THE IMPACTS OF CIRCADIAN DISRUPTION ON HIPPOCAMPAL PLACE CELL ACTIVITY

DAVID REUBEN ROBERTSON
Bachelor of Science in Neuroscience, University of Lethbridge, 2022

A thesis submitted
in partial fulfilment of the requirements for the degree of

MASTER OF SCIENCE

in

NEUROSCIENCE

Department of Neuroscience
University of Lethbridge
LETHBRIDGE, ALBERTA, CANADA

The Impacts of Circadian Rhythm Disruption on Hippocampal Place Cell Activity

David Reuben Robertson

Oral Defense Date: July 15th, 2024

Dr. R. McDonald Thesis Supervisor	Professor	Ph.D.
Dr. A. Gruber Thesis Examination Committee Member	Professor	Ph.D.
Dr. M. Tatsuno Thesis Examination Committee Member	Professor	Ph.D.
Dr. S. Pellis Chair, Thesis Examination Committee	Professor	Ph.D.

Abstract

Circadian rhythms are daily physiological cycles with wide-reaching influence on biological, mental and behavioural functions. We are at our best when our circadian rhythms function in a stable and consistent manner synchronous with stable and consistent patterns of day and night. Disruptions to circadian rhythms cause all manner of negative effects. One effect that is of particular interest to this study is that spatial memories formed while circadian rhythms are in disarray are not retained as well as those formed in stable conditions. The sorts of memories affected this way have a common factor. They all rely heavily on the hippocampal memory system. Methods have already been devised to read and decipher the neural code of hippocampal place cell firing patterns. However, until now, no attempt has been made to view how circadian disruption influences these hippocampal neural patterns. This experiment bridges that gap.

Acknowledgements

I am exceedingly grateful to the kind and wise people who have inspired and supported me throughout the past two years. With their guidance and timely aid, the many obstacles of this endeavor, which would have been overwhelming, were instead made simple. My sincerest thanks go to my supervisor Robert McDonald whose lessons instilled in me my interest and enthusiasm for this field, and who gave me the opportunity to become involved in research. To Nhung Hong, for always knowing what to do when I am at a loss. To Yagika Kaushik for her boundless patience and wisdom. To Amanda Huber for her diligence and insight. To HaoRan Chang for his cleverness. To Ingrid De Miranda Esteves for her time and skill. To Sorina Truica for her friendship and encouragement. Lastly to my parents, Fred and Sue Robertson whose love and faith has been a source of strength for me from the beginning.

Table of Contents

List of Tables

List of Figures

Chapter 1.

Introduction

This experiment concerns an intersection of two fields of research, namely the study of the role of the hippocampus in spatial memory, and the study of the cognitive effects of circadian rhythm disruption. As such, a brief introduction to these fields is given below.

1.1. Hippocampus and Memory

1.1.1. Overview of the neural basis of memory

The search for the brain regions that support learning and memory began in earnest with Karl Lashley's lesion studies. By severing or removing different parts of the brains of rats and testing their learning and retention abilities with mazes, he sought to identify which brain regions are most necessary for learning. He failed to find any specific location, instead finding that the severity of learning and memory impairments were related to lesion size. He concluded that memory is not localized but distributed throughout the brain (Lashley, 1950). In the years since then, much progress has been made in identifying the neural basis of memory. These discoveries overturning Lashley's conclusion have notably relied heavily on the study of subcortical areas, which were not targeted by Lashley's lesion studies (Eichenbaum, 2016).

The involvement of the hippocampus in memory was first identified through the groundbreaking work of Milner, Penfield and Scoville in studying the severe memory deficits of Henry Molaison, typically known as H.M. To treat H.M.'s epilepsy, Dr. Scoville performed a bilateral medial temporal lobe resection on him, entirely removing his hippocampi and some of the surrounding structures. After the surgery, H.M. no longer experienced epileptic seizures but instead had an extreme case of anterograde amnesia, being unable to learn and remember new factual information or autobiographical events (Scoville & Milner, 1957; Squire, 2009; Xia, 2006). He often described his state as being "like waking from a dream" (Milner et al., 1968). Though less severe, distinctive memory impairments had previously been identified in two patients of Dr. Penfield known as P.B. and F.C. who had undergone surgeries removing portions of one or both of their temporal lobes (Penfield & Milner, 1958). In examining the symptoms caused by these surgeries, it was concluded that the medial temporal lobe, and in particular the hippocampus is critical to the formation of conscious memories of facts and events, which were from then on described as declarative memories. Certain types of learning such as skill learning, habit learning,

simple conditioning, and emotional learning were not impaired in H.M., and were hereafter referred to as non-declarative memories. (Squire, 2009).

This work on H.M. provided clear evidence for the multiple memory systems theory, which asserts that different types of learning and memory are performed by different networks of brain regions. To explore the conceptual and physical anatomy of the multiple memory systems, a variety of double dissociation experiments were performed, searching for situations where removal of a brain region would impair one type of memory and not another. Double dissociation lesion experiments using rodents monkeys and humans distinguished between a hippocampal system involved in declarative memory, spatial navigation and context conditioning, and a dorsal striatal system involved in stimulus-response procedural learning and habit formation (Devan et al., 1999; Devan & White, 1999; Packard et al., 1989; Packard & McGaugh, 1992; Squire, 1992; Squire et al., 1993; Squire & Zola-Morgan, 1991; Yin et al., 2004). Additional such double dissociation studies revealed that emotional memory appears to rely on a distinct memory system focused on the amygdala (Bechara et al., 1995; Kesner & Hardy, 1983; McDonald & White, 1993; Phillips & LeDoux, 1992; Selden et al., 1991; Zola-Morgan et al., 1991).

The commonly accepted paradigm of multiple memory systems divides memory into three broad networks, one focused around the hippocampus, one around the dorsal striatum and one around the amygdala (Ferbinteanu, 2019; Gruber & McDonald, 2012; White & McDonald, 2002). However, each of these systems are themselves made of distinct components with dissociable functions (Bucci et al., 2000; Burwell et al., 2004; Gaffan et al., 2001; Hunt et al., 1994; Kesner et al., 1989). The interactions within and between these memory systems is still being explored.

Although the hippocampus is of central importance to the memory system devoted to declarative memory, there have been various theories regarding the specific role of the hippocampus within this system. To shed light on the functions of the hippocampus, one must first consider its central role in spatial memory in the context of cognitive map theory.

1.1.2. Cognitive map theory

Cognitive map theory asserts that the process of learning to navigate a new environment consists “not in stimulus-response connections but in the building up in the nervous system of sets which function like cognitive maps” (Tolman, 1948). Although this theory is generalizable to domains other than literal space (Tavares et al., 2015), for the purposes of the present research I will be focusing on cognitive map theory as it pertains to navigation in literally spatial environments.

There are various areas of the brain where neurons with location-dependent, behavior-independent activity have been found, such as in the dorsal hippocampus, entorhinal cortex, presubiculum and parasubiculum. These neurons and their higher order interactions form the basis of cognitive maps of spatial environments (Moser et al., 2017).

1.1.3. Place cells and spatial navigation

The idea that the hippocampus constructs a cognitive spatial map was first put forth by O'Keefe and Dostrovsky (1971) when they first discovered individual signals from the CA1 region of the hippocampus with spatially localized firing patterns. In 1978, O'Keefe and Nadel published "The Hippocampus as a Cognitive Map" which proposed that the hippocampus is "the core of a neural memory system providing an objective spatial framework within which the items and events of an organism's experience are located and interrelated". Much research has been done since then to investigate the behaviour of hippocampal place cells, confirming that they encode location, and attempting to determine how they do so (Moser et al., 2017).

The behaviour of place cells reflect an allocentric model of navigation, meaning position is encoded in a way that seems to rely on fixed landmarks and not to the orientation of the subject. A place cell activates when the subject enters the space that cell encodes for, called a place field, regardless of what the subject is doing or where it is facing (Muller et al., 1994). Place fields do not shift when individual landmarks in their environment are moved or removed (J. O'Keefe & Conway, 1978; J. O'Keefe & Speakman, 1987; Speakman & O'Keefe, 1990). Individual place cells can have multiple separate place fields within the same large environment, with some place cells encoding for many place fields, and others encoding for one or few (Rich et al., 2014). This fixed allocentric map behaviour of place cells must be derived from sensory information which is naturally egocentric. This raises questions of how the brain converts egocentric sensory information into an allocentric model of the environment, and how these place cells continue to function even when sensory input is limited (Quirk et al., 1990).

Head direction cells suggest a possible answer. Head direction cells, first found in the postsubiculum of rats, are cells that activate whenever the head is pointed in a particular direction in the horizontal plane. These cells behave independently from location, behaviour, and the posture of the rest of the body. The discovery of head direction cells (Taube et al., 1990a, 1990b) was an important finding because it bridged the gap from egocentric sensory information to the allocentric model of space reflected in the place cells. The existence of head direction cells supported and gave rise to the hypothesis that the cognitive map may use path integration based on idiothetic (self-motion) cues to determine changes in position (McNaughton et al., 1996; Samsonovich & McNaughton, 1997). This path integration system is necessary to explain how it

is possible to maintain knowledge of allocentric location even in the absence of light or landmarks. In short, Head direction cells use egocentric sensory data about self-motion to reliably produce orientation information necessary for path integration. Without accurate path integration, allocentric spatial representations like those of hippocampal place cells could not function in environments devoid of landmarks (Quirk et al., 1990).

Attempts have been made to determine how place cell place fields are influenced by visual information when it is decoupled from self-motion information (Bures et al., 1998; G. Chen et al., 2013). It was found that both are used, and that “individual cells are independently driven by different strengths of visual and motor-related path integration inputs” (G. Chen et al., 2013).

There are other types of spatial encoding cells aside from place cells and head direction cells. Grid cells, first discovered in the medial entorhinal cortex (Fyhn et al., 2004; Hafting et al., 2005), are cells that each have multiple evenly spaced firing fields arranged in a hexagonal tiling pattern that fills the entire environment. Grid cells differ from one another in the phases, orientations and spacing of their grids. Border cells, also initially found in the medial entorhinal cortex (Savelli et al., 2008; Solstad et al., 2008), are cells with firing fields along the edges of the environment. The entorhinal cortex is also home to grid cells that only fire when the head is pointed in a certain direction. More work is yet to be done to determine the mechanisms of how these cell types interact with each other to facilitate spatial learning and memory (Moser et al., 2008).

The place field of a place cell is typically conceptualized as being the region of space which when occupied by the animal will cause the place cell to fire. However, their behaviour is a touch more complicated and adaptive than that. Prior research involving head-fixed and consequently stationary mice, has found that place cells can have place fields representing regions of a virtual space (Harvey et al., 2009) or along a linear treadmill track (Royer et al., 2012).

Additionally, place cells are known to change their activity patterns within an environment in a process called remapping. When used without additional qualifiers the word remapping can refer to changes in either firing rates or place field locations in either a single place cell or a population of place cells. For the sake of clarity, in this paper the word remapping will be used to refer to changes in an individual cell’s place field. Rate remapping refers to changes in firing rates. Global, or complete remapping is the total shift of place fields and firing rates that occurs when the animal enters a new environment (Muller & Kubie, 1987). Global remapping can also sometimes occur when an environment is considerably altered (Bostock et al., 1991; Hayman et al., 2003), although minor environmental changes usually only cause rate remapping (Colgin et al., 2008). Gradual remapping in a population of place cells is often referred to as

representational drift. Recent studies have demonstrated that passage of time and amount of experience have different effects on hippocampal spatial representational drift. Khatib et al. (2023) found evidence that the amount of time spent exploring a spatial environment is related to more remapping of place fields. They also found that this representation drift leads to decreased numbers of cells functioning as place cells in the environment and increased total spatial information. In other words, “efficiency of hippocampal representation increases with experience without compromising its accuracy”. Note that this research involved single day experiments and may not be perfectly comparable to multiday experiments. Meanwhile, Geva et al. (2023) performed multiday experiments that found that “time drives day-to-day changes in neuronal activity rates, whereas experience drives changes in spatial tuning”.

1.1.4. Theories on the role of the hippocampus

The preceding sections have depicted one perspective on the role of the hippocampus, however, there are several other theories on its function, not all of which are mutually exclusive. To get a wider overview of what the hippocampus is thought to do, I will summarize a few of the most influential theories here.

One major theory on the role of the hippocampus was described by Hirsch (1974). He proposed that the hippocampus serves as a context retrieval system. His idea was that the components of memories are not stored in the hippocampus per se, but that the hippocampus acts like an index. In this model, environmental and cognitive cues would be used by the hippocampus to determine which memories to access, so that those relevant memories could be applied to the current situation. Once accessed or activated by action of the hippocampus, the contextual memories would modify the behaviour of the stimulus-response associations believed to directly control behaviour. The accessed information would do this by specifying “objects of attention and intention” (Hirsh, 1974). Hirsh noted that hippocampally ablated animals fall back on a stimulus-response system of learning characterized as habit formation.

Teyler and DiScenna (1986) Built on Hirsch’s index idea and applied it to episodic memory. They referred to this model of hippocampal function as ‘hippocampal memory indexing theory’. The theory, in brief, is that the component parts of memories are stored dispersed throughout the neocortex and other brain regions, and that the hippocampus contains only the “location and temporal sequencing” (Teyler & DiScenna, 1986) of which parts of the brain need to be reactivated to facilitate recall. Once a memory is formed, if enough of the brain regions pertaining to a memory activate at once, this would cause activation of the corresponding stored hippocampal index, triggering all associated brain regions to reactivate which constitutes recall of that memory.

The other major theory of the role of the hippocampus was described by O'Keefe and Nadel (1978). They drew inspiration from Tolman's (1948) idea of cognitive maps and proposed that the hippocampus is the site of these cognitive maps. They divided the functions they believed the hippocampus to be responsible for into the two categories of map-based (locale) navigation and route-based (taxon) navigation. In their terminology, locale navigation uses two-dimensional or three-dimensional cognitive maps, such as the ones used in spatial learning, while taxon navigation has no clear dimensional limit, and is involved in stimulus-response based habit learning.

McNaughton et al. (1996) as mentioned previously, paid particular attention to the activity patterns of place cells and head direction cells, and from that developed a model of understanding the role of the hippocampus in spatial navigation. They proposed that the hippocampus and related structures calculate position in space using self-motion data with a path integration system. In essence their idea is that animals use motor and proprioceptive data to determine how their position in space has changed over time, and corrects errors made in that process using visual data. This theory provided a framework for explaining certain characteristics of hippocampal place cells such as their ability to keep track of position in total darkness (Quirk et al., 1990).

Buzsáki and Tingley (2018) brought into question an underlying paradigm of much of hippocampal research when they proposed that neither the hippocampus nor the brain in general deals with space or time, but rather with sequences of events. They assert that the concept of the hippocampus as a space and time calculator does not fit with many experimental observations, and they suggest that the hippocampus "may be 'blind' regarding the modality of its inputs" (Buzsáki & Tingley, 2018). They pointed out that the neuronal circuitry of the hippocampus indicates that it processes all incoming information in much the same way regardless of what brain region the inputs are coming from. This is important because the hippocampus is bidirectionally connected to the neocortex, which in primates is proportionally much less concerned with sensory and motor processing than in rodents. It is thus reasonable that the time and place focus of the hippocampus experimentally identified in many previous studies is merely one facet of the true function of the hippocampus, which is not inherently specialized to those modalities. If this is true it would mean that whether any given experiment "implies that the hippocampus is computing space, time, memory, planning, abstract concepts, or other relationships may depend on the experimental design and the cortical input rather than on hippocampal computation per se" (Buzsáki & Tingley, 2018). To explain the behaviour of hippocampal place cells and other place and time related findings without using the concepts of place or time, Buzsáki and Tingley put forth the idea that the hippocampus may be a sequence generator. This is a modification of indexing theory wherein each fundamental hippocampal unit is

not a single index but an ordered series of indices. If true this means that “the hippocampal system is responsible for concatenating neocortical information chunks into sequences for both encoding and retrieval” (Buzsáki & Tingley, 2018). It is important to note that although Buzsáki and Tingley disagree with the concept of a brain mechanism directly representing or calculating space or time, they specifically do not take issue with relating neuronal observations to measurements of space and time.

1.2. Circadian Rhythms

Circadian rhythms are daily cycles of physiological and neurological function. These regular rhythms influence many aspects of behavior across nearly all light sensitive organisms (Schibler, 2005). Disruptions to circadian rhythms are known to have negative effects on many different aspects of health. It is important to identify all the many effects of circadian rhythms disruption because for many people these disruptions are common in day to day life, as a result of shift-work, 24-hour business, jetlag, and late-night exposure to bright light.

1.2.1. Central and peripheral circadian clocks

The expression of circadian rhythms is produced primarily by the suprachiasmatic nucleus (SCN) which functions as a master clock by synchronizing the cycles of peripheral clocks throughout the body (Van Esseveldt et al., 2000). The SCN produces an oscillating signal with a period of approximately 24 hours, though the timing of the SCN’s circadian rhythm uses exogenous environmental cues to stay calibrated to a 24-hour period. These external cues, called zeitgebers, ensure that circadian rhythms remain in sync with the environmental day-night cycle (Sharma & Chandrashekaran, 2005; Van Esseveldt et al., 2000). This system relies on zeitgebers like sunrise, sunset, meals, physical activity and social contact occurring with regularity. As such, unusual changes in the timing of any of these signals can cause a shift or disruption in an organism’s circadian rhythm as it seeks to adapt and realign with the zeitgebers (Aschoff et al., 1975). Since light exposure is the most reliable and influential zeitgeber (Münch & Bromundt, 2012), phase shifts in light-dark schedules are frequently used to study the effects of circadian disruption.

1.2.2. Methods of circadian disruption

There are a variety of ways to phase shift light-dark schedules in research, which can prove problematic in directly comparing the results of these studies to one another (Knutsson, 2004). Human studies often use shift workers with inconsistent work schedules as an

experimental group compared to a stably diurnal control group, though such studies generally lack consistency in how frequently the subjects shift their sleep schedules. Human studies are also frequently confounded by self-selection issues, which make animal models particularly valuable in this field. Some studies test the effects of a single abrupt phase shift, though the size of the shift varies from study to study (A.-M. Chang et al., 2023; Loh et al., 2010). Other studies, primarily using rodents, have used a middle-ground approach involving regular phase advancement in accordance with a set schedule to induce complete circadian disruption during a particular window of time (Craig & McDonald, 2008; Deibel et al., 2014, 2022; Gibson et al., 2010; Iggena et al., 2017; Martino et al., 2008; McDonald et al., 2013). Whenever the circadian rhythm is disrupted in any way there are a variety of effects, some obvious and some subtle.

1.2.3. Health effects circadian disruption

Circadian disruption has been linked to many negative health effects (Baron & Reid, 2014; Mehta et al., 2021; Roenneberg et al., 2019; Roenneberg & Merrow, 2016). These include but are not limited to cancer (Bracci et al., 2019; Filipski et al., 2006; Wendeu-Foyet et al., 2020; Zienolddiny et al., 2013), obesity (W.-P. Chang & Lin, 2022; Chaput et al., 2023), cardiovascular risk factors (Chellappa et al., 2019; Martino et al., 2008), decreased glucose tolerance (Yuan et al., 2021), and mood disorders (Vadnie & McClung, 2017). Circadian disruption has also been linked to age-related dementias such as Alzheimer's disease (Musiek et al., 2015), as well as age-related memory decline in general (Antoniadis et al., 2000).

1.2.4. Memory effects of circadian disruption

The first indications that phase shifting light-dark schedules cause impairments in memory tasks came from experiments testing retention in active and passive avoidance tasks (Davies et al., 1974; Tapp & Holloway, 1981; Fekete et al., 1985, 1986; Stone et al., 1992). This apparent link between circadian rhythms and memory raised questions regarding how each memory system is affected by circadian disruption. The first step to addressing such questions for any memory system or brain region is to find a task that relies on that memory system and compare the performance of phase shifted subjects with unshifted controls. Of relevance to the current research are animal studies which have demonstrated a link between circadian disruption and impairments of learning and memory functions known to rely on the hippocampus. Devan et al. (2001), used the Morris water task (Brandeis et al., 1989; R. Morris, 1984) to assess the effects of phase shifting on the hippocampus. This task was chosen because the spatial memory it tests has been shown to rely on the hippocampus (Kolb et al., 1983; R. G. Morris et al., 1982; Okaichi, 1987; J. O'Keefe et al., 1975; Sutherland et al., 1982; Sutherland & Rudy, 1989). Devan

et al. (2001) trained rats on the Morris water task on five days while the experimental group experienced a 3-hour phase advance each day, including the day before training began. The retention test was done after 17 days of stable 24-hour days to re-entrain their circadian rhythms. It was found that the phase shifting did not affect learning during the training days, but that the performance on the retention test was impaired in rats that were being phase shifted during the training. In short, they found that circadian disruption caused impaired retention and normal acquisition of spatial memory. This finding has been replicated (Deibel et al., 2022; Zelinski et al., 2014). Other experiments with different phase shift schedules have found disruption induced impairments to Morris water task (Iggena et al., 2017), contextual fear conditioning (Loh et al., 2010; Steiger et al., 2022), and conditioned place preference (Gibson et al., 2010; McDonald et al., 2013) which are all tasks that rely on hippocampal and parahippocampal functions.

1.3. Purpose of current research

Because circadian disruption has been found to impair performance in spatial memory tasks known to depend on the hippocampus, the simplest interpretation is that the activity of the hippocampus is being impaired or disrupted in some way by circadian disruption. The next step is to attempt to confirm this by observing patterns of neural activity in the hippocampus during and after acquisition of a new spatial memory to see if there are significant changes between phase shifted and control groups. It is hypothesized that the formation and stability of representations of space encoded in the hippocampus will directly parallel the behavioural outcomes observed in Devan et al.'s (2001) study. Namely, that multi-day phase shifting will not impair acquisition of a new spatial memory and will impair the retention of that memory after phase shifting has ended.

To test this, representations of space encoded in the hippocampus were observed and analyzed by recording the firing rates of place cells in mice as they moved through an environment on multiple days. The spatial representational drift between days was measured in terms of mean tuning curve correlations (Geva et al., 2023). Low rates of representational drift mean high degrees of place cell stability across days, while high rates of representational drift mean impaired stability of place cells across days. If the hypothesis holds true, then it is expected that the rates of representational drift between acquisition days and retention tests would be increased for phase shifted mice, relative to controls.

Chapter 2.

Methods

Thy1-GCaMP6 mice each with an implanted window over the right hippocampus were trained to run along a treadmill for a sugar water reward. Two-photon calcium imaging of the same population of CA1 neurons across multiple days was performed for each mouse. The experimental group experienced a phase advanced light/dark schedule during initial imaging sessions. The effects of this shifting lighting schedule on the behaviour of CA1 place cells was assessed.

2.1. Subjects

2.1.1. Thy1-GCaMP6

Seventeen adult transgenic Thy1-GCaMP6 mice were used in this experiment. Thy1-GCaMP6 mice are transgenic mice which express calcium ion sensors in cortical neurons, which allows for 2-photon imaging of their hippocampal neurons (T.-W. Chen et al., 2013; Dana et al., 2014). Specifically, the mice produce a GCaMP6 calcium indicator in excitatory neurons in the brain using the Thy1 promotor.

2.1.2. Hippocampal cranial window surgical procedure

The mice underwent cranial window surgeries to make a section of their right hippocampus accessible for imaging.

In preparation, each window was made by attaching a circular piece of glass to one end of a metal tube. The stainless steel tube was 1.5mm long with a 3mm outside diameter. A 0.15mm thick, 3mm diameter round cover glass (made by Deckglasser) was affixed to one end of the tube using optic glue (NOA71, Norland).

Prior to surgery, mice were injected with 0.075 mg/kg of buprenorphine (0.03 mg/mL, s.c.). They were anesthetized with isofluorane (1–1.5%, O2; 1 L/min) and were head-fixed in a stereotactic frame while laid on a heating pad to maintain their body temperature at 37.0 ± 0.5°C. Once in position, the mice were injected with 0.5 mL of saline (s.c.) to prevent dehydration during surgery, 0.05 mL of dexamethasone (i.m.) to suppress inflammation, and 0.1 mL of lidocaine (s.c. below scalp) as a local anesthetic.

The surgery was performed by removing the scalp, opening a 3mm diameter hole in the cranium to the right of the sagittal suture and anterior to the right lambdoid suture, then aspirating enough of the cortex to expose the fibers of the corpus collosum. The tube was then inserted, glass-side down into the hollowed-out space, where it was then affixed to the craniotomy using Vetbond (3M). Metabond (Parkell) was used to affix a titanium headplate to the exposed skull. Dental Acrylic (Jet tooth Shade Powder and Liquid, Lang Dental Manufacturing Co.) was used to cover the skull between the tube and the head-plate. A rubber ring was attached over the headplate to allow for water immersion imaging. See figure 2.1 for an example of this headplate apparatus.

Once the cement set, the mice were injected with 0.05 mL of Inflacam (s.c.) to suppress inflammation and 0.05 mL of Baytril (s.c.) which is an antibiotic. These two injections were repeated once per day for two days following surgery.

Figure 2.1: Mouse 1's cranial window and headplate apparatus.

2.1.3. Cohorts and schedule

Subjects were divided into two cohorts, the first being imaged in the summer of 2023 and the second being imaged in the spring of 2024. Cohort 1's experimental group consisted of 1 female and 4 males. Cohort 1's control group initially consisted of 4 males, one of which later had

to be excluded from the study for inadequate lap numbers during imaging days. Cohort 2's experimental group initially consisted of 2 females and 2 males, but one of the females was excluded when it was found that they lacked detectable levels of GCaMP6, despite testing positive for the GCaMP6 genotype. Thus, after exclusions the total experimental group includes 3 females and 6 males, while the total control group includes 2 females and 6 males.

Table 2.1: Mouse identification numbers and sexes by cohort and group

	Cohort 1	Cohort 2	Totals
Control Group	#3(M), #4(M), #8(M)	#14(F), #15(M), #16(F), #17(M), #18(F), #19(M)	3 females and 6 males
Experimental Group	#1(F), #2(M), #5(M), #6(M), #9(M)	#10(F), #11(M), #13(M)	2 females and 6 males

Since all imaging was done by one person on one set of imaging equipment it was deemed unfeasible to image all nine mice of cohort 1 on the same days. As such, the two groups of cohort 1 were staggered to prevent schedule overlap. For context, imaging the five mice from cohort 1's experimental group including set up, take down, data transfer and the occasional equipment repair required eleven and a half hours per imaging day on average, not including breaks. The first imaging day of the cohort 1 control group was May 28th, 2023. The first imaging day of the cohort 1 experimental group was June 14th, 2023. Due to a short notice scheduling conflict, the six control group mice of cohort 2 needed to be separated into two groups of three mice each. The first imaging day of the cohort 2 experimental group was February 20th, 2024. The first imaging day of the first half of the cohort 2 control group (mice 14, 15 and 16) was March 12th, 2024. The first imaging day of the second half of the cohort 2 control group (mice 17, 18 and 19) was March 22nd, 2024.

2.2. Design

The treadmill and 2-photon microscopy procedure described below is largely identical to prior experiments performed using the same equipment (H. Chang et al., 2020, 2023; Esteves et al., 2021, 2023; Ivan et al., 2024).

2.2.1. Treadmill training

After a minimum of nine days to recover from surgery, each mouse began water restriction and subsequently began treadmill training once per day. For 3 days prior to water restriction each mouse was weighed to determine a baseline weight. During water restriction,

each mouse was weighed daily before and after being given water, both to confirm that they drank, and to ensure that their weight after drinking never dropped below 85% of their baseline weight. All weights were recorded on water restriction log sheets.

While water restriction is ongoing, the activity of the mice was recorded using infrared motion sensors (Actimetrics) attached to their cages. This was done to monitor the circadian rhythms of the mice allowing for confirmation of three assumptions this experiment relies on. Firstly, the mice were expected to have consistent circadian rhythms of activity. Secondly, phase shifting the experimental group's light-dark schedule was expected to disrupt their circadian rhythms. Thirdly, imaging the control group without altering their housing room's light-dark schedule was expected to not disrupt their circadian rhythms. These assumptions did in fact hold true as can be seen in figure 2.2 which shows some of the actogram data obtained by the motion sensors.

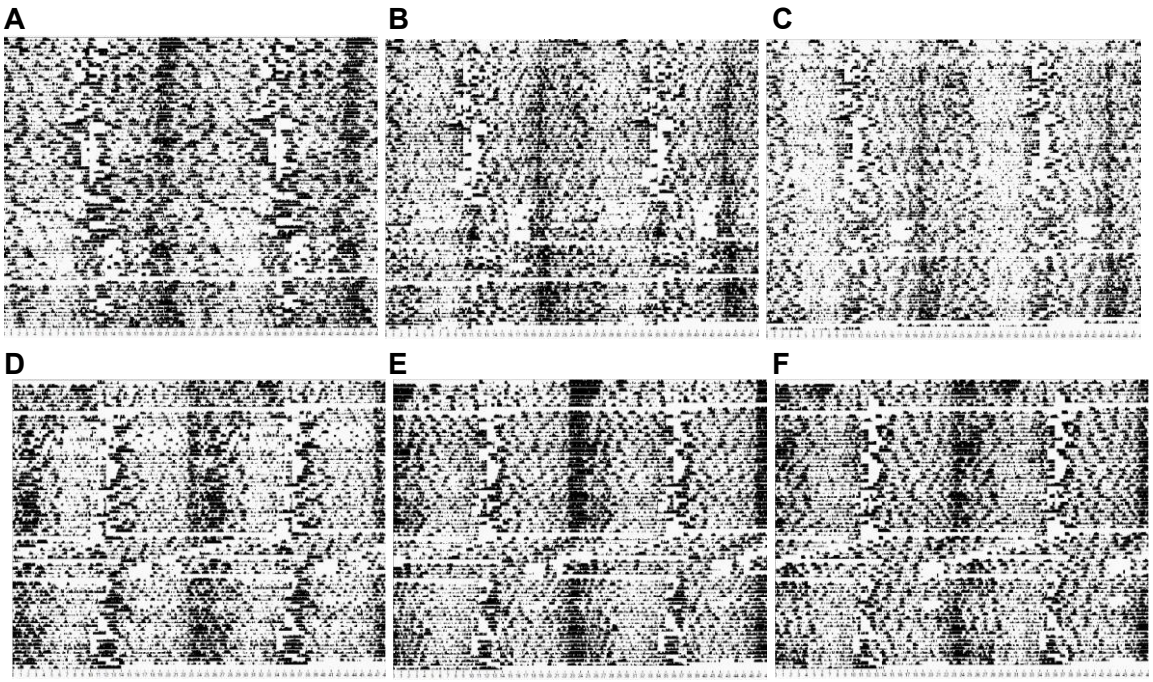

Figure 2.2: Actograms of 6 mice from cohort 2. Data was obtained using cage-mounted infrared motion sensors (Actimetrics). Each figure is double plotted such that each row contains 48 hours of data. A, B and C are actograms from 3 control group mice. The vertical lines that remain uninterrupted before during and after the imaging days shows that imaging did not disrupt their circadian rhythms. D, E and F are actograms from 3 experimental group mice. The diagonal disruptions to the otherwise consistent vertical lines show that the phase shifting these mice experienced disrupted their circadian rhythms, as expected.

The treadmill belt was a 150 cm long strip of loop side Velcro (Country Brook), with the ends connected by a piece of matching hook side Velcro (Country Brook). The training treadmill was blank other than the velcro connector. The belt went around two 10 cm diameter wheels positioned so that the portion of the top of the belt between the two wheels would slide across a

stable metal platform with side walls, such that a mouse, when head-fixed in place there, would be standing on top of the treadmill belt supported by the metal platform, and not directly the metal. Speed and direction of the treadmill's motion was recorded by an optical encoder (Avago Tech) attached to the rear wheel. A piece of reflective tape hot glued to inner surface of the treadmill allowed a photoelectric sensor (Omron) to indicate whenever a full lap was completed, which would send a signal to reset the position data and trigger a reward. The tube leading from the sugar water to the spout was kept pinched shut by solenoid pinch valve (Bio-Chem) that would dispense rewards by briefly unclamping the tube. The optical encoder, photoelectric sensor and solenoid pinch valve were coordinated by a custom-designed circuit with a microcontroller (Arduino UNO, Farnell).

Training began on the 6th day of water restriction and was done once per day up until the first imaging day. For cohort 1 training lasted between 54 and 93 days, which was deemed unnecessarily long for the purposes of habituation to head-fixation and maximization of lap frequency, so for cohort 2 training lasted between 43 and 53 days.

During training sessions, a mouse was head-fixed in place on the treadmill. Completing forward laps was rewarded by 10% sugar water from a spout held in place within reach of the tongue. During training there was no upper limit on the number of laps a mouse was permitted to run. The first training session for each mouse was 5 minutes of running with no wait times before or after. Training session durations gradually ramped up to 20 minutes of running with the treadmill being clamped in place for 15 minutes before and 10 minutes after.

2.2.2. Imaging schedule and lighting schedule

Throughout the training period, the control group were housed in a room with lights on from 7:30 to 19:30, while the experimental group were housed in a room with a 10:30 to 22:30 lighting schedule. The experimental group's baseline light-dark schedule was set at 10:30 to minimize the amount of imaging that would need to be done at inconvenient times of day. Every mouse had 10 consecutive imaging days and 3 retention tests for a total of 13 imaging days per mouse.

For the both the control and experimental groups, all recording sessions took place when their housing room would be lit. Because multiple mice were being imaged each day, different mice within the same group were imaged at different times of day. The first 10 imaging days occurred one after another. The first retention test, hereafter referred to in figures as day 11, took place 7 days after day 10. The second retention test, hereafter referred to in figures as day 12, took place 1 day after the first retention test, or 8 days after day 10. The third and final retention

test, hereafter referred to in figures as day 13, took place 15 days after the second retention test, or 23 days after day 10.

For the experimental group, phase shifting began one day before the first day of imaging. Their usual 10:30 to 22:30 lighting schedule was phase advanced by 3 hours per day until the time of lights on returned to 10:30. In other words, they experienced 8 consecutive 21-hour days. The first of these 21-hour days was the day before the first day of imaging, meaning that the first 7 imaging days occurred while the phase shifting was ongoing, with days 8 to 10 and the retention tests taking place on normal 24-hour days with the lights remaining on from 10:30 to 22:30.

Table 2.2: Lighting schedule

	Experimental Group		Control group	
	Lights Turn On	Lights Turn Off	Lights Turn On	Lights Turn Off
During Training	10:30	22:30	7:30	19:30
Final training day	7:30	19:30	7:30	19:30
Day 1	4:30	16:30	7:30	19:30
Day 2	1:30	13:30	7:30	19:30
Day 3	22:30	10:30	7:30	19:30
Day 4	19:30	7:30	7:30	19:30
Day 5	16:30	4:30	7:30	19:30
Day 6	13:30	1:30	7:30	19:30
Day 7	10:30	22:30	7:30	19:30
Day 8	10:30	22:30	7:30	19:30
Day 9	10:30	22:30	7:30	19:30
Day 10	10:30	22:30	7:30	19:30
Day 11 (R1)	10:30	22:30	7:30	19:30
Day 12 (R2)	10:30	22:30	7:30	19:30
Day 13 (R3)	10:30	22:30	7:30	19:30

The experimental group day 1 recording began as close to 4:30 as feasible, and each subsequent day the target start time receded by 2 hours until it reached 16:30 on day 7. The control group for cohort 1 had a day 1 target start time of 13:30 which receded by 1 hour per day until reaching 7:30 on day 7. This was intended to minimize the amount of variation between the groups in regard to the spacing of the imaging sessions, while still keeping all imaging sessions within hours of housing room light. Thus the first 7 imaging sessions for each experimental group mouse is spaced apart by approximately 22 hours, and the first 7 imaging sessions for each cohort 1 control group mouse is spaced apart by approximately 23 hours. Unfortunately, due to scheduling limitations involved in sharing use of the imaging with other researchers it was not possible to do this for the cohort 2 control group, so all their first 10 imaging sessions remain spaced apart by 24 hours.

2.2.3. 2-photon equipment, imaging parameters and procedures

The treadmill apparatus used during 2-photon imaging was largely the same as the training treadmill apparatus (2.2.1), with three key differences. First, a sensor was clipped to the spout to track the timing of each time the spout was licked by the mouse. Second, infrared LED lights and an infrared camera were positioned to record video of the mouse's head during imaging sessions. Third, the treadmill belt used during imaging sessions had three tactile cues attached to it in addition to the usual Velcro connector, two made of solidified glue, and one made of reflective tape. See figure 2.3 for comparison of the belt used during training to the belt used during imaging.

Figure 2.3: Tactile cue distribution across both belts.

All 2-photon imaging was done using a Bergamo II multi-photon microscope (Thorlabs). The Ti:Sapphire pulsed laser (Cohorent) was tuned to 920 nm and focused through a 16x objective lens (Nikon, 0.8 N.A.). Its power output was kept between 80 and 100 mW during imaging, as measured at the sample using a handheld optical power and energy meter (Thorlabs). Fluorescent light emitted by GCaMP6 during imaging were detected and amplified by a GaAsP photomultiplier tube (Hamamatsu). All imaging is performed at 19.2 fps over a square field of view (FOV) with a width and length of 835.76μm and a resolution of 800x800 pixels.

The relative timing of treadmill position and velocity data with respect to the microscope data was measured using AxoScope software (Molecular Devices).

Setup for each imaging session consisted of clamping the treadmill belt in place, placing the mouse onto the treadmill, and clamping their headplate into a fixed position. The tape covering the inset stainless-steel tube was removed and the surrounding dental acrylic was wiped clean with a cotton tipped applicator soaked in 70% ethanol. Enough distilled water was added to the headplate apparatus to allow for water immersion imaging. The sugar water spout with the lick sensor clamped to it was then positioned within reach of the mouse's tongue, and the objective lens of the microscope was centered above the window and lowered into position. A Velcro loop around the objective lens was slid down to the headplate to block out light from around the sides. A black tarp curtain surrounding the entire treadmill and microscope apparatus

was then closed and the room lights were turned off to further darken the environment. The exact position and depth of the objective lens was chosen on day 1 to maximize the number of excitatory neurons visible within the FOV. On all subsequent imaging days the lateral positioning and depth of the FOV were adjusted to match the reference images of the day 1 FOV.

Once the proper FOV was found, three recording sessions were done on each imaging day for each mouse. The first and third imaging sessions were pre-run and post-run sessions lasting 24000 frames each (~20 minutes), and both done with the treadmill clamped in place. The second recording session was the running session. Immediately after the start of recording, the treadmill was unclamped allowing the mouse to run freely, receiving a 10% sugar water reward with each lap, just as in training. Day 1 of imaging would be each mouse's first experience with the tactile cues of the imaging belt. After the completion of their 20^{th} lap the treadmill was again clamped. This was done to avoid extreme disparity between mice in the total number laps, as would occur if there was not an upper limit. If a mouse did not complete a minimum of 10 laps in a running session, the data obtained that day was disregarded in later data analysis steps. On day 1 the running session lasted 24000 frames (~20 minutes), however if a mouse was found to reliably complete all 20 laps in less than 10 minutes, the duration of future running sessions was shortened by up to 12000 frames on a case-by-case basis.

2.3. Single session analysis

The preprocessing of individual sessions uses the same overall methodology as described in previous studies using the same treadmill and 2-photon microscope apparatus (Chang et al., 2020, 2023; Esteves et al., 2021, 2023). A description of this process can be found below.

2.3.1. Identification of cells

The raw video files obtained from the microscope were processed in Suite-2p (Pachitariu et al., 2016). This program performed motion correction, identified of regions of interest (ROIs) that might be cells, and determined the fluorescence level of each ROI over time. The ROIs identified by Suite-2p were visually inspected and sorted one-by-one on the basis of their shape, size, and fluorescence fluctuation to determine whether or not they are actual cells. See figure 2.4B for an example of one session's ROIs after sorting.

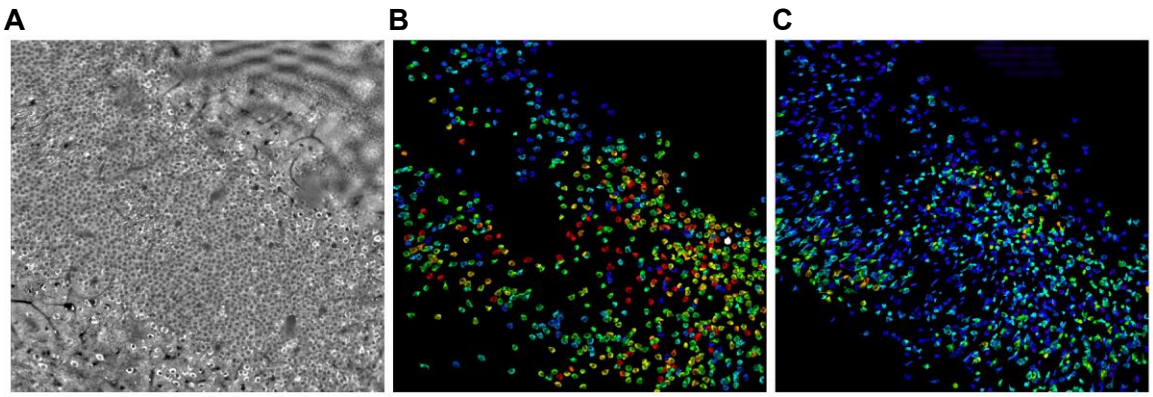

Figure 2.4: Example of Suite-2p ROI sorting. **A**, Enhanced mean FOV from the mouse 6 day 1 recording session. **B**, Masks of ROIs manually identified in Suite-2p as being cells, with colour indicating likelihood of being a cell as determined by Suite-2p's built-in classifier tool. **C**, Masks of ROIs manually identified in Suite-2p as not being cells, with colour indicating likelihood of being a cell as determined by Suite-2p's built-in classifier tool.

For each ROI, the calcium fluorescence fluctuations are refined by correcting for neuropil contamination signals. This is done by estimating neuropil signals from the signal fluctuations of the immediate surroundings of the ROI, and subtracting that from the ROI's signal fluctuations (Bonin et al., 2011), such that Fcorrected = Fraw – Fmotion – Fneuropil. The fluorescence signal of each ROI was also adjusted relative to their baseline level Fo, such that $\Delta F/F$ = (Fcorrected – Fo)/Fo x 100.0. The firing spikes underlying the signal fluctuations were calculated by deconvolving the $\Delta F/F$ time courses with constrained non-negative matrix factorization (Pnevmatikakis et al., 2016). All subsequent analysis of cell activity was done in MATLAB using this deconvolved spiking activity normalized between 0 and 1.

During these steps, Suite-2p uses all three sessions (pre-run, running and post-run) as a single input. Once sorting is finalized, Suite-2p outputs each session's data separately. It outputs the fluorescence signal of each cell in the form of a matrix with a height equal to the total number of cells and a width equal to the number of frames in the recording session. It also provides the shape and position of each cell, and the timing of each frame.

2.3.2. Merging data sources and identifying place cells

All subsequent analysis was performed in MATLAB.

The length of the treadmill was divided into 50 equally spaced 3 cm-long bins. Position along the treadmill over time was simplified to bin number over microscope frame number, and spatial tuning curves were made by finding each cell's total activity while in each bin, normalizing

them by relative amount of time spent in each bin, and filtering them with a Gaussian window (4 cm standard deviation smoothing kernel).

In order for a cell to be identified as a place cell, two criteria had to be met (Chang et al., 2020, 2023; Esteves et al., 2021, 2023):

First, potential place cells are tested to determine if they contain sufficiently high spatial information. spatial information in bits was calculated for each cell using the formula given by Skaggs et al. (1992) as $I = \sum_{i=1}^{N} p_i \frac{f_i}{f} log_2 \frac{f_i}{f}$ where I is spatial information in bits, f_i is mean activity in bin i, f is overall mean firing rate of the cell, and p_i is probability of the mouse being in bin i. To meet the first criteria, a place cell had to contain more spatial information than the 95th percentile threshold of a null distribution of spatial information made by circularly shuffling the time courses 1000 times. Some prior studies have used only this first test as their means of determining whether a cell is a place cell (Geva et al., 2023; Khatib et al., 2023).

Second, potential place cells are tested to determine if they have an actual place field. To do this, a continuous wavelet transform was made for each cell's spatial tuning curve using the Ricker wavelet, also known as the Mexican Hat wavelet. An example of a tuning curve and wavelet transforms on that tuning curve are shown in figure 2.5, along with an example of the full results of the continuous wavelet transform on that tuning curve in figure 2.6. The local maxima of the transform indicate the locations and widths of potential place fields as shown in figure 2.7A. Any potential place fields narrower than 5% or wider than 80% of the length of the treadmill were discarded, followed by noise filtering to remove local maxima of insufficient magnitude (figure 2.7B). After that, local maxima centered within any larger potential place field were discarded (figure 2.7C). Finally the reliability of each remaining potential place field (figure 2.8) is tested in two ways. First, potential place fields with less than 2.5 times the firing activity within the place field than outside it were discarded. Second, for each potential place field the laps with peak activation for that cell within the place field under consideration were identified. Gaps between successful laps that were only 5% the total number of laps long rounded down were treated as though they were successful. After that, place fields that did not have a string of consecutive successful laps at least as long as 33% of the total number of laps were discarded.

All cells with sufficient spatial information and a sufficiently coherent place field are added to the place cell list for that recording session.

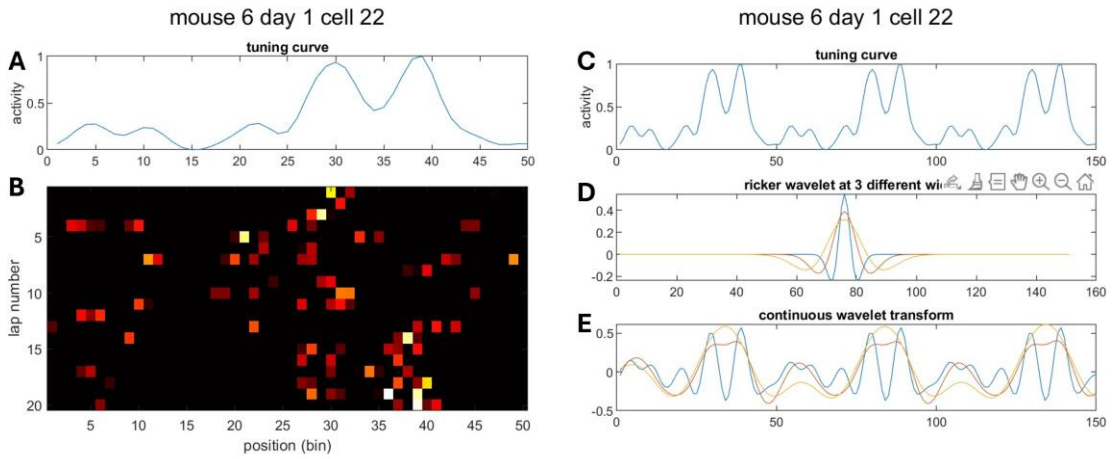

Figure 2.5: Activation data, tuning curve and continuous wavelet transform of a single place cell. The cell used for these figures cell 22 from mouse 6 on day 1. **A**, Spatial tuning curve of this place cell. **B**, Normalized activation intensity of this place cell grouped by each of the 50 bins of the treadmill (each bin being 3 cm long), and each of the 20 laps. Lap number is indicated by the y-axis, bin number is indicated by the x-axis, and total activation intensity is indicated by shade, with white indicating highest activation and black indicating zero activation. **C**, Extended tuning curve used in the continuous wavelet transform. **D**, Three of the fifty ricker wavelets used in the continuous wavelet transform. To be specific, the blue wavelet has a width of 2*sd=5, the orange wavelet has a width of 2*sd=10, and the yellow wavelet has a width of 2*sd=15. **E**, The products of performing a wavelet transform using the extended tuning curve in C, and each of the three ricker wavelets in D.

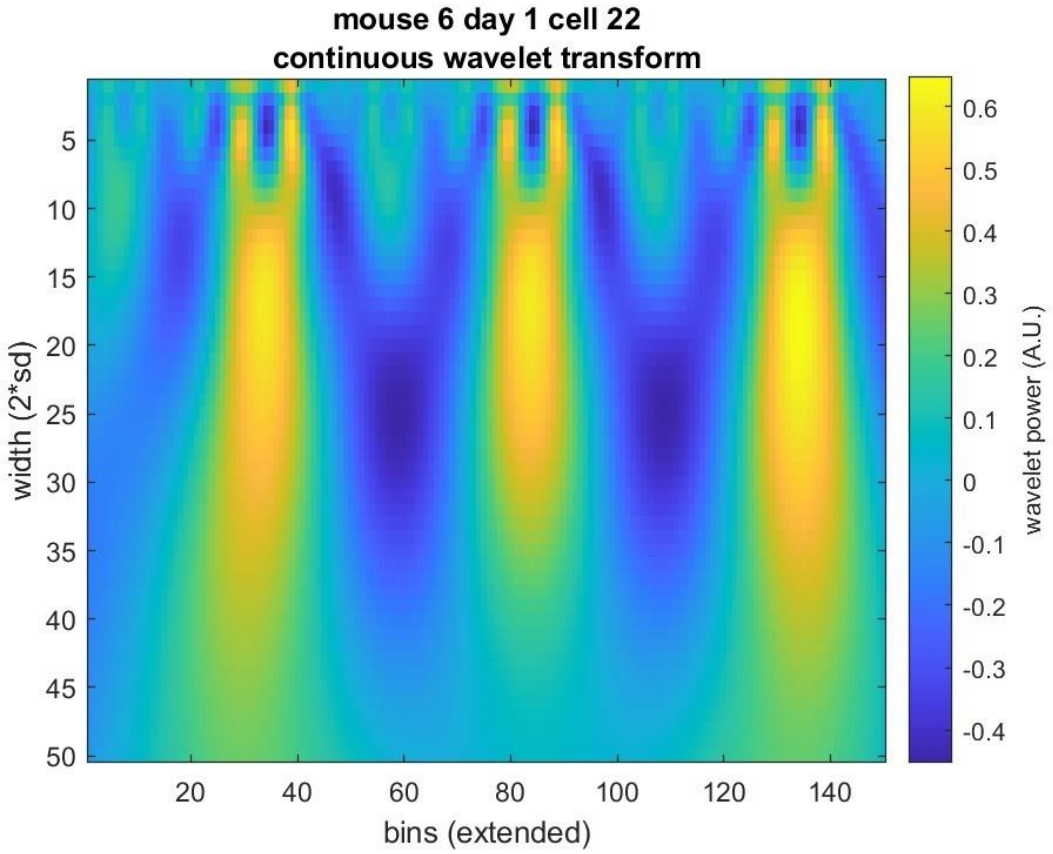

Figure 2.6: Uncropped results of a continuous wavelet transform using 50 different ricker wavelets and the extended tuning curve of a single place cell. The cell used for these figures cell 22 from mouse 6 on day 1.

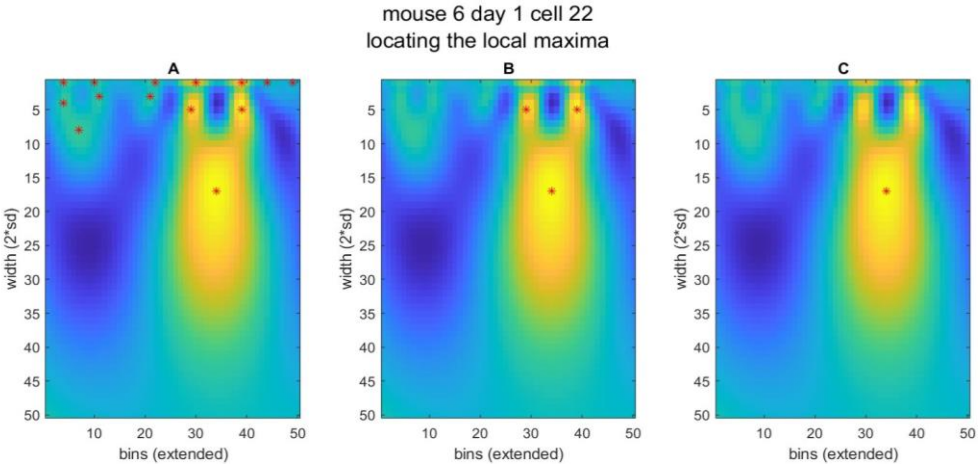

Figure 2.7: Process of identifying the correct place field using a single example place cell. The cell used for these figures cell 22 from mouse 6 on day 1. **A**, Identification of all local maxima in the continuous wavelet transform. **B**, Noise filtering. Exclusion of all local maxima that indicate a potential place field narrower than 5% or wider than 80% of the length of the treadmill. Additional local maxima were excluded for having less

wavelet power than the median plus mean absolute deviation of the wavelet transform made with the ricker wavelet of width 2*sd=1, i.e. the first row. **C**, Removal of all local maxima located within a wider potential place field.

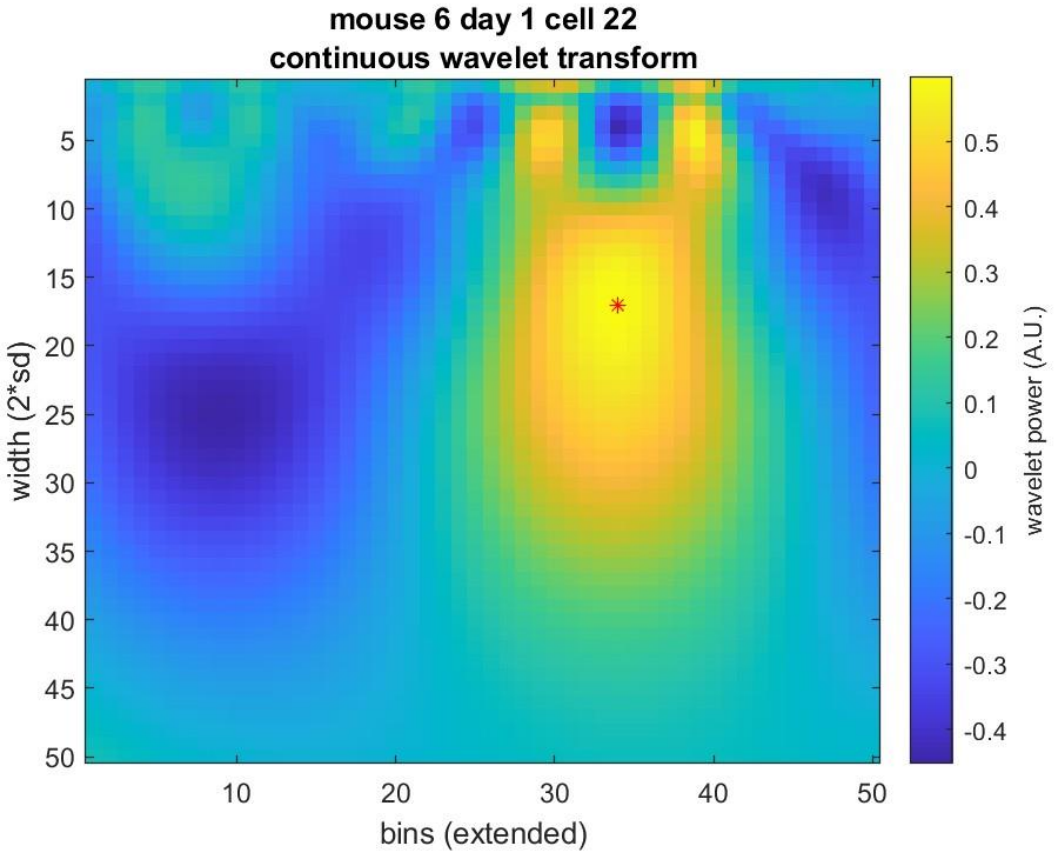

Figure 2.8: results of a continuous wavelet transform using 50 different ricker wavelets and the extended tuning curve of a single place cell. The cell used for these figures cell 22 from mouse 6 on day 1. This cell only has one potential place field, with it's location and width indicated by the x and y coordinates of the red asterisk. This potential place field, once identified, passed the reliability test resulting in this cell meeting the criteria of possessing at least one sufficiently coherent place field. Since it had previously passed the criteria of possessing a sufficient amount of spatial information, this cell was then identified as being a place field.

2.3.3. Firing consistency of place cells

The criteria used for identifying place cells are focused on spatial information and place field coherence. The requirements for place field reliability, in the sense of how consistently the place cells fire on each lap are minimal. A few tests were performed to assess this characteristic of the place cells observed in this experiment and their place fields.

It is common to describe the ideal place cell as firing every time the animal enters its place field and continuing to fire while the animal occupies that space, then going nearly or completely inactive when the animal is outside the place field. Although many of the place cells observed in this experiment matched that description, many others were entirely inactive on certain laps. Figure 2.9 shows that not all place cells have each lap's location of peak activation occur within its place field(s). The difference between figure 2.9A and 2.9B indicates that many of these missed laps are not due to spikes of activation outside the place field(s), but are rather due to silent laps, where the place cell does not fire at all throughout the entire lap. Figure 2.9 indicates that place cells are mostly, but not perfectly, consistent in having their peak activation for each lap fall within their place field(s).

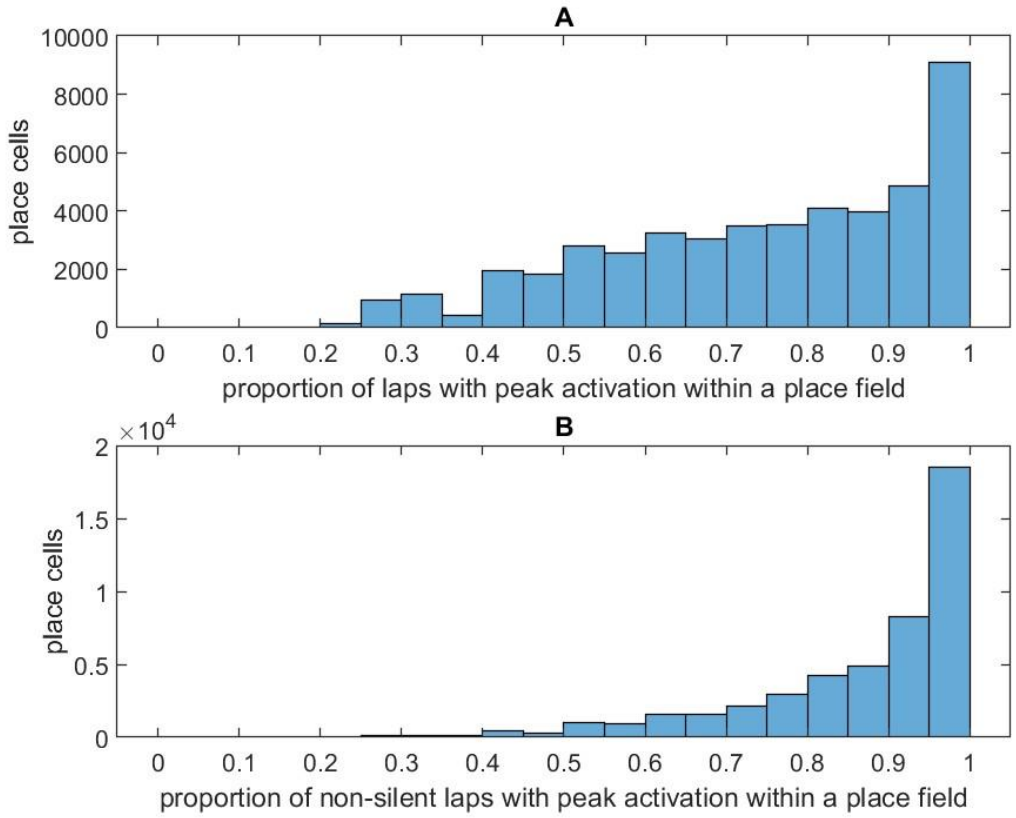

Figure 2.9: Consistency of peak activation of each lap occurring within place fields. Data for this figure was drawn from all place cells from all possible days from both cohorts (see appendix A) using the offset optimizer protocol (see section 3.2). **A**, Histogram of the proportion of laps in which the bin containing the greatest total activation is within a place field. The treadmill is divided into 50 bins each 3 cm long. For each cell identified as a place cell (see section 2.3.2) the bin with the greatest total activity is determined for each lap. The number of laps where the peak bin is within a place field is counted and then divided by the total number of laps, giving a single proportion value between 0 and 1 for each place cell. A proportion of 1 indicates that the place cell activated at least once during every lap, and that its bin of highest activation was

always inside its place field(s). **B**, Histogram of the proportion of non-silent laps in which the bin containing the greatest total activation is within a place field. This was calculated nearly the same way as A, except for dividing the count by the number of non-silent laps instead of the total number of laps. A non-silent lap is a lap in which the cell activated at least once.

Looking at each place field individually, figure 2.10A shows that most place cells at least occasionally fail to activate when the mouse passes through its place field. Figure 2.10B was made to assess whether place cells tend to increase or decrease in consistency over the course of an individual session. The slight positive skew (mean = 0.0744 and skew = 0.0922) suggests that it is a slightly more likely for a place cell to become more consistent over the course of a session than for it to become less consistent.

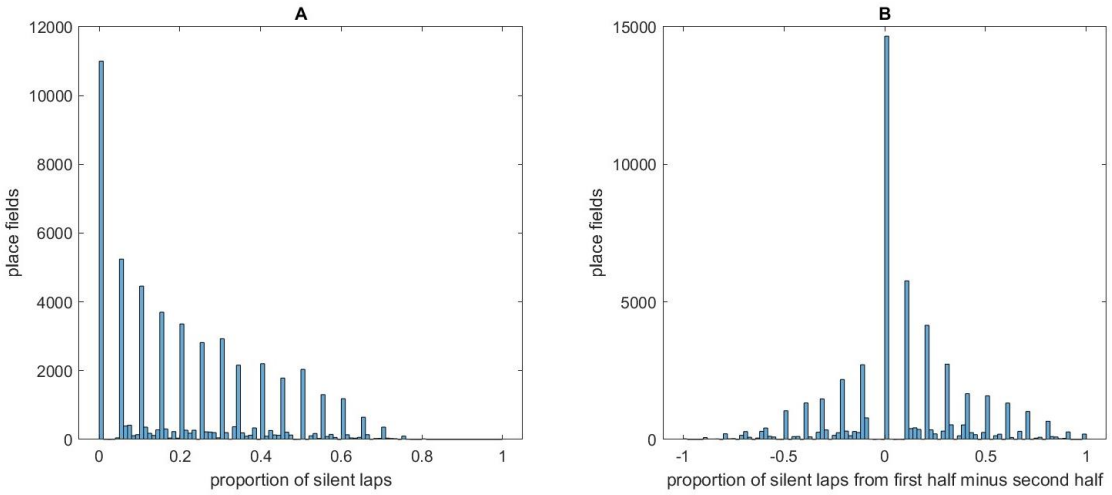

Figure 2.10: Place field activation consistency. Data for this figure was drawn from all place cells from all possible days from both cohorts (see appendix A) using the offset optimizer protocol (see section 3.2). **A**, Histogram of the proportion of laps in which a place cell fails to fire within its place field. For cells with more than one place field, a separate proportion value is calculated for each place field. For each place field the proportion was calculated by dividing the number of silent laps by the total number of laps, which for most mice on most days was 20. **B**, Comparison of place field activation consistency in the first and second half of each session. Each session was separated into two halves of an equal number of laps. For sessions with an odd number of laps the middle lap was disregarded. Each value in this histogram was obtained from a single place field. Each value was calculated by subtracting the proportion of silent laps in the second half of the session from the proportion of silent laps in the first half of the session. A value of -1 indicates that the place cell did not activate at all in the first half of the session, and then activated within the place field on every lap in the second half. A value of 1 indicates that the place cell activated within the place field on every lap in the first half of the session, and then did not activate at all in the second half.

One final test of place field reliability was done, which tested for drift within place fields over the course of a session. Although histograms of figure 2.11 have high kurtosis indicating that

most place fields do not appear to drift, there were nonetheless a small proportion of outliers with substantial drift.

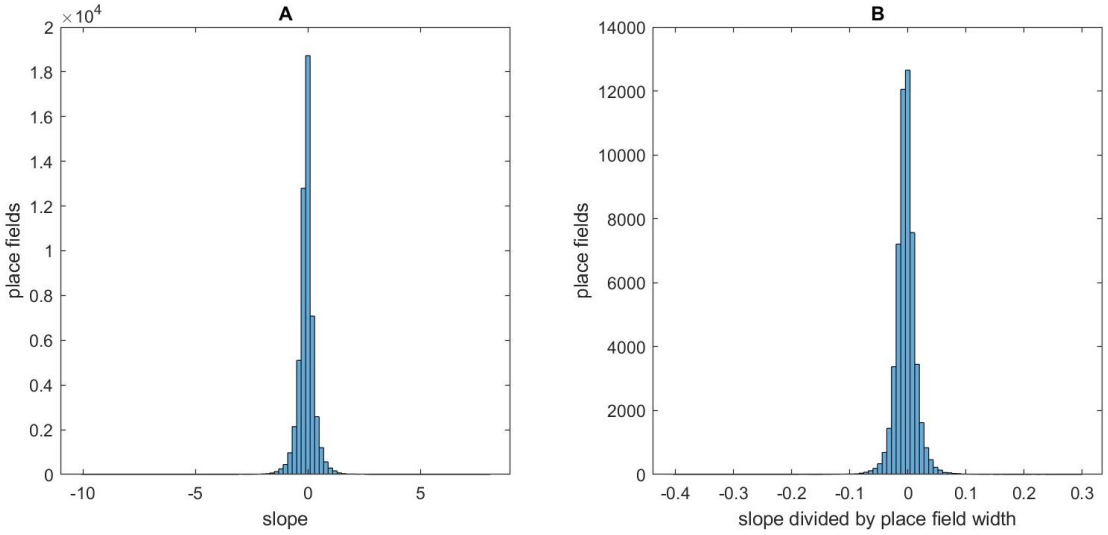

Figure 2.11: Degree of drift within each place field. Data for this figure was drawn from all place cells from all possible days from both cohorts (see appendix A) using the offset optimizer protocol (see section 3.2). **A**, Histogram of slopes of linear lines of best fit for the positions of mean activation on each lap within each place field. A separate value is calculated for each place field. To calculate each value, the activation data outside the place field was disregarded and for each lap the mean position of activation was calculated, with each bin being weighted according to its level of activation. Once each lap (other than silent laps) had a single position value, a line of best fit was found for the hypothetical scatter plot with lap number as the x-axis and mean position of activation as the y-axis. The linear line of fit was found using simple linear regression. A value of zero indicates that activation within the place field remained centered and constant throughout the session, with no drifting over time. **B**, Histogram of slopes of best fit divided by the width of the place field. To normalize for varying widths of place fields, this histogram was made with the same data as A, and merely has each value divided by the corresponding place field width.

2.4. Within-subject analysis

2.4.1. Registration between days and cell pair verification

To find the neurons whose activity was recorded on more than one day, the ROI masks of a pair of days were registered against one another using only rotation and translation. After two days were registered to one another (see figure 2.12A), all cross-day cell pairs with at least one pixel of mask overlap were added to a list, along with their Jaccard index, which is a measure of how overlapped they are. An example of the distribution of this list of Jaccard indexes from one pair of days is shown in figure 2.12B's top subfigure. All potential cell pairs where both cells were

more heavily overlapped with other cells were classified as non-nearest neighbours and were discarded. See figure 2.12B middle subfigure for an example of the distribution of the Jaccard indexes remaining after this step. The list of cell pairs was then sorted into two groups entitled cluster 1 and cluster 2 using k-means clustering on their Jaccard index values. The cluster 1 cell pairs had low Jaccard index values and were an approximate grouping of the cell pairs that were unlikely to be the same cell recorded from on both days. The cluster 2 cell pairs had comparatively high Jaccard index values and were an approximate grouping of the cell pairs that were likely to be the same cell recorded from on both days. See figure 2.12B bottom subfigure for an example of a single pair of days' remaining cell pairs after being sorted into cluster 1 and cluster 2.

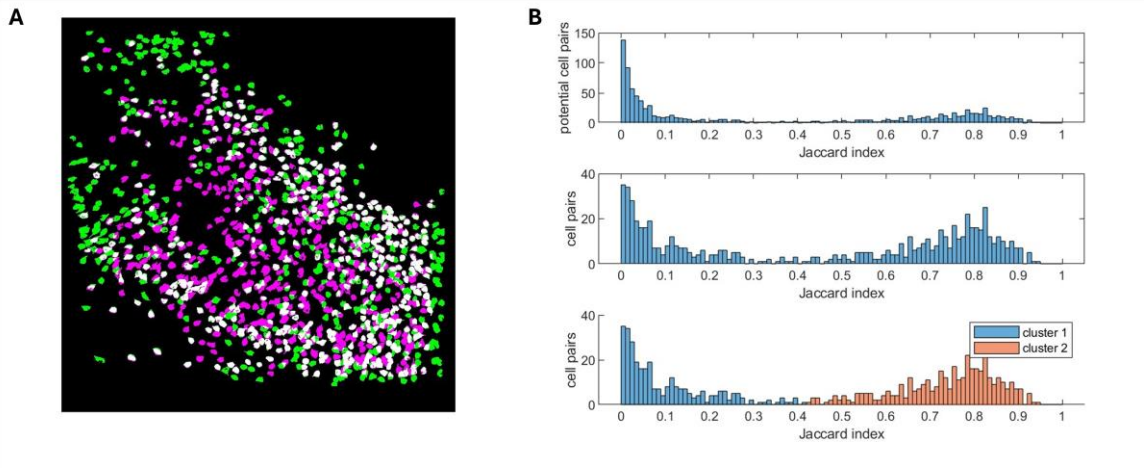

Figure 2.12: Process of converting ROIs from mouse 6 day 1 and day 2 into a list of cell pairs divided into two clusters based on Jaccard index. **A**: ROIs of mouse 6 day 1 in green and mouse 6 day 2 in magenta, with overlapping regions shown in white. Any day 1 ROI that at least partially overlaps with a day 2 ROI is regarded as a potential cell pair. **B**: Histograms of Jaccard index for three steps of analyzing cell pairs. Potential cell pairs (top) are narrowed down to only nearest neighbour cell pairs (middle), which are then sorted by k-means clustering. Cluster 1 shown in blue consists of slightly overlapped cell pairs, while cluster 2 shown in orange consists of relatively heavily overlapped cell pairs.

For each mouse, these cluster 1 and cluster 2 lists were calculated for every possible pair of the 13 imaging days, excluding comparisons of a day to itself, totaling 78 possible pairs of days. All 78 lists were combined, and the histogram of Jaccard index values was found to be bimodal in all mice. An example of the combined cluster 1 and cluster 2 histograms from all pairs of days from a single mouse is shown in figure 2.13A and 2.12C. Since k-means clustering is a rough approximation of the shape of the overlapping probability distributions of the two clusters, lines of best fit were made using beta distributions for each cluster using maximum likelihood estimation. An example of a single mouse's beta distributions is shown in figure 2.13B and 2.13C.

The Jaccard threshold for each mouse was set at the Jaccard index value higher than 99% of the area under the cluster 1 beta curve for that mouse.

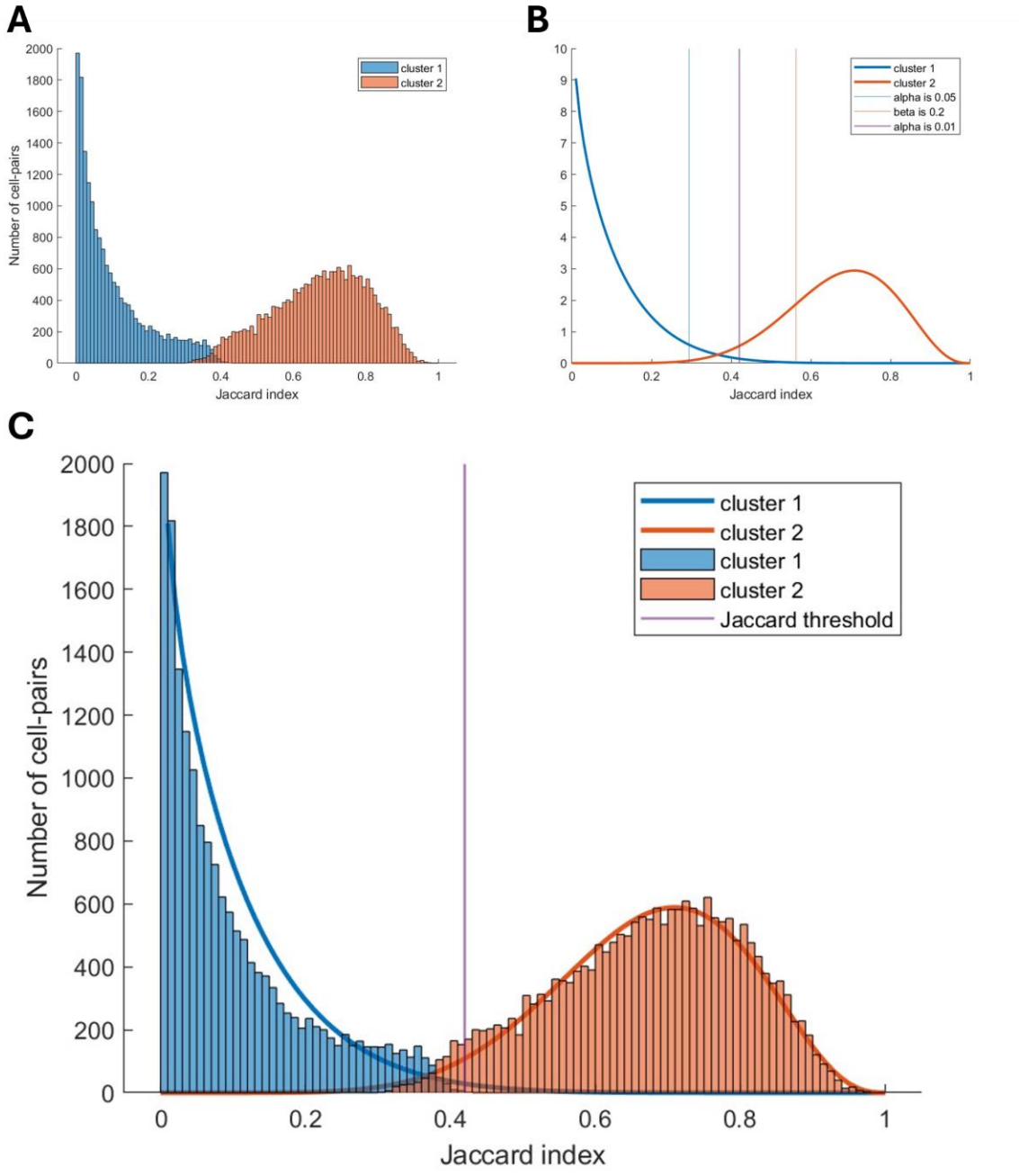

Figure 2.13: Process for determining a Jaccard threshold, using mouse 6 as an example. **A**: Histogram of overlap between cell pairs, measured in Jaccard index values, from mouse 6. Data for this histogram was drawn from comparisons of all possible pairs of days and does not include potential cell pairs designated as non-nearest neighbours. All cell pairs in this bimodal distribution have been sorted into two clusters by k-means clustering. Cluster 1 is an approximation of the group of cell pairs likely to be differing cells, whereas

cluster 2 is an approximation of the group of cell pairs likely to be persistent cells. **B**: Beta distributions fitted to the distributions of cluster 1 and cluster 2 by maximum likelihood estimation. Beta distributions are probability density functions with a range of 0 to 1, for which the area under the curve is equal to 1. The blue line labelled 'alpha is 0.05' in the legend indicates the threshold at which 95% of cluster 1 would be excluded, leaving a false positive rate of 5%. The orange line labelled 'beta is 0.2' in the legend indicates the threshold at which 20% of cluster 2 would be excluded, leaving a statistical power of 80%. The purple line indicates the selected Jaccard threshold for mouse 6 at which 99% of cluster 1 is excluded. **C**: An overlay of both clusters' histograms, beta distributions and the Jaccard threshold for which alpha is 0.01.

This method of using beta lines of fit mapped to distributions as a way to find optimal thresholds that fall within acceptable limits was drawn from (Sheintuch et al., 2017), who used centroid distance and spatial correlations as their measures of mask similarity. My use of Jaccard index was motivated by (H. Chang et al., 2023), which used a fixed Jaccard index threshold of 0.5 across all subjects.

2.4.2. Combinations of four filter options and centroid distance redundancy

When comparing two days within the same subject, correlations were calculated between the tuning curve of each cell on one day and the tuning curve of that same cell on the other day. Before this can be done, a level of specificity must be decided on regarding which cells are to be included in the analysis. Starting from a list of every possible pair of cells with one cell drawn from each of the two days being compared, the bare minimum level of strictness is the exclusion of non-nearest neighbors as described in section 2.4.1. However, additional filters were also used. One filter, referred to in figure 2.14 as 'above' removes all cell pairs with a Jaccard index below the Jaccard threshold (see 2.4.1) for that mouse. The purpose of the 'above' filter is to narrow down the list of cell pairs to only those pairs which are highly likely to be the same cell across two days. Another potential filter, referred to in figure 2.14 as 'pc' removes all cell pairs that were not classified as place cells (see 2.3.2) on either of the two days. An alternative to the 'pc' filter, referred to in figure 2.14 as 'strict' removes all cell pairs that were not classified as place cells (see 2.3.2) on both of the two days.

To check the reliability of the Jaccard index and Jaccard threshold as a measure of how likely a cell pair is to be the same cell, an alternative thresholding filter, referred to in figure 2.14 as 'cent', was made. It was expected to remove the same subset of cell pairs as the 'above' filter. This filter was made using the same procedure as described in 2.4.1 using centroid distance instead of Jaccard index. The distributions of cluster 1 and cluster 2 cell pairs from all 78 pairs of days were closer and more overlapped for centroid distances than for Jaccard index. As such setting a threshold that disposed of 99% of cluster 1 on the basis of centroid distance would have

in some mice simultaneously disposed of more than 20% of cluster 2. This was deemed an unacceptable loss of statistical power, so the centroid distance threshold was raised to the point that would dispose of 95% of cluster 1.

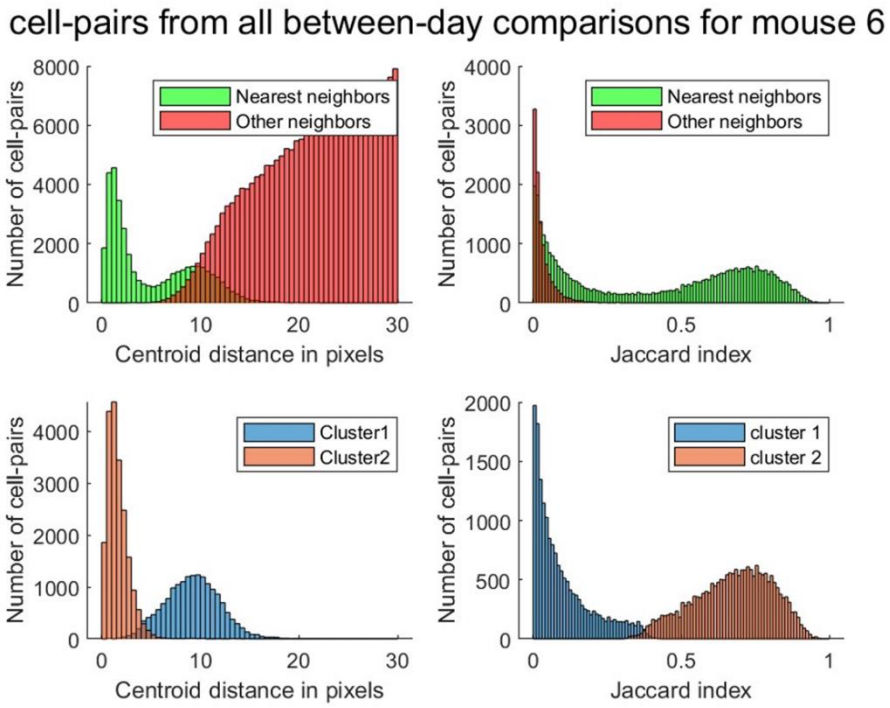

Figure 2.14: Example of distributions of all cell pairs from all 78 pairs of days for a single mouse on the basis of centroid distance (left two subfigures) and Jaccard index (right two subfigures) showing preliminary of excluded non-nearest neighbours (top two subfigures) and k-means clustering separated cluster 1 and cluster 2 (bottom two subfigures).

To test the effects of the various combinations of filters, The total number of cell pairs that met the criteria for each filter combination was plotted for a single example mouse (see figure 2.15). For mouse 6 it was found that the number of cell pairs permitted by ‘cent’ without ‘above’ was between 5 and 6% larger than the number permitted by ‘above’ without ‘cent’. This indicates that as expected, the centroid distance threshold of 95% of cluster 1 is less restrictive than the Jaccard threshold of 99% of cluster 1. The number of cell pairs permitted by ‘above’ is approximately 1% larger than the number of cell pairs permitted by both ‘cent’ and ‘above’ which indicates the existence of a small number of outlier cell pairs with high enough Jaccard index to pass the ‘above’ filter and enough centroid distance to fail to pass the ‘cent’ filter.

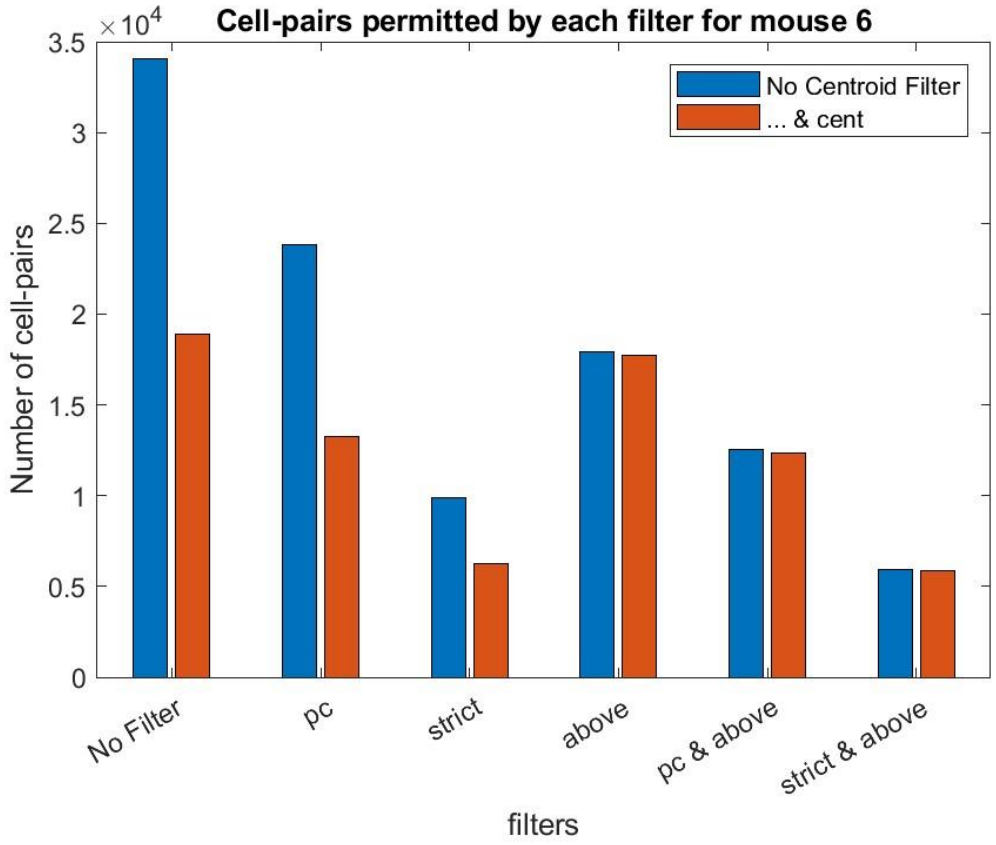

Figure 2.15: Total numbers of cell pairs from mouse 6, from all 78 possible combinations of days that meet the criteria of various combinations of filters.

The relative strictness of combinations of filters is visually depicted in figure 2.15 and quantified in table 2.3. The purpose of showing this data is to demonstrate the importance of using either 'above' or 'cent' and to compare their relative strictness.

Table 2.3: Total numbers of cell pairs from mouse 6, from all 78 possible combinations of days that meet the criteria of various combinations of filters, and the proportion of these counts relative to the baseline count prior to filtering.

	Number of cell pairs	Proportion to baseline
No Filter	34050	1.0000
'cent'	18902	0.5551
'above'	17894	0.5255
'above' and 'cent'	17704	0.5199
'cent' and 'pc'	13246	0.3890
'above' and 'pc'	12510	0.3674
'above', 'cent', and 'pc'	12375	0.3634
'cent' and 'strict'	6225	0.1828
'above' and 'strict'	5904	0.1734
'above', 'cent' and 'strict'	5847	0.1717

This comparison of the Jaccard threshold filter ‘above’ to the centroid distance threshold filter ‘cent’ indicates that the two filter options are similar in outcome and that applying both is mostly but not entirely redundant. It also indicates that the ‘above filter’ based on Jaccard index (H. Chang et al., 2023) can have use a stricter threshold without as much loss of statistical power compared to the ‘cent’ filter based more closely on the methodology of Sheintuch et al. (2017). For these reasons, ‘above’ was used and ‘cent’ was not used in later analyses.

An additional test of these filter options was made to search for what will be referred to as AJAK problems. An AJAK problem is when the list of cell pairs includes two different cell pairs that share a cell. In other words, when day 1 and day 2 are compared, if Cell A from day 1 is partially overlapping with both Cell J and Cell K from day 2, then the place cell list might contain two different cell pairs, AJ and AK which both involve Cell A, despite it being impossible for Cell A to be Cell J and Cell K at the same time. Whether a filter removes all AJAK problems is thus a simple test of whether it is completely removing all secondary cell pairs from the cell pair list even without being coded to do that directly. A search for AJAK problems in mouse 6 for six filter combinations not including ‘cent’ was performed. The results of this search for six combinations of filters is shown in the six subfigures of figure 2.16. Each subfigure shows the total number of AJAK problems found in the comparison of each pair of days, with number of AJAK problems indicated by color and days indicated by the x and y axes.

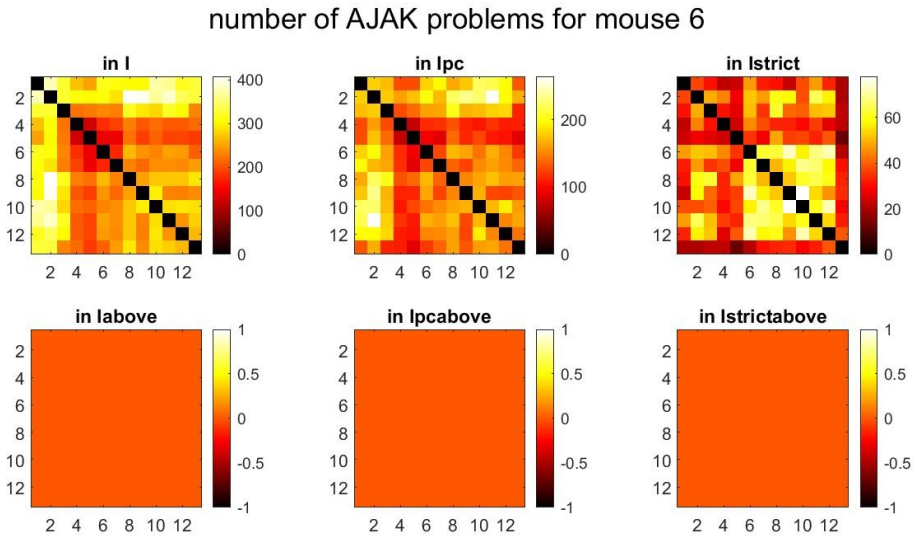

Figure 2.16: Search for AJAK problems in one subject across the six combinations of filters that do not include the ‘cent’ filter.

Figures 2.16 and 2.15 indicate that the ‘above’ filter which uses a the Jaccard index threshold to remove 99% of cluster 1, is reliable in identifying the cell pairs which are in reality the

same cell being recorded from across days. The ‘above’ filter does nothing to identify which of these cells are place cells. For that, the ‘strict’ filter would be ideal, as it only accepts cell pairs that meet the place cell criteria described in 2.3.2 on both days. However, combined use of both ‘above’ and ‘strict’ results was found to be excessively restrictive for some pairs of days with some mice, yielding uselessly small cell pair lists, which would undermine the statistical power of any analysis being done on them. As such, the combination of the ‘above’ filter with the ‘pc’ filter was chosen for subsequent analysis. The ‘pc’ filter requires that a cell meet the 2.3.2 place cell criteria on at least one of the two days being compared. The cell pairs that meet these two filters are hereafter referred to as ‘pcabove’ cell pairs. This approach of accepting cell pairs which only register as place cells on one of the two days has been used in prior studies (Geva et al., 2023; Khatib et al., 2023).

2.4.3. Mean of tuning curve correlations as a measure of representational drift

To quantify the representational drift in a mouse’s place cell activity between two days, Pearson’s correlation values were calculated between the tuning curves of ‘pcabove’ cell pairs. The list of ‘pcabove’ cell pairs for a given pair of days represents the subset of neurons that were successfully imaged on both days, and that were identified as behaving recognizably like a place cell on at least one of those days. To measure the reliability of the tuning curves of these cells, Pearson’s correlation values were calculated comparing the tuning curve of each ‘pcabove’ cell from one day with the tuning curve of each ‘pcabove’ cell from the other day. This produces a grid of correlation values for which each value along the diagonal represents the correlation of the two tuning curves of a single cell pair, while each value outside the diagonal represents the correlation of tuning curves from differing cells on differing days.

For each mouse, this grid of correlation values was calculated for every possible pair of days, and for each combination of filters presented in figure 2.15, although only the correlation values calculated using the ‘pcabove’ filter condition was used in further analysis. As an example of this complete set of correlation grids from a single subject, mouse 6 ‘pcabove’ correlations grid is displayed in figure 2.17. Note that in figure 2.17, the subfigures comparing a day to itself have the most vibrant internal diagonals because each data point along the diagonal would be at the maximum Pearson’s correlation of 1. Also note that the total absence of a visible diagonal in a subfield indicates substantial differences in the tuning curves of those cells between those days.

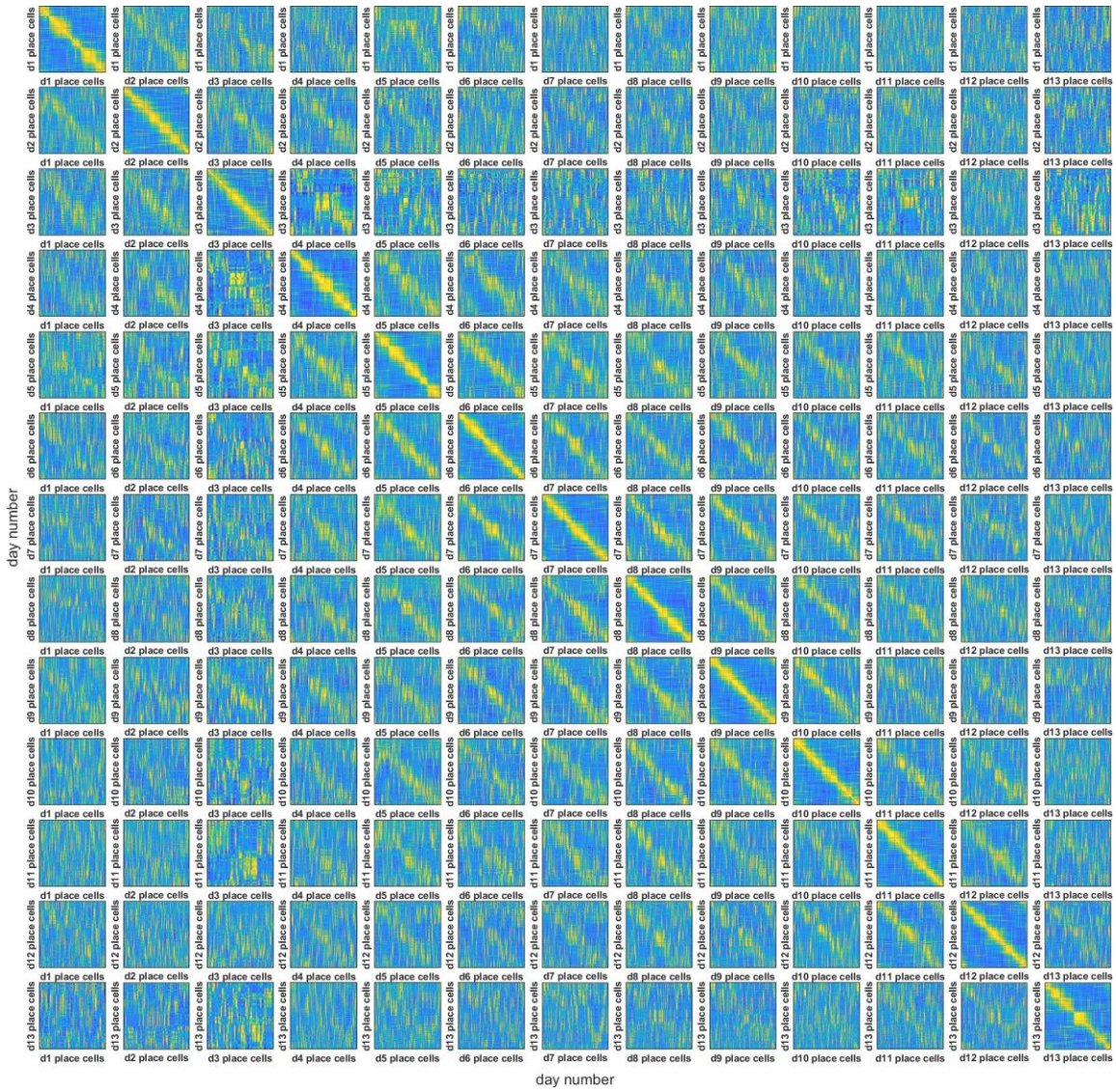

Figure 2.17: All correlation values obtained from mouse 6 using 'pcabove' filter protocol. Each subfigure represents the comparison of two days, with each data point representing the Pearson's correlation between the tuning curves of two cells from differing days, arranged in order such that the data points along the top-left to bottom-right diagonal of each subfigure represents the comparison of a cell to itself between days. High correlation values are indicated by yellow, low correlation values are indicated by blue.

To simplify and narrow the focus, figure 2.18 displays only the mean of the correlation values comparing each cell to its pair (presumably itself) across days, which is represented in figure 2.17 as the values along the diagonal of each subfigure.

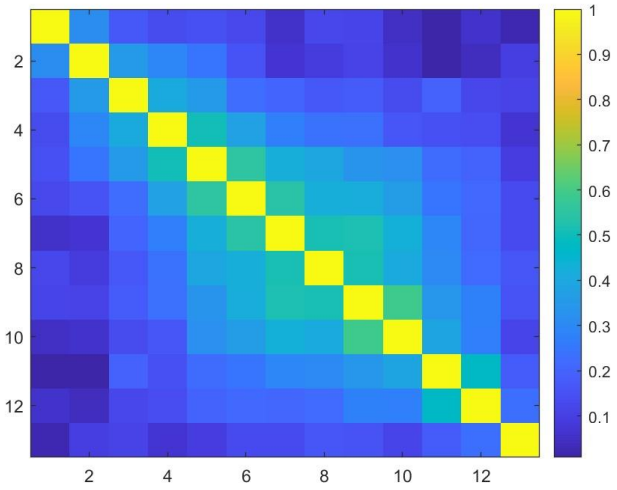

Figure 2.18: Mean of Pearson's correlations of each cell's tuning curves between a pair of days. The pair of days is indicated by x and y coordinates. Mean of the correlations from each pair of days is indicated by color with high mean correlations indicated by yellow and low mean correlations indicated by blue. Data is obtained from mouse 6 using 'pcabove' filter protocol. Note that day 11 occurred 7 days after day 10, day 12 occurred 1 day after day 11, and day 13 occurred 15 days after day 12.

2.4.4. Visual assessment of an individual place cell across days

After obtaining cell pair lists for all possible pairs of days for a mouse, it becomes possible to check for irregularities in the activity of a single cell across multiple days. Using mouse 6 as an example, figure 2.19 demonstrates that not many recorded cells are found in all 13 recording sessions.

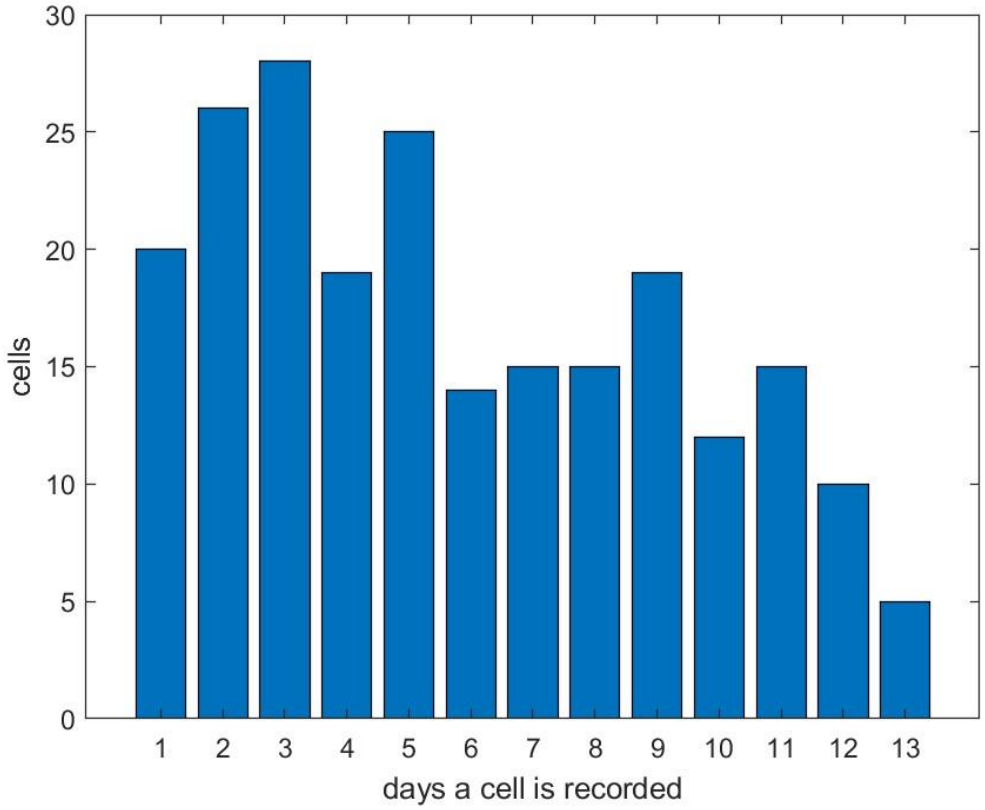

Figure 2.19: Number of days on which each of the cells initially observed in mouse 6 on day 1 were imaged.

To help clarify what the data processing steps in the preceding sections do, a single cell from mouse 6 will be used as an example in the following figures. The cell chosen for this purpose was one of the five cells from mouse 6 that were successfully imaged on all 13 sessions.

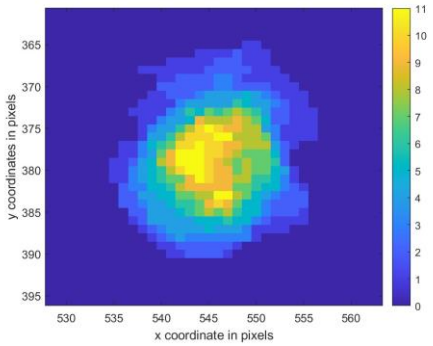

Figure 2.20: Overlayed ROI masks of a single example cell from mouse 6. Yellow indicates areas overlapped by multiple days.

Looking at figure 2.20 one may notice that this neuron does not appear in precisely the same location each day. This causes there to be substantial variation in the Jaccard index of this neuron depending on which pair of days is being compared, as shown in figure 2.21.

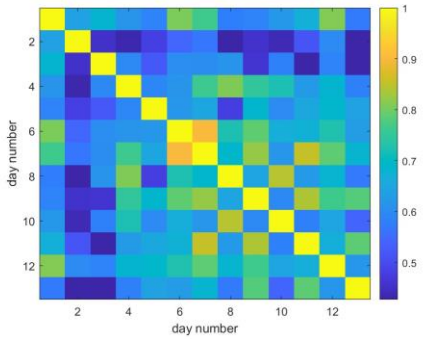

Figure 2.21: Jaccard index of each pair of days' ROI masks for a single example cell from mouse 6. Yellow indicates higher degrees of overlap between the ROIs.

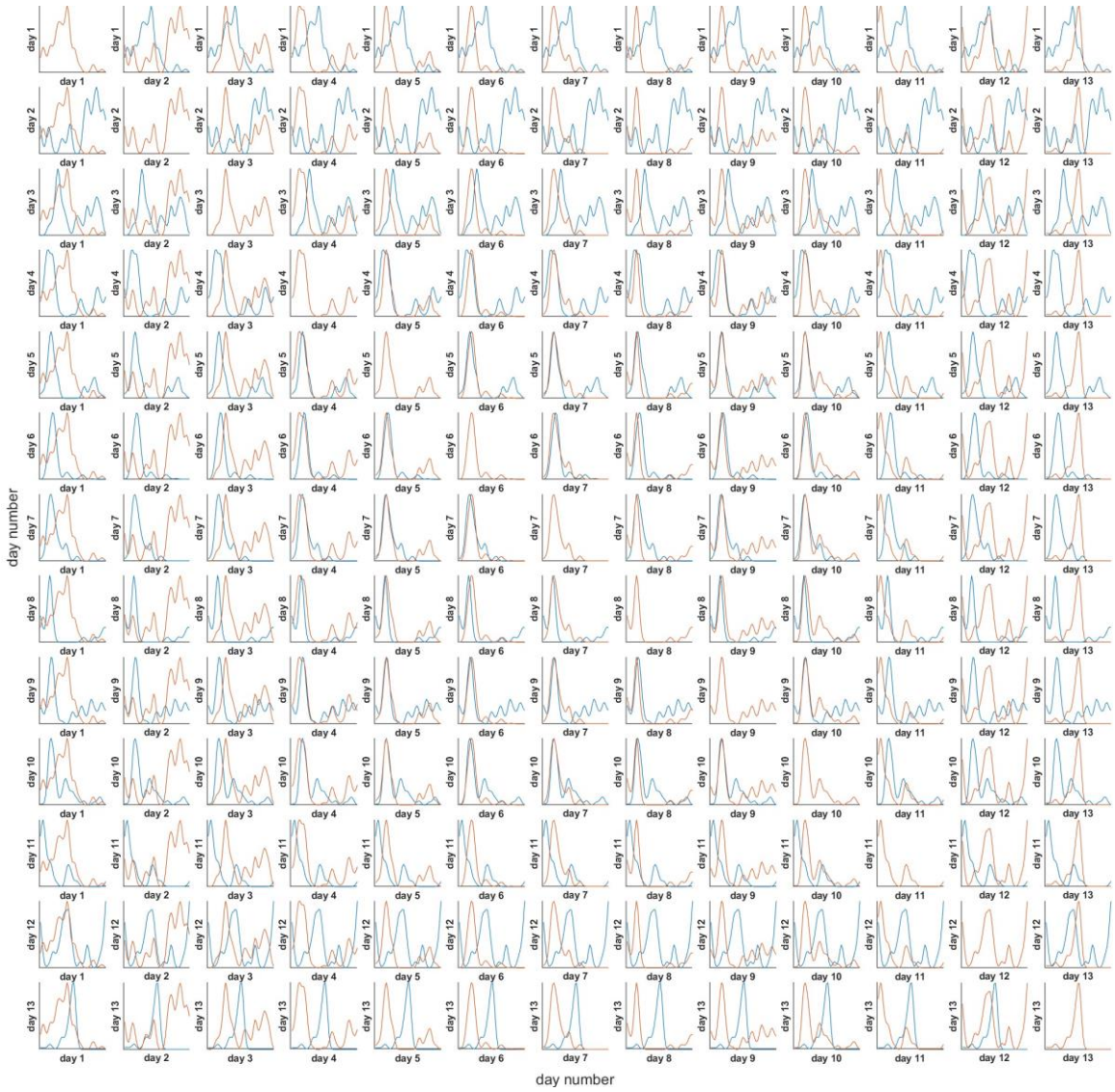

Figure 2.22: Every tuning curve from the example cell from mouse 6. Each subfigure displays tuning curve of two days.

Pearson's correlation coefficient between each pair of the thirteen tuning curves found for this example cell are shown in figure 2.23 using the x and y axis to indicate the pair of days. The actual tuning curves themselves are shown in figure 2.22. It is visibly apparent in both figures that the place field of this place cell remapped considerably across the first four imaging days before holding still between day 4 and day 10, and then remapping again during the three retention tests.

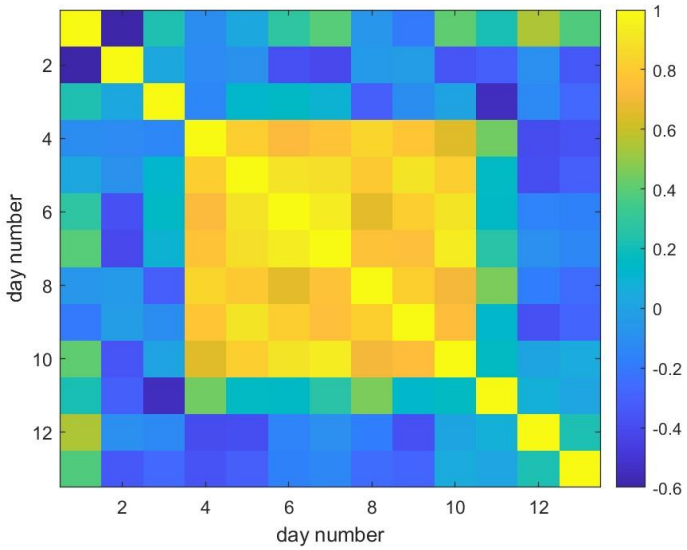

Figure 2.23: Pearson's correlation of the mouse 6 example cell's tuning curves from each pair of days. Note that day 11 occurred 7 days after day 10, day 12 occurred 1 day after day 11, and day 13 occurred 15 days after day 12.

Chapter 3.

Results

3.1. Cohort 1 results obtained with true offsets

To assess representational drift in the observed population of CA1 cells of a single mouse, comparisons between the spatial tuning curves of day 10 are made with the tuning curves of every other day. The degree to which tuning curves differ between days indicates the relative stability of the hippocampus-based spatial memory of the treadmill.

When the means of tuning curve correlations are calculated for each pair of days for a single mouse, the method for doing so follows the method described in 2.4.3, and in particular the method for the creation of figure 2.18. It is worth noting here that when comparing a mouse's tuning curves of day 10 to another day, the only cells considered were those from cells that were identified on both day 10 and the other day in question. Since not all place cells were identified in Suite2p every session, each comparison of day 10 to another day uses a different subset of the cells recorded on day 10. As such there is considerable variation in the number of cell pairs available for analysis between pairs of days.

Most pairs of days for each mouse are disregarded in the creation of figure 3.1, to focus only on the pairs that include day 10. When the mean of tuning curve correlations for these pairs of days is plotted for each mouse in cohort 1, they show the expected increase in correlation to day 10 throughout days 1 to 9. The three retention tests (plotted as days 11 to 13) tend to show correlation values between what was found on day 1 and day 9, as expected.

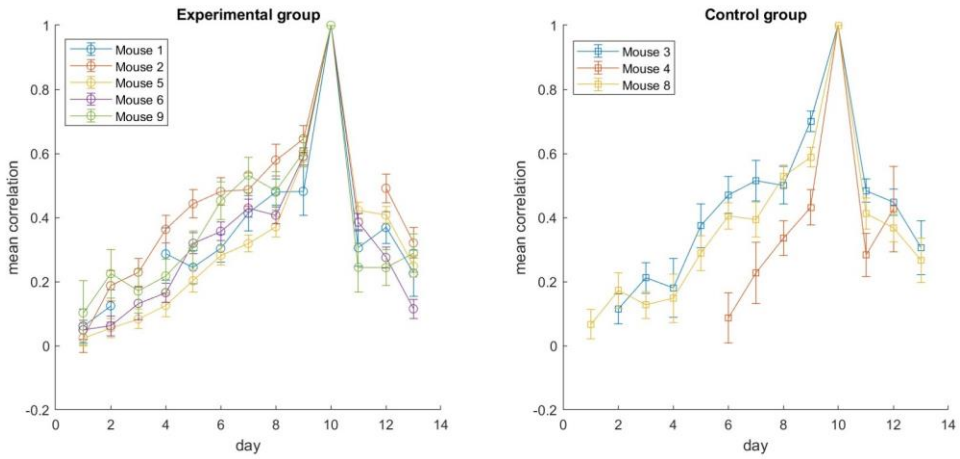

Figure 3.1: Cohort 1 comparisons of the place maps of all days to day 10 using true offsets, with each mouse plotted separately. The only Pearson's correlation values used to calculate the displayed means and standard errors were from 'pcabove' cell pairs, from pairs of days that included day 10.

When averaging these figure 3.1 results within each group to create figure 3.2, the means and standard errors are calculated from the set of means of each pair of days. This has a few consequences. Firstly, each mouse is weighted equally, regardless of how many cell pairs worth of tuning curve correlation data points went into the identification of each mouse's mean correlation for that pair of days. In other words, because each mouse is weighted equally and different mice have different numbers of cell pairs, the data points from individual cell pairs are not weighted equally. Secondly because of the gaps in some mice's data, the number of mice contributing to each data point in figure 3.2 varies between pairs of days. For example, in considering the control group in figure 3.1 it becomes apparent that the comparison of day 1 to day 10 only has data from one mouse, namely mouse 8.

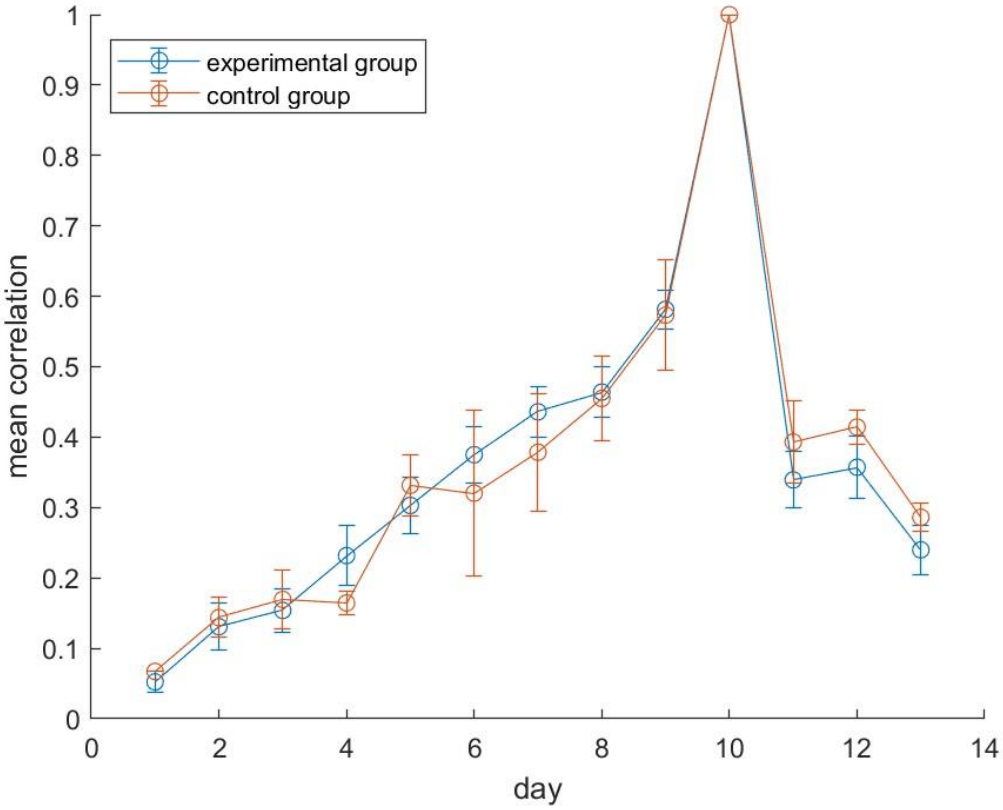

Figure 3.2: Cohort 1 between-group comparison of the place maps of all days to day 10 using true offsets. The mean of each mouse's tuning curve correlations for each pair of days were calculated independently. The mean and standard error of those means within each group are shown. The only Pearson's correlation values used were from 'pcabove' cell pairs, from pairs of days that included day 10. Due to unusable sessions, the number of subjects contributing to each data point varies between pairs of days.

As shown in figure 3.2, when using purely the data from cohort 1, the experimental group has little if any variation from the control group in the stability of their CA1 tuning curves across sessions. For the sake of thoroughness, Welch's two-sample t-test was performed for each pair of days comparing the experimental group to the control group. Welch's t-test was chosen because the two groups being compared are independent samples with differing sample sizes. The data sets compared by the t-test contained one data point from each mouse, namely the mean of each mouse's tuning curve correlations from the pair of days in question. Since some mice had days with unusable data, the number of mice contributing data to these tests varied from one pair of days to another. The number of mice considered in each t-test as well as the p-value of those t-tests are listed in table 3.1. The null hypothesis being tested is that the experimental group values and the control group values come from populations that share the same mean. A 5% significance level was used, meaning that the null hypothesis would be rejected for any pair of days in which the p-value was calculated as being below 0.05. As shown

in table 3.1, this did not happen on any pair of days. As such the null hypothesis is not rejected for cohort 1.

Table 3.1: Results of Welch's two-sample t-tests between the experimental group and the control group of cohort 1 for each day compared to day 10. Due to some mice having some days with unusable data, the number of mice contributing data to each analysis varies between pairs of days. Significance threshold of $p < 0.05$ is used.

	Experimental mice (n)	Control mice (n)	p-value	t-value
Day 1	5	1	NaN	-1.0206
Day 2	5	2	0.7828	-0.2955
Day 3	4	2	0.7915	-0.2990
Day 4	5	2	0.2006	1.4801
Day 5	5	2	0.6634	-0.4810
Day 6	5	3	0.6972	0.4375
Day 7	5	3	0.5758	0.6316
Day 8	5	3	0.9047	0.1287
Day 9	5	3	0.9283	0.0993
Day 11	4	3	0.4933	-0.7580
Day 12	5	3	0.3075	-1.1207
Day 13	5	2	0.3013	-1.1532

Because of the low number of mice in cohort 1, made worse by the loss of mouse 7 from the control group, the statistical power of these tests was problematically low. For this reason, as second cohort was run.

3.2. Offset optimizer

3.2.1. The problem with cohort 2

A problem was found in the data of all cohort 2 sessions, which prevented the normal method of accurately synchronizing the microscope data with the position and velocity data. The AxoScope software (Molecular Devices) records the time of each frame recorded by the 2-photon microscope, as well as the time of each event recorded by the computer that monitors the treadmill's position over time through the optical encoder and photoelectric sensor. This software is critical for identifying the framerates and start times of both systems which are necessary for synchronizing the two sources of data. Without proper synchronization of position data and cellular firing rate data, there would be inaccuracies in the shape and relative position of all tuning

curves. For reasons that remain unclear, the offset in start times for these two data sources erroneously appears to be zero seconds for all cohort 2 recording sessions. Using an offset of zero yielded obviously incorrect output data from cohort 2, and so attempts were made to find the correct offset values of each recording session without using the AxoScope files. Two potential methods were devised, and their accuracy was tested using cohort 1 data. The method that produced estimated offsets of cohort 1 sessions closest to those sessions' real offsets was used on both cohort 1 and 2.

3.2.2. Two potential solutions and their relative merits

The two potential solutions used different methods of obtaining an estimate of a recording session's offset in start times.

The first potential method used a custom-made optimizer code to find the offset value that would result in the highest possible correlation between the velocity over time and the total neural activity over time for that session. Total neural activity over time was calculated as the sum of the smoothed (kernel standard deviation of 8) and normalized deconvolved firing activity of all cells identified in Suite-2p. This method operates on the assumption that increases in total neural activity in the CA1 region are synchronized with the timing of voluntary movement. An example of the reason this assumption was made can be found in figure 3.3, which shows a visually apparent similarity between the timings of bursts of speed and bursts of CA1 neural activity.

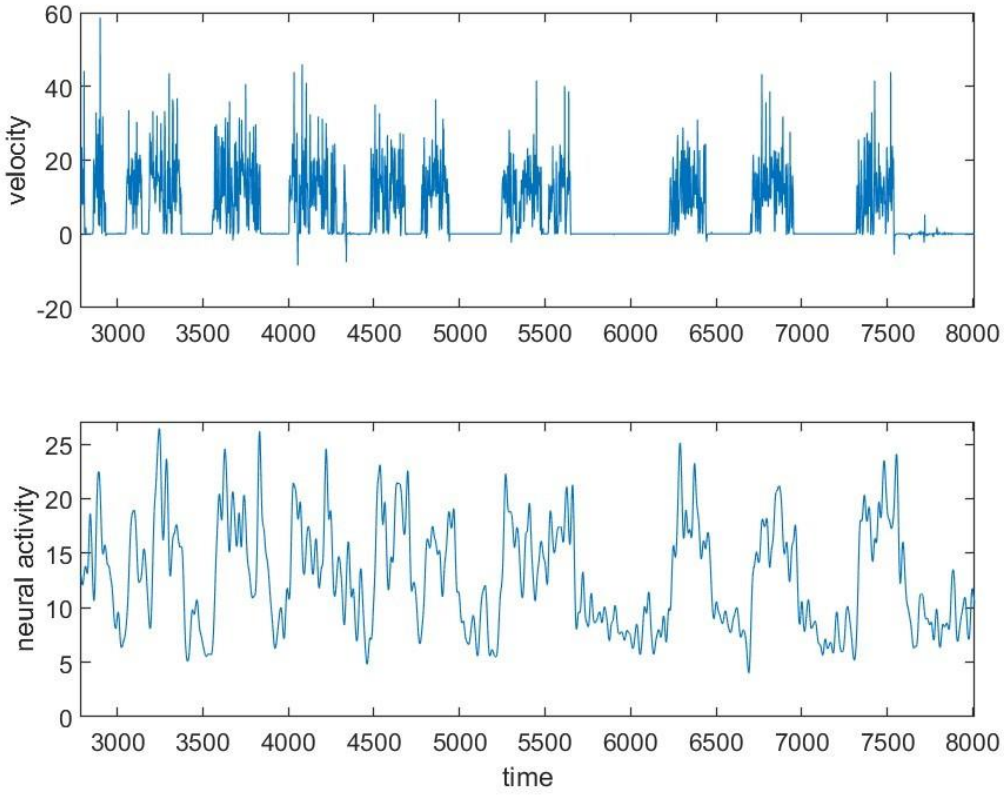

Figure 3.3: A portion of mouse 6, day 1 comparing velocity over time to neural activity over time. Time is measured here in microscope frames (19.2 fps).

The second potential method comes from the observation that the raw data files to be synchronized contain timestamps that are accurate to the second. Using the difference in whole seconds between the timestamps as the offset value is intuitive, but seeing as the microscope operates at 19.2 frames per second, this is problematically imprecise from the onset.

For each session in cohort 1, the true offset was subtracted from the optimized offset, and also from the timestamp offset, to measure how inaccurate these estimates are. These measurements of offset error were then plotted on the following histogram (figure 3.4). The mean error of the optimizer method is 0.8442 seconds with a standard deviation of 0.3013 seconds. The mean error of the timestamp method is 3.5107 seconds with a standard deviation of 1.1043 seconds. In this context, mean error is a measure of inaccuracy and standard deviation is a measure of imprecision. It is presumed that the degree of accuracy and precision of the optimizer method as well as the precision of the timestamp method will be the same in cohort 2 as they were in cohort 1. If neither computer's internal clocks drifted or were adjusted between cohort 1 and 2, then the same could be said of the accuracy of the timestamp method. Since the optimizer

method was more accurate and more precise, it was used on both cohorts instead of the timestamp method.

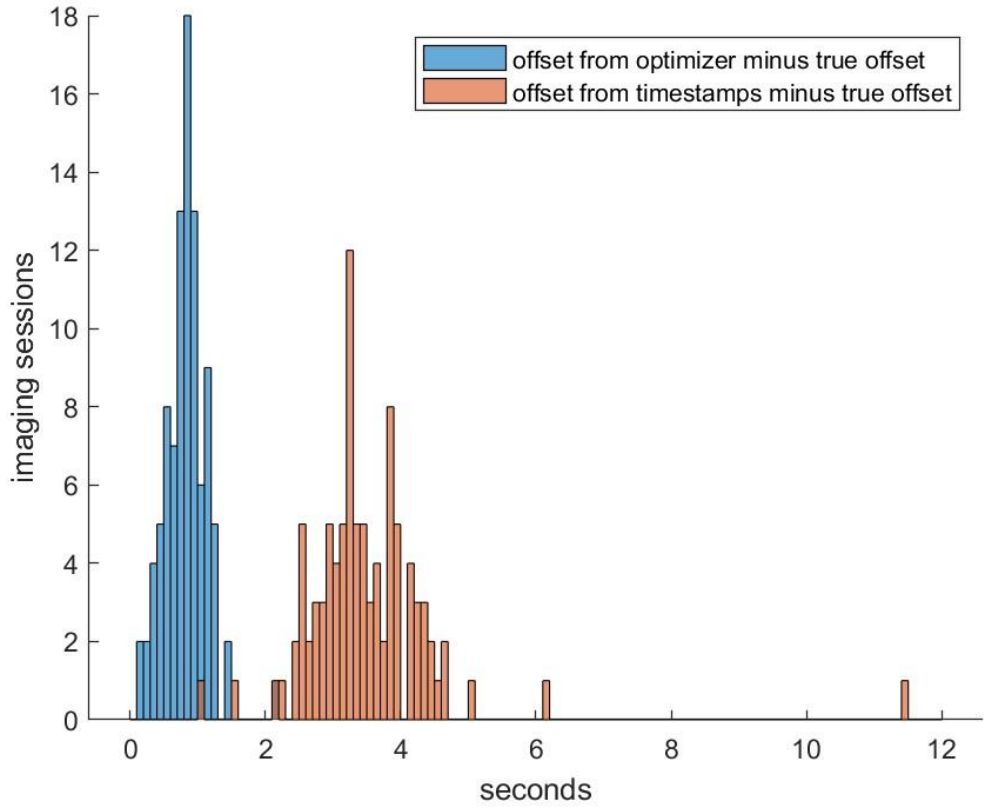

Figure 3.4: Accuracy and precision of the two offset estimator methods when tested on cohort 1. 'Offset' refers to the difference in start times of the recordings of the 2-photon microscope and the Matlab program monitoring the treadmill. Each value contributing to this histogram is an estimated offset for a cohort 1 recording session, subtracted by the true offset for that session obtained from the AxoScope recording of that session.

3.2.3. Cohort 1 results obtained with the offset optimizer

Before using the offset optimizer on cohort 2, it is first applied to cohort 1 so that comparisons can be made between the ultimate results it produces can be compared to the cohort 1 results already obtained using the true offsets (see 3.2).

When the data of cohort 1 is processed using estimated offset values obtained from the optimizer function instead of the accurate offset values obtained from AxoScope, the data processing pipeline functions normally on all subsequent steps. After calculating the mean of tuning curve correlations to day 10 for each mouse, the results as shown in figure 3.5 appear

roughly similar to the results of figure 3.1 which were made with the true offsets. The mouse with the most noticeable deviation from expected pattern is mouse 1, though it is not yet known why this occurred.

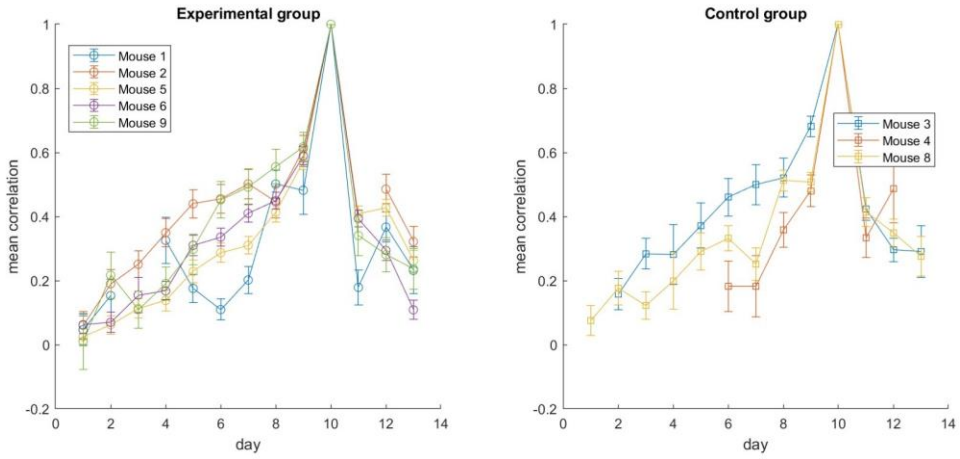

Figure 3.5: Cohort 1 comparisons of the place maps of all days to day 10 using optimized offsets, with each mouse plotted separately. The only Pearson's correlation values used to calculate the displayed means and standard errors were from 'pcabove' cell pairs, from pairs of days that included day 10.

The means and standard errors of each group shown in figure 3.6 were calculated from the means of each mouse's tuning curve correlations, as shown in figure 3.5.

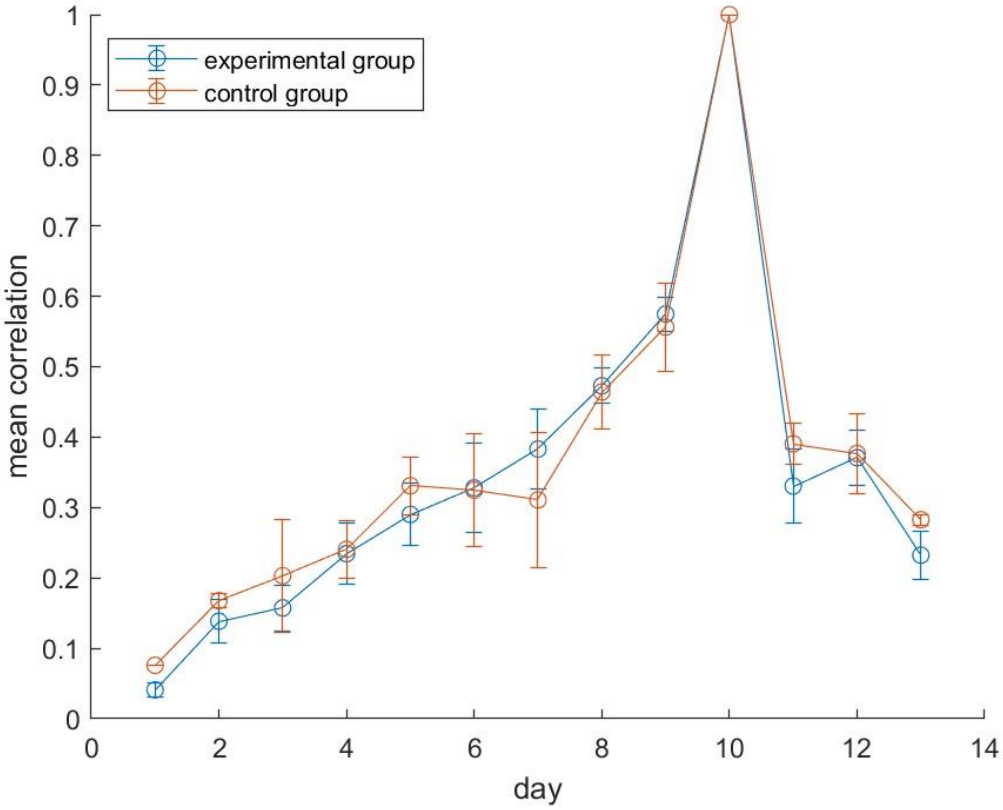

Figure 3.6: Cohort 1 between-group comparison of the place maps of all days to day 10 using optimized offsets. The mean of each mouse's tuning curve correlations for each pair of days were calculated independently. The mean and standard error of those means within each group are shown. The only Pearson's correlation values used were from 'pcabove' cell pairs, from pairs of days that included day 10. Due to unusable sessions, the number of subjects contributing to each data point varies between pairs of days.

3.2.4. Comparison of cohort 1 offset methods

To assess the reliability of the optimizer offset method, the results it gave for cohort 1 are compared to the cohort 1 results obtained using the true offsets. This will inform the interpretation of the cohort 2 results for which there are only optimized offsets and no true offsets.

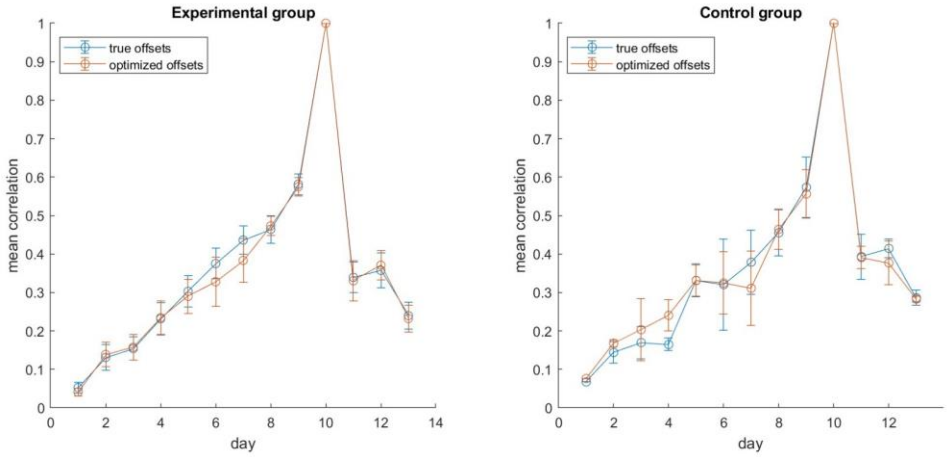

Figure 3.7: Effects of using optimized offsets instead of true offsets in cohort 1. This displays the same data as figure 3.2 which was made using true offsets, and figure 3.6 which was made using estimated offsets obtained using the optimizer method.

Welch's t-test was used to verify that there are no significant differences between the means of the populations of tuning curve correlation values obtained by these two offset methods in cohort 1. Since each t-test looks at a particular pair of days and is either comparing the experimental group to the experimental group, or the control group to the control group, the number of mice in both compared samples is always equal. The number of mice considered in each t-test and the p-values obtained from those t-tests are shown in table 3.2.

Table 3.2: Results of Welch's two-sample t-tests between the true offset results and the optimized offset results for both groups of cohort 1 for each day compared to day 10. Due to each t-test being performed between data sets calculated with from the same raw data, the number of mice contributing to both samples is always equal within a t-test, so only one n-value is listed for each t-test. Due to some mice having some days with unusable data, the number of mice contributing data to each analysis varies between pairs of days. Significance threshold of $p < 0.05$ is used.

	Experimental Group			Control group		
	n (# of mice)	p-value	t-value	n (# of mice)	p-value	t-value
Day 1	5	0.5447	0.6357	1	0	-∞
Day 2	5	0.8694	-0.1698	2	0.5500	-0.7996
Day 3	4	0.9405	-0.0778	2	0.7574	-0.3687
Day 4	5	0.9649	-0.0454	2	0.2845	-1.7360
Day 5	5	0.8374	0.2120	2	0.9936	0.0090
Day 6	5	0.5490	0.6309	3	0.9782	-0.0294
Day 7	5	0.4593	0.7844	3	0.6243	0.5307
Day 8	5	0.8438	-0.2043	3	0.9148	-0.1141

Day 9	5	0.8605	0.1816	3	0.8736	0.1700
Day 11	4	0.8998	0.1317	3	0.9721	0.0381
Day 12	5	0.8261	-0.2272	3	0.5900	0.6090
Day 13	5	0.8810	0.1546	2	0.8899	0.1667

These uniformly high p-values shown in table 3.2 assert that the null hypothesis is not at any point rejected for the comparison of the results shown in figure 3.7. This means that the offsets made by the optimizer function do not lead to significantly different results than the true offsets, when applied to cohort 1. Given that all cohort 2 used the same experimental procedure as cohort 1, this indicates that it is should be acceptable to use optimized offsets in the absence of true offsets. This allows the data from cohort 2 to be analyzed.

3.3. Cohort 2 results obtained with offset optimizer

When the data of cohort 2 is processed using estimated offset values obtained from the optimizer function all subsequent steps of the data analysis pipeline functioned normally. After calculating the mean of tuning curve correlations to day 10 for each mouse, the results are shown in figure 3.8. Unfortunately, since mouse 11's data for day 10 was unusable, no comparisons between day 10 and other days are possible for that mouse. This combined with the various unusable days of mice 10 and 13, causes the experimental group of cohort 2 to appear rather sparse.

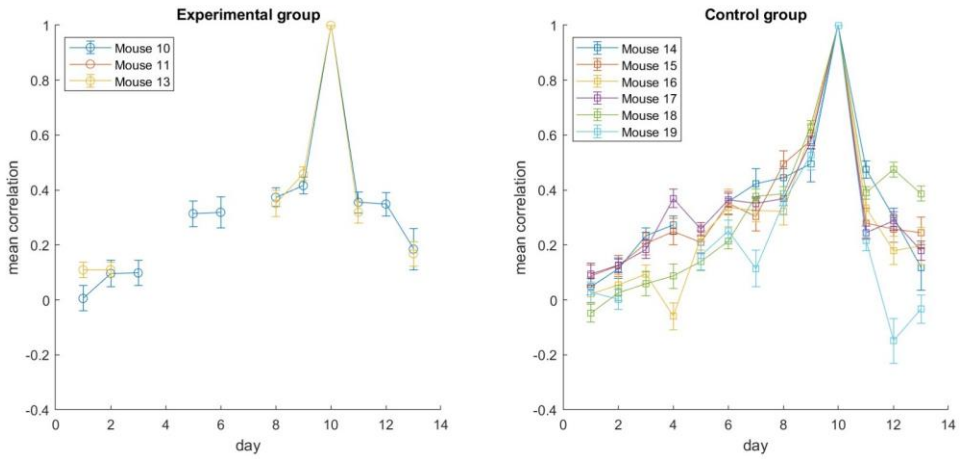

Figure 3.8: Cohort 2 comparisons of the place maps of all days to day 10 using optimized offsets, with each mouse plotted separately. The only Pearson's correlation values used to calculate the displayed means and standard errors were from 'pcabove' cell pairs, from pairs of days that included day 10. Data from mouse 11 is missing because the day 10 data for that mouse is unusable (see appendix A.).

The means and standard errors of each group shown in figure 3.9 were calculated from the means of each mouse's tuning curve correlations, as shown in figure 3.8.

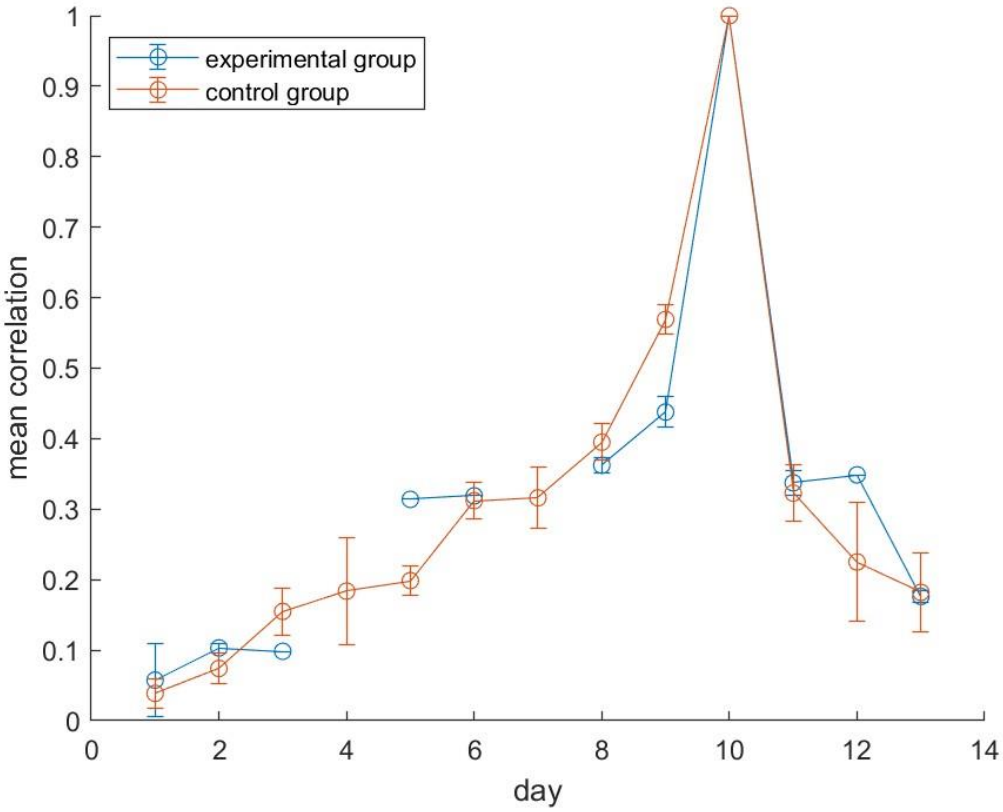

Figure 3.9: Cohort 2 between-group comparison of the place maps of all days to day 10 using optimized offsets. The mean of each mouse's tuning curve correlations for each pair of days were calculated independently. The mean and standard error of those means within each group are shown. The only correlation values used were from 'pcabove' cell pairs, from pairs of days that included day 10. Due to unusable sessions, the number of subjects contributing to each data point varies between pairs of days.

3.4. Combined cohort results obtained with offset optimizer

3.4.1. Group differences

The results of both cohorts obtained using optimized offsets are shown in the following figures. Only data from day pairs that include day 10 are included. Figure 3.10 contains both the cohort 1 data of figure 3.5 and the cohort 2 data of figure 3.8.

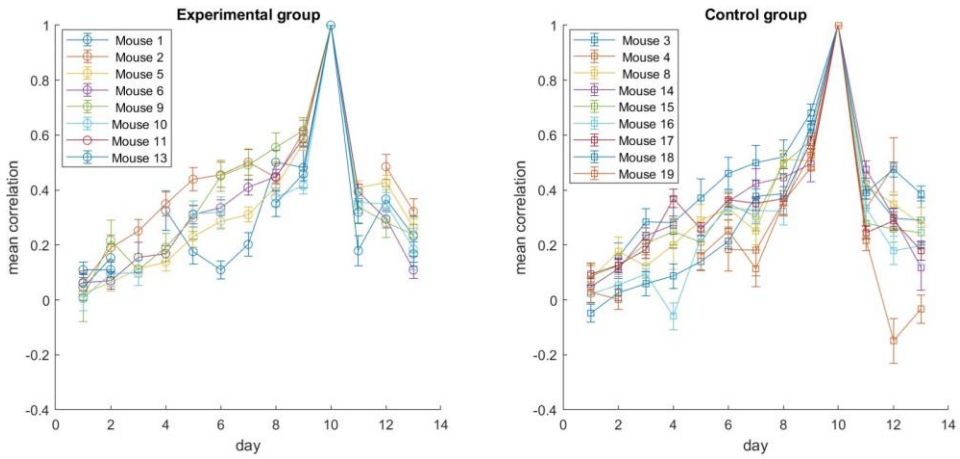

Figure 3.10: Comparisons of the place maps of all days to day 10 using optimized offsets, with each mouse plotted separately. The only Pearson's correlation values used to calculate the displayed means and standard errors were from 'pcabove' cell pairs, from pairs of days that included day 10. Data from mouse 11 is missing because the day 10 data for that mouse is unusable (see appendix A).

The means and standard errors of each group shown in figure 3.11 were calculated from the means of each mouse's tuning curve correlations, as shown in figure 3.10.

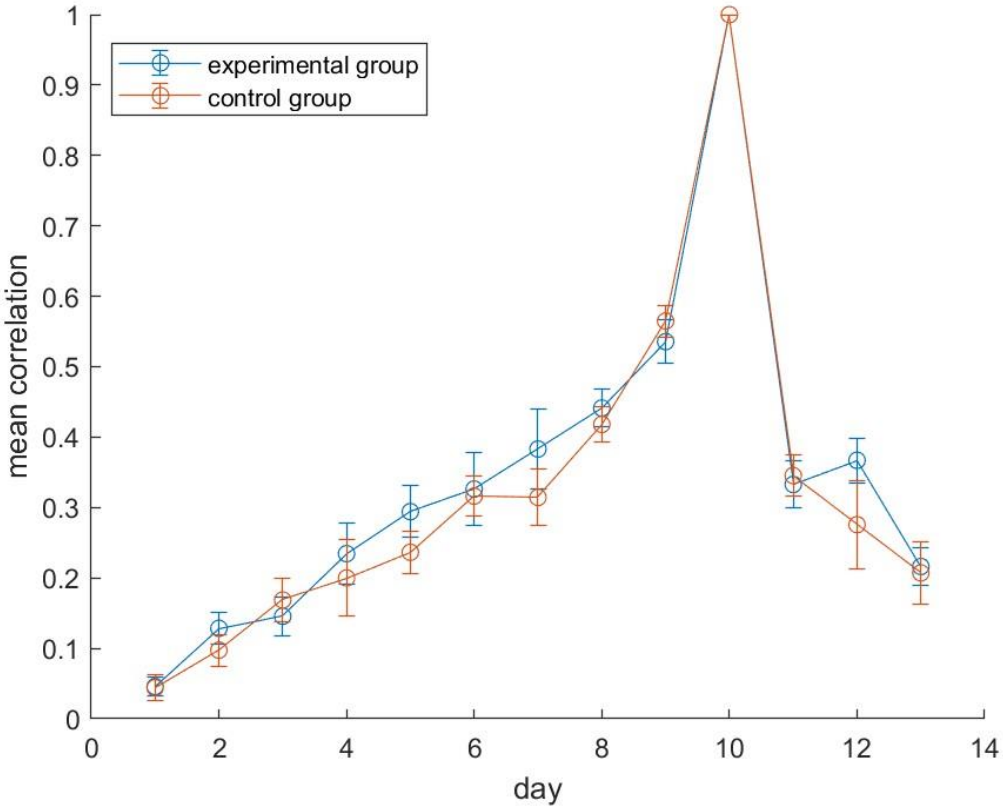

Figure 3.11: Combined cohorts between-group comparison of the place maps of all days to day 10 using true offsets. The mean of each mouse's tuning curve correlations for each pair of days were calculated independently. The mean and standard error of those means within each group are shown. The only correlation values used were from 'pcabove' cell pairs, from pairs of days that included day 10. Due to unusable sessions, the number of subjects contributing to each data point varies between pairs of days.

As shown in figure 3.11, when using data from both cohorts, the experimental group appears to have little to no variation from the control group in the stability of their CA1 tuning curves across sessions. To verify this, Welch's two-sample t-test was performed for each pair of days comparing the experimental group to the control group. The data sets compared by the t-test contained one data point from each mouse, namely the mean of each mouse's tuning curve correlations from the pair of days in question. Since some mice had days with unusable data, the number of mice contributing data to these tests varied from one pair of days to another. The number of mice considered in each t-test as well as the p-value of those t-tests are listed in table 3.3. The null hypothesis being tested is that the experimental group values and the control group values come from populations that share the same mean. A 5% significance level was used, meaning that the null hypothesis would be rejected for any pair of days in which the p-value was calculated as being below 0.05. As shown in table 3.3, this did not happen on any pair of days. As such the null hypothesis is not rejected at any point.

Table 3.3: Results of Welch's two-sample t-tests between the experimental group and the control group of the combined cohorts for each day compared to day 10. Due to some mice having some days with unusable data, the number of mice contributing data to each analysis varies between pairs of days. Significance threshold of $p < 0.05$ is used.

	Experimental mice (n)	Control mice (n)	p-value	t-value
Day 1	7	7	0.9402	0.0767
Day 2	7	8	0.3475	0.9749
Day 3	5	7	0.5888	-0.5588
Day 4	5	7	0.6287	0.4988
Day 5	6	7	0.2497	1.2209
Day 6	6	9	0.8696	0.1694
Day 7	5	9	0.3512	0.9906
Day 8	7	9	0.5392	0.6300
Day 9	7	9	0.4588	-0.7663
Day 11	6	9	0.7822	-0.2831
Day 12	6	9	0.2177	1.3042
Day 13	7	8	0.8639	0.1755

3.4.2. Sex differences

An additional analysis was performed searching for any sex differences in the stability of tuning curves across days. This analysis was done using the data from both cohorts obtained using optimized offsets.

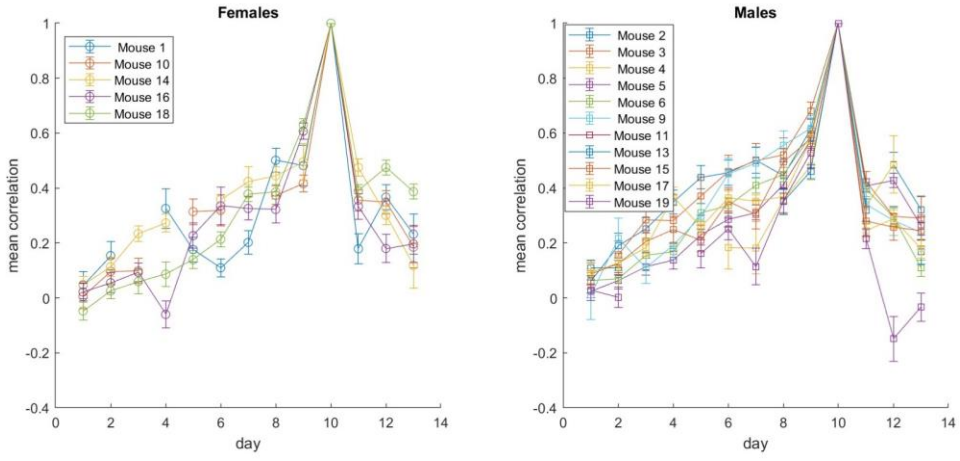

Figure 3.12: Comparisons of the place maps of all days to day 10 using optimized offsets, with each mouse plotted separately overlayed with others of the same sex. The only Pearson's correlation values used to

calculate the displayed means and standard errors were from ‘pcabove’ cell pairs, from pairs of days that included day 10. Data from mouse 11 is missing because the day 10 data for that mouse is unusable (see appendix A).

The means and standard errors of each group shown in figure 3.13 were calculated from the means of each mouse’s tuning curve correlations, as shown in figure 3.12.

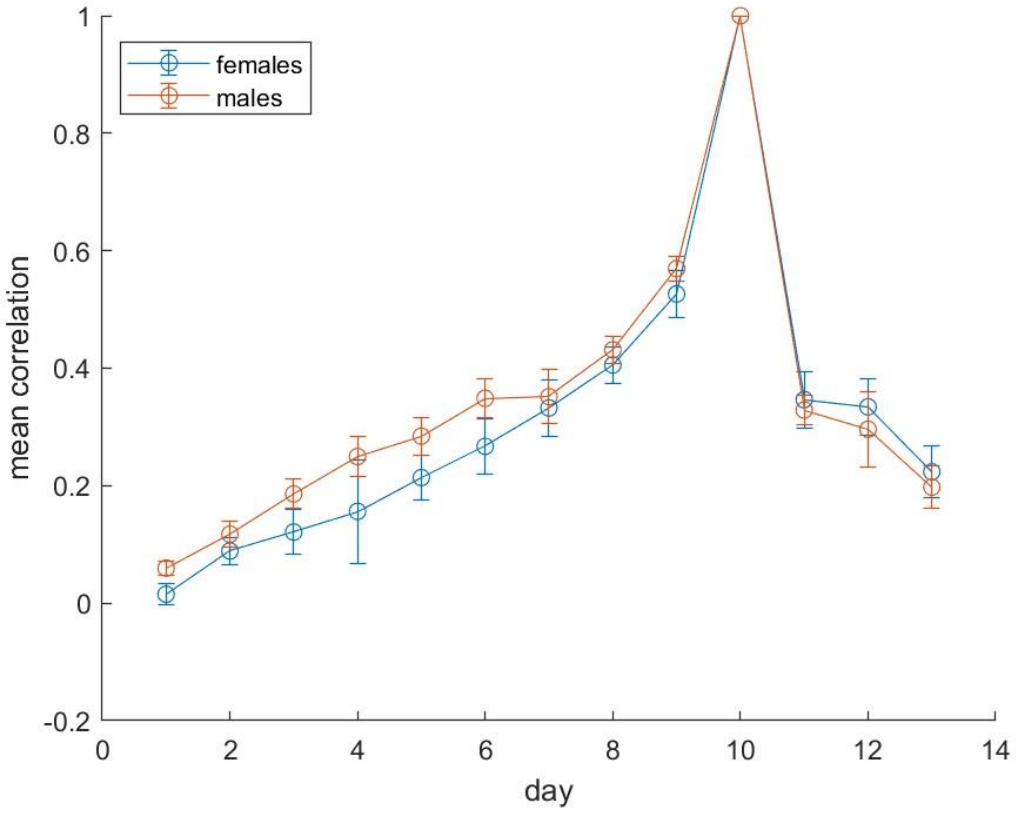

Figure 3.13: Combined cohorts between-sexes comparison of the place maps of all days to day 10 using true offsets. The mean of each mouse’s tuning curve correlations for each pair of days were calculated independently. The mean and standard error of those means within each group are shown. The only correlation values used were from ‘pcabove’ cell pairs, from pairs of days that included day 10. Due to unusable sessions, the number of subjects contributing to each data point varies between pairs of days.

As shown in figure 3.13, there appears to be no effect of sex on the stability of their CA1 tuning curves across sessions. To verify this, Welch’s two-sample t-test was performed for each pair of days comparing females to males. The data sets compared by the t-test contained one data point from each mouse, namely the mean of each mouse’s tuning curve correlations from the pair of days in question. Since some mice had days with unusable data, the number of mice contributing data to these tests varied from one pair of days to another. The number of mice considered in each t-test as well as the p-value of those t-tests are listed in table 3.4. The null

hypothesis being tested is that the female group values and the male group values come from populations that share the same mean. A 5% significance level was used, meaning that the null hypothesis would be rejected for any pair of days in which the p-value was calculated as being below 0.05. As shown in table 3.4, this did not happen on any pair of days. As such the null hypothesis is not rejected at any point.

Table 3.4: Results of Welch's two-sample t-tests between the females and males of both cohorts for each day compared to day 10. Due to some mice having some days with unusable data, the number of mice contributing data to each analysis varies between pairs of days. Significance threshold of $p < 0.05$ is used.

	Female mice (n)	Male mice (n)	p-value	t-values
Day 1	5	8	0.0745	-2.0508
Day 2	5	9	0.3825	-0.9110
Day 3	4	7	0.2107	-1.4145
Day 4	4	7	0.3807	-0.9875
Day 5	4	8	0.1968	-1.4219
Day 6	5	9	0.1875	-1.4426
Day 7	4	9	0.7806	-0.2875
Day 8	5	10	0.5240	-0.6639
Day 9	5	10	0.3766	-0.9520
Day 11	5	9	0.7559	0.3252
Day 12	5	9	0.6398	0.4802
Day 13	5	9	0.6607	0.4539

3.4.3. Place field widths

In addition to assessments of representational drift, a brief analysis was performed to determine the distribution of place field widths, and to search for any group effects or sex differences in these distributions. Figure 3.14 demonstrates that the distribution of place field widths is highly consistent between groups, sexes and days.

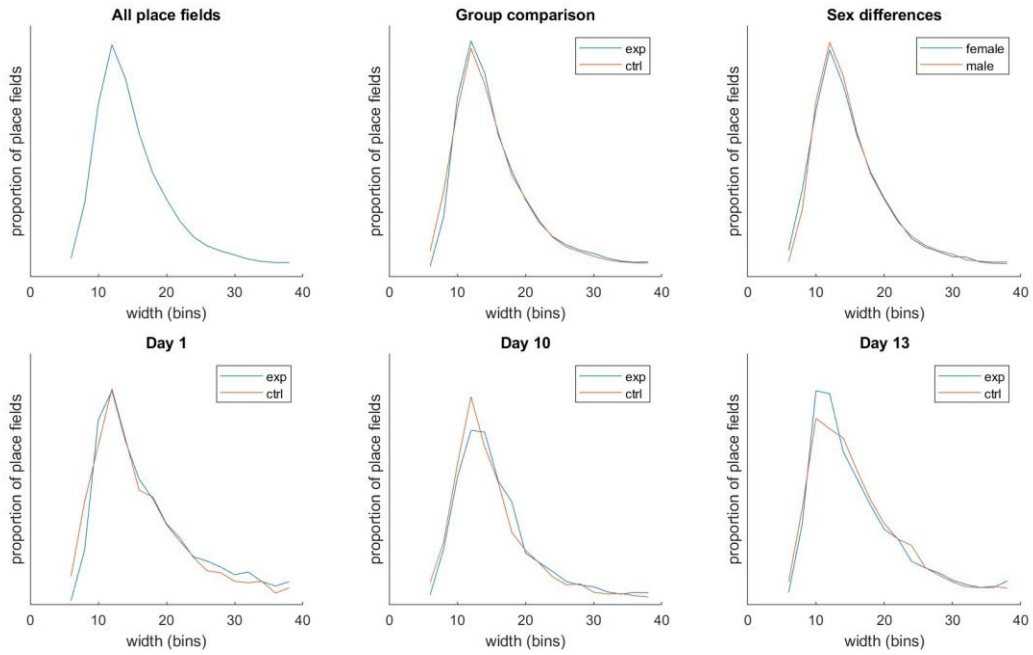

Figure 3.14 Distribution of place field widths. The top left subfigure shows the distribution curve for all place fields from all place cells across all days for all mice. The top middle and top right subfigures show the same data separated either by group or by sex respectively. Each of the three bottom subfigures shows the place field distribution curves for all mice separated by group on either their first, tenth or thirteenth imaging days respectively.

Chapter 4.

Discussion

4.1. Summary and interpretation of findings

Circadian disruption has been shown to have a wide variety of effects on health and cognition, and the phase shifting of light-dark schedules has been shown to be an effective and reliable method of inducing circadian disruption. One of these known effects is an impairment in spatial memory retention for memories formed during phase shift induced circadian disruption This experiment is an attempt to confirm that the neural basis of this behavioural phenomenon is tightly associated with the activity of the spatial maps of the hippocampus, as has been suspected (Deibel et al., 2022; Devan et al., 2001; Zelinski et al., 2014). To do this, this experiment examines the effects of circadian disruption, by way of phase shifting, on CA1 place cell activity in mice across multiple days. The phase shifting done to the experimental group was a daily 3-hour phase advance, referred to in other literature as a T21 light-dark schedule, which occurred 8 times starting with the day before the first imaging day. Each mouse had a portion of the CA1 of their right hippocampus imaged using 2-photon microscopy once per day for 10 days, and then again on three retention test days taking place 7, 8 and 23 days after the 10^{th} imaging day. Each mouse ran along a treadmill during imaging, with tactile cues affixed to the treadmill belt. For each day of imaging, the spatial tuning curve of each cell was identified, and used to determine which cells met a previously established mathematical definition of a place cell (H. Chang et al., 2020, 2023; Esteves et al., 2021, 2023).

Due to technical errors during the second cohort's data acquisition, a suboptimal method for synchronizing the timing of the neural activation with the timing of the position and velocity data had to be developed. The synchronization method operated by finding the offset in start times between the 2-photon imaging data and the treadmill position data that would optimize for the highest possible correlation between velocity and total neural activity. This synchronization method was tested on cohort 1 and found to yield offset values that were on average 0.8442 seconds larger than the correct offset as calculated. This indicates that there is normally a delay between bursts of movement and bursts of neural activity in the CA1 region. Although the optimizer method for calculating offsets is inaccurate by a consistent amount, it nonetheless was found to have no significant effect on the mean tuning curve values. When compared to those calculated using accurate offsets. This indicates that average of 0.8442 seconds offset inaccuracy is not enough time to ruin the tuning curves.

The data analysis that has thus far been completed has focused primarily on analyzing place cell activity in terms of mean tuning curve correlation which is a measure of representational drift between days. To calculate tuning curve correlations between days, the cells imaged on a pair of days were identified, the Pearson's correlation of each cell's tuning curves were compared, and the mean of those correlations was calculated for each mouse. t-tests were calculated between the phase-shifted group and the control group using those mean tuning curve correlation values. No effect of circadian disruption on representational drift has been found between the 10th acquisition day and any of the retention test days. This lack of any significant between-group differences holds true both for the cohort 1 data analyzed with accurate offset values, and for the combined cohorts analyzed with optimized offsets. These findings runs contrary to the hypothesis that patterns of neural activity in this particular brain region would directly reflect the patterns of spatial memory acquisition and retention demonstrated in behavioural testing by Devan et al. (2001) and others (Deibel et al., 2022; Zelinski et al., 2014). This may be because representational drift was the wrong metric to examine. If so, then some of the numerous potential methods of analysis of this data that have not yet been attempted may reveal the expected pattern in the hippocampus.

4.2. Limitations of this study

This experiment has been plagued from beginning to end with a litany of hardware malfunctions and software glitches. The vast majority of these issues caused nothing more than minor delays, however a few of them negatively impacted the data. The most severe of these is the missing cohort 2 offset data, and the errors that caused some properly performed recording sessions to be unusable in later analysis (see appendix A).

Beyond these concerns with the practical application of this experimental procedure, there are also some limitations inherent to the experimental procedure itself. This experiment is meant to follow up on the findings of Devan et al. (2001) who used a Morris water maze procedure to test the spatial memory of rats. To allow for 2-photon imaging, certain dissimilarities to Devan et al.'s procedure had to be introduced, each one of which weakens the parallels between their experiment and this experiment.

The first dissimilarity is that this experiment uses transgenic mice instead of rats. It is possible that the subspecies of mouse used in this experiment might not be as prone to phase-shift induced impairments to spatial memory as the subspecies of rat used in Devan et al.'s (2001) experiments. That having been said, it would have been impossible to safely perform 2-photon imaging on rats using the available equipment, so the alteration was necessary.

With the current equipment, 2-photon imaging necessitated the use of a (dry) treadmill as the environment instead of a 2-dimensional water maze. 2-photon imaging also requires that the mice must have their heads fixed in place during imaging which is not a natural posture. Running on a treadmill while head-fixed deprives the mouse of translational vestibular feedback that would normally contribute to the path integration system that is directly involved with place cell activity (McNaughton et al., 1996). For this same reason the treadmill model is also problematic in the way it restricts optical flow when done without virtual reality tools. An experiment done by Aghajan et al. (2015) shows that even with virtual reality to provide optical flow and body-fixing instead of head-fixing, the CA1 place cells of rats exploring a 2-dimensional virtual environment while physically stationary show impaired spatial selectivity compared to the CA1 place cells of mobile rats exploring a real 2-dimensional environment. The differences in methodology between the present research and the work of Devan et al (2001) weaken the comparison between them to an unclear degree, while also suggesting a variety of possible methodological changes that could be made with access to superior equipment.

An additional possible issue with the treadmill methodology is the necessity of pretraining on a blank treadmill. It is possible, albeit unlikely, that the hippocampal representation of the training environment is having some manner of influence on the representation of the imaging environment. The distinct similarities between these two environments lends support to this concern, seeing as both environments involve head-fixing and treadmills of the same length and material. However, prior research has shown that global remapping occurs even when moving an animal between identical chambers in different places (Leutgeb et al., 2005). Given that the training and imaging treadmills were in different rooms, with different sounds, different scents and drastically different visual landmarks in addition to the tactile cues on the imaging belt, it is extremely unlikely that the hippocampal representations of these two environments would be noticeably similar to one another.

Another potential weakness of the present study is the criteria used to identify place cells. A careful examination of the example place cells in figure C.1 reveals that some of the cells that met all criteria for being a place cell do not have the high level of consistency between laps that is expected of true place cells. The most obvious way to expand the exclusion criteria would be to redefine the minimum threshold for between lap consistency, as the current rules are rather minimalistic. A second way to expand exclusion criteria would be to set an outer threshold for how much drift is deemed too much. Figure 2.11 shows the distribution of drift among place fields, and the same calculations used in creating that figure could be applied to each cell, so as to exclude those with place fields that drift too quickly in either direction over the course of the session.

4.3. Future directions

4.3.1. Further analysis of this experiment

Much of the data obtained in this experiment has not yet been fully utilized, which leaves open many avenues for additional investigation into the influence of phase shifting on neural activity in the hippocampus.

The most promising of these possibilities is an analysis of changes in spatial information per place cell or spatial information per cell between days. As found by Geva et al. (2023), representational drift has a tendency toward creating greater efficiency in hippocampal place maps, with fewer total place cells and greater total spatial information. It is entirely possible that an analysis of spatial information could reveal correlations not seen in the analysis of representational drift shown in chapter 3. Much of the work for this analysis has already been done, as calculating spatial information (in bits) for each and every cell was already done to facilitate the identification of place cells (see section 2.3.2), and these values were all saved.

During each recording session, some measures of mouse behaviour were recorded. Namely, the position and velocity of the treadmill were recorded, the timing of each lick was recorded, and an infrared camera aimed at the left side of the mouse's head was running. There is reason to expect that mice with clear memory of where along the treadmill rewards are administered will more frequently pause their running immediately before that location, will begin licking in anticipation immediately before that location, and will show anticipatory pupil dilation (Yamada & Toda, 2022). There is variation between mice in their median pause position and variance in where they pause as shown in appendix D. Analyses could be done to identify whether mice with more consistent anticipatory pausing behaviour are more likely to have less representational drift or more spatial information per place cell. Similar analyses could be done using anticipatory lick timing or anticipatory pupil dilation, though certain technological issues with the lick sensor and the infrared camera would make those analyses more challenging and time-consuming than would normally be expected.

Drawing inspiration again from Geva et al. (2023), ensemble rate correlations could be calculated between days for each mouse. The firing rates of place cells were found to decrease over the course of several days after initial exposure to an environment in a predicable manner that was not influenced by the amount of experience in the environment during that time (Geva et al., 2023). Analyses could be done to identify any effect of phase shifting on these ensemble rate correlations.

A closer look at the experimental group actogram data reveals that there is a visible diagonal shift in peak activity timing during the phase advance days (Figure 2.2 D, E and F), and that this diagonal line more noticeable for some mice than others. This raises the distinct possibility that some mice are better than others at adapting gracefully to phase-shifting. If some mice in the experimental group are more severely impacted by the phase-shifting than others, then there might be a relationship between severity of disruption and rate of representational drift. To do this analysis, the first step would be to devise a method of quantifying the severity of disruption from the actogram data. Future work will assess this interesting possibility.

One field of analysis that is currently being pursued is an investigation of replay signals in these mice. This analysis is making use of the pre-run and post-run recording sessions and will identify effects of phase shifting on the occurrence, frequency and other characteristics of ensemble replay signals before and after running on the treadmill. Replay signals in the hippocampus are when sequential neural firing patterns that occur during an activity are reactivated when this activity is not ongoing. Hippocampal place cell replay signals have been identified at compressed timescales during deep sleep, at normal timescales during REM sleep, and at compressed timescales typically in reverse order while awake (Foster & Wilson, 2006; Hasselmo, 2008; Louie & Wilson, 2001). Replay signals during sleep are thought to be involved with memory consolidation, whereas the role of awake replay signals such as those collected in this experiment are thought to support learning (Foster, 2017; Foster & Wilson, 2006). Circadian disruption induced modifications to any of these types of replays would provide useful insights, however, compared to disruptions to awake replay patterns, a disruption to consolidation related processes would more neatly explain Devan et al.'s (2001) pattern of unaffected acquisition and impaired retention.

Another possible area of investigation would be to test whether the spatially sensitive cells associated with the positions of tactile cues on the treadmill are more stable across days, or more likely to be involved in replay signals, using the analysis procedures described by Chang et al. (H. Chang et al., 2023).

4.3.2. Potential future research

Determining that hippocampal representational drift is unaffected by phase shifting, does not invalidate the idea that circadian disruption driven impairments to spatial memory should be reflected in some way in hippocampal neural activity. It does raise the question of what aspects of neural activity in the hippocampus other than representational drift might reflect this observed impairment. To assess the effects of circadian disruption on total hippocampal activity and its functional connectivity to other brain regions, a human fMRI experiment has already been

designed and prepared. This fMRI experiment was initially intended to be the main focus of this thesis with the 2-photon mouse experiment intended a secondary project. This fMRI project had to be abandoned due to administrative issues after approximately one year of training, imaging practice, MRI certification, equipment repair, software coding, the creation of a data analysis pipeline, recruitment of volunteers, and the imaging of the first three volunteers.

Since hippocampal representational drift appears unaffected by phase shifting under the current experimental procedures, it is worth questioning what about those procedures could be improved upon. Much of the behavioural research this study is building upon was performed with freely moving animals exploring two-dimensional spaces. The head-fixed one-dimensional treadmill used in this experiment, while convenient, was not the most optimal parallel. The way to correct this would be to use a miniaturized head-mounted 2-photon microscope such as the one described by Zong et al. (2022). These 'miniscopes' weigh less than 3 grams with only slightly worse resolution than the large and immobile 2-photon microscope used in this experiment. The freedom of movement could allow for a conditioned place preference or novel object recognition task to be run while imaging is ongoing. The best possible parallel would be to use a waterproofed miniscope durable enough to be used on a transgenic GCaMP rat as it performs the Morris water task, following the same procedure as Devan et al. (2001).

Other experimenters in the past have used electrophysiological methods to record hippocampal activity in freely moving rodents (Muller et al., 1994; J. O'Keefe & Recce, 1993; J. O'Keefe & Speakman, 1987; Quirk et al., 1990; Wilson & McNaughton, 1993). This is a valid alternative to the use of miniaturized 2-photon microscopes with its own set of advantages and weaknesses. The main advantages of electrophysiology are the recording of large numbers of cells from multiple sites simultaneously, with comparatively minimal cortical damage and high temporal resolution. The main weakness compared to 2-photon microscopy is low spatial resolution such that the activity of neighbouring neurons are generally not distinguishable from one another.

There is also the distinct possibility that the effects of circadian disruption on the hippocampal memory system might not be focused on the hippocampus itself, but rather on other regions closely connected to the hippocampus. The retrosplenial cortex is an especially promising region to investigate given its roles in spatial behaviour and the way it is connected to a wide variety of spatial, sensory and motor regions. It is uniquely situated for using spatial information from the hippocampus to produce spatial behaviour, although the full nuances of what this region does and how it does it is still largely unclear (Mitchell et al., 2018).

4.4. Concluding thoughts

This experiment has demonstrated no significant effects of phase shifting on CA1 representational drift using spatial representations of a linear treadmill track as the environment. The preprocessing and initial analyses of the vast amount of data obtained in this experiment lays the groundwork for future investigations into the effects of circadian disruption on the hippocampal memory system. Indeed, some of the questions raised here may be able to be answered use the data produced in this experiment.

References

Aghajan, Z. M., Acharya, L., Moore, J. J., Cushman, J. D., Vuong, C., & Mehta, M. R. (2015). Impaired spatial selectivity and intact phase precession in two-dimensional virtual reality. *Nature Neuroscience*, *18*(1), 121–128. https://doi.org/10.1038/nn.3884

Antoniadis, E. A., Ko, C. H., Ralph, M. R., & McDonald, R. J. (2000). Circadian rhythms, aging and memory. *Behavioural Brain Research, 114*(1-2), 221-233. https://doi.org/10.1016/SO166-4328(00)00290-4

Aschoff, J., Hoffmann, K., Pohl, H., & Wever, R. (1975). Re-entrainment of circadian rhythms after phase-shifts of the Zeitgeber. *Chronobiologia*, *2*(1), 23–78.

Baron, K. G., & Reid, K. J. (2014). Circadian misalignment and health. *International Review of Psychiatry*, *26*(2), 139–154. https://doi.org/10.3109/09540261.2014.911149

Bechara, A., Tranel, D., Damasio, H., Adolphs, R., Rockland, C., & Damasio, A. R. (1995). Double dissociation of conditioning and declarative knowledge relative to the amygdala and hippocampus in humans. *Science*, *269*(5227), 1115–1118. https://doi.org/10.1126/science.7652558

Bostock, E., Muller, R. U., & Kubie, J. L. (1991). Experience-dependent modifications of hippocampal place cell firing. *Hippocampus*, *1*(2), 193–205. https://doi.org/10.1002/hipo.450010207

Bracci, Ciarapica, Zabaleta, Tartaglione, Pirozzi, Giuliani, Piva, Valentino, Ledda, Rapisarda, Stevens, & Santarelli. (2019). BRCA1 and BRCA2 Gene Expression: Diurnal Variability and Influence of Shift Work. *Cancers*, *11*(8), 1146. https://doi.org/10.3390/cancers11081146

Brandeis, R., Brandys, Y., & Yehuda, S. (1989). The use of the Morris Water Maze in the study of memory and learning. *The International Journal of Neuroscience*, *48*(1–2), 29–69. https://doi.org/10.3109/00207458909002151

Bucci, D. J., Phillips, R. G., & Burwell, R. D. (2000). Contributions of postrhinal and perirhinal cortex to contextual information processing. *Behavioral Neuroscience*, *114*(5), 882–894. https://doi.org/10.1037//0735-7044.114.5.882

Bures, J., Fenton, A. A., Kaminsky, Y. u, Wesierska, M., & Zahalka, A. (1998). Rodent navigation after dissociation of the allocentric and idiothetic representations of space. *Neuropharmacology*, *37*(4–5), 689–699. https://doi.org/10.1016/s0028-3908(98)00031-8

Burwell, R. D., Saddoris, M. P., Bucci, D. J., & Wiig, K. A. (2004). Corticohippocampal contributions to spatial and contextual learning. *The Journal of Neuroscience*, *24*(15), 3826–3836. https://doi.org/10.1523/JNEUROSCI.0410-04.2004

Buzsáki, G., & Tingley, D. (2018). Space and Time: The Hippocampus as a Sequence Generator. *Trends in Cognitive Sciences*, *22*(10), 853–869. https://doi.org/10.1016/j.tics.2018.07.006

Chang, A.-M., Anderson, C., Cain, S. W., Reichenberger, D. A., Ronda, J. M., Lockley, S. W., & Czeisler, C. A. (2023). Entrainment to gradual vs. Immediate 8-hour phase advance shifts with and without short-wavelength enriched polychromatic green light. *Sleep Health*, *10*(1, Suppl.), S67-S75. https://doi.org/10.1016/j.sleh.2023.09.007

Chang, H., Esteves, I. M., Neumann, A. R., Mohajerani, M. H., & McNaughton, B. L. (2023). Cortical reactivation of spatial and non-spatial features coordinates with hippocampus to form a memory dialogue. *Nature Communications*, *14*(1), 7748. https://doi.org/10.1038/s41467-023-43254-7

Chang, H., Esteves, I. M., Neumann, A. R., Sun, J., Mohajerani, M. H., & McNaughton, B. L. (2020). Coordinated activities of retrosplenial ensembles during resting-state encode spatial landmarks. *Philosophical Transactions of the Royal Society B: Biological Sciences*, *375*(1799), 20190228. https://doi.org/10.1098/rstb.2019.0228

Chang, W.-P., & Lin, Y.-K. (2022). Relationship between rotating shift work and white blood cell count, white blood cell differential count, obesity, and metabolic syndrome of nurses. *Chronobiology International*, *39*(2), 159–168. https://doi.org/10.1080/07420528.2021.1989447

Chaput, J.-P., McHill, A. W., Cox, R. C., Broussard, J. L., Dutil, C., da Costa, B. G. G., Sampasa-Kanyinga, H., & Wright, K. P. (2023). The role of insufficient sleep and circadian misalignment in obesity. *Nature Reviews Endocrinology*, *19*(2), 82–97. https://doi.org/10.1038/s41574-022-00747-7

Chellappa, S. L., Vujovic, N., Williams, J. S., & Scheer, F. A. J. L. (2019). Impact of circadian disruption on cardiovascular function and disease. *Trends in Endocrinology and Metabolism: TEM*, *30*(10), 767–779. https://doi.org/10.1016/j.tem.2019.07.008

Chen, G., King, J. A., Burgess, N., & O'Keefe, J. (2013). How vision and movement combine in the hippocampal place code. *Proceedings of the National Academy of Sciences*, *110*(1), 378–383. https://doi.org/10.1073/pnas.1215834110

Chen, T.-W., Wardill, T. J., Sun, Y., Pulver, S. R., Renninger, S. L., Baohan, A., Schreiter, E. R., Kerr, R. A., Orger, M. B., Jayaraman, V., Looger, L. L., Svoboda, K., & Kim, D. S. (2013). Ultrasensitive fluorescent proteins for imaging neuronal activity. *Nature*, *499*(7458), 295–300. https://doi.org/10.1038/nature12354

Colgin, L. L., Moser, E. I., & Moser, M.-B. (2008). Understanding memory through hippocampal remapping. *Trends in Neurosciences*, *31*(9), 469–477. https://doi.org/10.1016/j.tins.2008.06.008

Craig, L. A., & McDonald, R. J. (2008). Chronic disruption of circadian rhythms impairs hippocampal memory in the rat. *Brain Research Bulletin*, *76*(1–2), 141–151. https://doi.org/10.1016/j.brainresbull.2008.02.013

Dana, H., Chen, T.-W., Hu, A., Shields, B. C., Guo, C., Looger, L. L., Kim, D. S., & Svoboda, K. (2014). Thy1-GCaMP6 Transgenic Mice for Neuronal Population Imaging In Vivo. *PLoS ONE*, *9*(9), e108697. https://doi.org/10.1371/journal.pone.0108697

Deibel, S. H., Higdon, S., Cassell, T. T. S., House-Denine, M. L., Giberson, E., Webb, I. C., & Thorpe, C. M. (2022). Impaired Morris water task retention following T21 light dark cycle exposure is not due to reduced hippocampal c-FOS expression. *Frontiers in Behavioral Neuroscience*, *16*, 1025388. https://doi.org/10.3389/fnbeh.2022.1025388

Deibel, S. H., Hong, N. S., Himmler, S. M., & McDonald, R. J. (2014). The effects of chronic photoperiod shifting on the physiology of female Long-Evans rats. *Brain Research Bulletin*, *103*, 72–81. https://doi.org/10.1016/j.brainresbull.2014.03.001

Devan, B. D., Goad, E. H., Petri, H. L., Antoniadis, E. A., Hong, N. S., Ko, C. H., Leblanc, L., Lebovic, S. S., Lo, Q., Ralph, M. R., & McDonald, R. J. (2001). Circadian Phase-Shifted Rats Show Normal Acquisition but Impaired Long-Term Retention of Place Information in the Water Task. *Neurobiology of Learning and Memory*, *75*(1), 51–62. https://doi.org/10.1006/nlme.1999.3957

Devan, B. D., McDonald, R. J., & White, N. M. (1999). Effects of medial and lateral caudate-putamen lesions on place- and cue-guided behaviors in the water maze: Relation to thigmotaxis. *Behavioural Brain Research*, *100*(1–2), 5–14. https://doi.org/10.1016/s0166-4328(98)00107-7

Devan, B. D., & White, N. M. (1999). Parallel information processing in the dorsal striatum: Relation to hippocampal function. *The Journal of Neuroscience*, *19*(7), 2789–2798. https://doi.org/10.1523/JNEUROSCI.19-07-02789.1999

Eichenbaum, H. (2016). Still searching for the engram. *Learning & Behavior*, *44*(3), 209–222. https://doi.org/10.3758/s13420-016-0218-1

Esteves, I. M., Chang, H., Neumann, A. R., & McNaughton, B. L. (2023). Consolidation of cellular memory representations in superficial neocortex. *iScience*, *26*(2), 105970. https://doi.org/10.1016/j.isci.2023.105970

Esteves, I. M., Chang, H., Neumann, A. R., Sun, J., Mohajerani, M. H., & McNaughton, B. L. (2021). Spatial Information Encoding across Multiple Neocortical Regions Depends on an Intact Hippocampus. *The Journal of Neuroscience*, *41*(2), 307–319. https://doi.org/10.1523/JNEUROSCI.1788-20.2020

Ferbinteanu, J. (2019). Memory systems 2018 – towards a new paradigm. *Neurobiology of Learning and Memory*, *157*, 61–78. https://doi.org/10.1016/j.nlm.2018.11.005

Filipski, E., Li, X. M., & Lévi, F. (2006). Disruption of Circadian Coordination and Malignant Growth. *Cancer Causes & Control*, *17*(4), 509–514. https://doi.org/10.1007/s10552-005-9007-4

Foster, D. J. (2017). Replay Comes of Age. *Annual Review of Neuroscience*, *40*(Volume 40, 2017), 581–602. https://doi.org/10.1146/annurev-neuro-072116-031538

Foster, D. J., & Wilson, M. A. (2006). Reverse replay of behavioural sequences in hippocampal place cells during the awake state. *Nature*, *440*(7084), 680–683. https://doi.org/10.1038/nature04587

Fyhn, M., Molden, S., Witter, M. P., Moser, E. I., & Moser, M.-B. (2004). Spatial representation in the entorhinal cortex. *Science*, *305*(5688), 1258–1264. https://doi.org/10.1126/science.1099901

Gaffan, E. A., Bannerman, D. M., Warburton, E. C., & Aggleton, J. P. (2001). Rats' processing of visual scenes: Effects of lesions to fornix, anterior thalamus, mamillary nuclei or the retrohippocampal region. *Behavioural Brain Research*, *121*(1–2), 103–117. https://doi.org/10.1016/s0166-4328(00)00389-2

Geva, N., Deitch, D., Rubin, A., & Ziv, Y. (2023). Time and experience differentially affect distinct aspects of hippocampal representational drift. *Neuron*, *111*(15), 2357-2366.e5. https://doi.org/10.1016/j.neuron.2023.05.005

Gibson, E. M., Wang, C., Tjho, S., Khattar, N., & Kriegsfeld, L. J. (2010). Experimental 'Jet Lag' Inhibits Adult Neurogenesis and Produces Long-Term Cognitive Deficits in Female Hamsters. *PLoS ONE*, *5*(12), e15267. https://doi.org/10.1371/journal.pone.0015267

Gruber, A. J., & McDonald, R. J. (2012). Context, emotion, and the strategic pursuit of goals: Interactions among multiple brain systems controlling motivated behavior. *Frontiers in Behavioral Neuroscience*, *6*, 50. https://doi.org/10.3389/fnbeh.2012.00050

Hafting, T., Fyhn, M., Molden, S., Moser, M.-B., & Moser, E. I. (2005). Microstructure of a spatial map in the entorhinal cortex. *Nature*, *436*(7052), 801–806. https://doi.org/10.1038/nature03721

Harvey, C. D., Collman, F., Dombeck, D. A., & Tank, D. W. (2009). Intracellular dynamics of hippocampal place cells during virtual navigation. *Nature*, *461*(7266), 941–946. https://doi.org/10.1038/nature08499

Hasselmo, M. E. (2008). Temporally structured replay of neural activity in a model of entorhinal cortex, hippocampus and postsubiculum. *The European Journal of Neuroscience*, *28*(7), 1301–1315. https://doi.org/10.1111/j.1460-9568.2008.06437.x

Hayman, R. M. A., Chakraborty, S., Anderson, M. I., & Jeffery, K. J. (2003). Context-specific acquisition of location discrimination by hippocampal place cells. *The European Journal of Neuroscience*, *18*(10), 2825–2834. https://doi.org/10.1111/j.1460-9568.2003.03035.x

Hirsh, R. (1974). The hippocampus and contextual retrieval of information from memory: A theory. *Behavioral Biology*, *12*(4), 421–444. https://doi.org/10.1016/s0091-6773(74)92231-7

Hunt, M. E., Kesner, R. P., & Evans, R. B. (1994). Memory for spatial location: Functional dissociation of entorhinal cortex and hippocampus. *Psychobiology*, *22*(3), 186–194.

Iggena, D., Winter, Y., & Steiner, B. (2017). Melatonin restores hippocampal neural precursor cell proliferation and prevents cognitive deficits induced by jet lag simulation in adult mice. *Journal of Pineal Research*, *62*(4), e12397. https://doi.org/10.1111/jpi.12397

Ivan, V. E., Tomàs-Cuesta, D. P., Esteves, I. M., Curic, D., Mohajerani, M., McNaughton, B. L., Davidsen, J., & Gruber, A. J. (2024). The Nonclassic Psychedelic Ibogaine Disrupts Cognitive Maps. *Biological Psychiatry Global Open Science*, *4*(1), 275–283. https://doi.org/10.1016/j.bpsgos.2023.07.008

Kesner, R. P., & Hardy, J. D. (1983). Long-term memory for contextual attributes: Dissociation of amygdala and hippocampus. *Behavioural Brain Research*, *8*(2), 139–149. https://doi.org/10.1016/0166-4328(83)90050-5

Kesner, R. P., Walser, R. D., & Winzenried, G. (1989). Central but not basolateral amygdala mediates memory for positive affective experiences. *Behavioural Brain Research*, *33*(2), 189–195. https://doi.org/10.1016/S0166-4328(89)80050-6

Khatib, D., Ratzon, A., Sellevoll, M., Barak, O., Morris, G., & Derdikman, D. (2023). Active experience, not time, determines within-day representational drift in dorsal CA1. *Neuron*, *111*(15), 2348-2356.e4. https://doi.org/10.1016/j.neuron.2023.05.014

Knutsson, A. (2004). Methodological Aspects of Shift-Work Research. *Chronobiology International*, *21*(6), 1037–1047. https://doi.org/10.1081/CBI-200038525

Kolb, B., Sutherland, R. J., & Whishaw, I. Q. (1983). A comparison of the contributions of the frontal and parietal association cortex to spatial localization in rats. *Behavioral Neuroscience*, *97*(1), 13–27. https://doi.org/10.1037/0735-7044.97.1.13

Lashley, K. S. (1950). In search of the engram. In *Physiological mechanisms in animal behavior. (Society's Symposium IV.)* (pp. 454–482). Academic Press.

Leutgeb, S., Leutgeb, J. K., Barnes, C. A., Moser, E. I., McNaughton, B. L., & Moser, M.-B. (2005). Independent codes for spatial and episodic memory in hippocampal neuronal ensembles. *Science*, *309*(5734), 619–623. https://doi.org/10.1126/science.1114037

Loh, D. H., Navarro, J., Hagopian, A., Wang, L. M., Deboer, T., & Colwell, C. S. (2010). Rapid Changes in the Light/Dark Cycle Disrupt Memory of Conditioned Fear in Mice. *PLoS ONE*, *5*(9), e12546. https://doi.org/10.1371/journal.pone.0012546

Louie, K., & Wilson, M. A. (2001). Temporally structured replay of awake hippocampal ensemble activity during rapid eye movement sleep. *Neuron*, *29*(1), 145–156. https://doi.org/10.1016/s0896-6273(01)00186-6

Martino, T. A., Oudit, G. Y., Herzenberg, A. M., Tata, N., Koletar, M. M., Kabir, G. M., Belsham, D. D., Backx, P. H., Ralph, M. R., & Sole, M. J. (2008). Circadian rhythm disorganization produces profound cardiovascular and renal disease in hamsters. *American Journal of Physiology-Regulatory, Integrative and Comparative Physiology*, *294*(5), R1675–R1683. https://doi.org/10.1152/ajpregu.00829.2007

McDonald, R. J., & White, N. M. (1993). A triple dissociation of memory systems: Hippocampus, amygdala, and dorsal striatum. *Behavioral Neuroscience*, *107*(1), 3–22. https://doi.org/10.1037//0735-7044.107.1.3

McDonald, R. J., Zelinski, E. L., Keeley, R. J., Sutherland, D., Fehr, L., & Hong, N. S. (2013). Multiple effects of circadian dysfunction induced by photoperiod shifts: Alterations in context memory and food metabolism in the same subjects. *Physiology & Behavior*, *118*, 14–24. https://doi.org/10.1016/j.physbeh.2013.04.010

McNAUGHTON, B. L., Barnes, C. A., Gerrard, J. L., Gothard, K., Jung, M. W., Knierim, J. J., Kudrimoti, H., Qin, Y., Skaggs, W. E., Suster, M., & Weaver, K. L. (1996). Deciphering The Hippocampal Polyglot: The Hippocampus as a Path Integration System. *Journal of Experimental Biology*, *199*(1), 173–185. https://doi.org/10.1242/jeb.199.1.173

Mehta, P., Kaur, G., Thakur, N., & Kaur, N. (2021). Circadian Dysregulation: A Mainstream Mess of the Present World. *Journal of Pharmaceutical Research International*, 272–281. https://doi.org/10.9734/jpri/2021/v33i54B33786

Milner, B., Corkin, S., & Teuber, H.-L. (1968). Further analysis of the hippocampal amnesic syndrome: 14-year follow-up study of H.M. *Neuropsychologia*, *6*(3), 215–234. https://doi.org/10.1016/0028-3932(68)90021-3

Mitchell, A. S., Czajkowski, R., Zhang, N., Jeffery, K., & Nelson, A. J. D. (2018). Retrosplenial cortex and its role in spatial cognition. *Brain and Neuroscience Advances*, *2*, 2398212818757098. https://doi.org/10.1177/2398212818757098

Morris, R. (1984). Developments of a water-maze procedure for studying spatial learning in the rat. *Journal of Neuroscience Methods*, *11*(1), 47–60. https://doi.org/10.1016/0165-0270(84)90007-4

Morris, R. G., Garrud, P., Rawlins, J. N., & O'Keefe, J. (1982). Place navigation impaired in rats with hippocampal lesions. *Nature*, *297*(5868), 681–683. https://doi.org/10.1038/297681a0

Moser, E. I., Kropff, E., & Moser, M.-B. (2008). Place cells, grid cells, and the brain's spatial representation system. *Annual Review of Neuroscience*, *31*, 69–89. https://doi.org/10.1146/annurev.neuro.31.061307.090723

Moser, E. I., Moser, M.-B., & McNaughton, B. L. (2017). Spatial representation in the hippocampal formation: A history. *Nature Neuroscience*, *20*(11), 1448–1464. https://doi.org/10.1038/nn.4653

Muller, R. U., Bostock, E., Taube, J. S., & Kubie, J. L. (1994). On the directional firing properties of hippocampal place cells. *The Journal of Neuroscience, 14*(12), 7235–7251. https://doi.org/10.1523/JNEUROSCI.14-12-07235.1994

Muller, R. U., & Kubie, J. L. (1987). The effects of changes in the environment on the spatial firing of hippocampal complex-spike cells. *Journal of Neuroscience*, *7*(7), 1951–1968. https://doi.org/10.1523/JNEUROSCI.07-07-01951.1987

Münch, M., & Bromundt, V. (2012). Light and chronobiology: Implications for health and disease. *Dialogues in Clinical Neuroscience*, *14*(4), 448–453.

Musiek, E. S., Xiong, D. D., & Holtzman, D. M. (2015). Sleep, circadian rhythms, and the pathogenesis of Alzheimer disease. *Experimental & Molecular Medicine*, *47*(3), e148. https://doi.org/10.1038/emm.2014.121

Okaichi, H. (1987). Performance and dominant strategies on place and cue tasks following hippocampal lesions in rats. *Psychobiology*, *15*(1), 58–63. https://doi.org/10.3758/BF03327264

O'Keefe, J., & Conway, D. H. (1978). Hippocampal place units in the freely moving rat: Why they fire where they fire. *Experimental Brain Research*, *31*(4), 573–590. https://doi.org/10.1007/BF00239813

O'Keefe, J., & Dostrovsky, J. (1971). The hippocampus as a spatial map. Preliminary evidence from unit activity in the freely-moving rat. *Brain Research*, *34*(1), 171–175. https://doi.org/10.1016/0006-8993(71)90358-1

O'Keefe, J. M., Nadel, L., & O'Keefe, J. (1978). *The hippocampus as a cognitive map*. Oxford University Press, Oxford.

O'Keefe, J., Nadel, L., Keightley, S., & Kill, D. (1975). Fornix lesions selectively abolish place learning in the rat. *Experimental Neurology*, *48*(1), 152–166. https://doi.org/10.1016/0014-4886(75)90230-7

O'Keefe, J., & Recce, M. L. (1993). Phase relationship between hippocampal place units and the EEG theta rhythm. *Hippocampus*, *3*(3), 317–330. https://doi.org/10.1002/hipo.450030307

O'Keefe, J., & Speakman, A. (1987). Single unit activity in the rat hippocampus during a spatial memory task. *Experimental Brain Research*, *68*(1), 1–27. https://doi.org/10.1007/BF00255230

Pachitariu, M., Stringer, C., Dipoppa, M., Schröder, S., Rossi, L. F., Dalgleish, H., Carandini, M., & Harris, K. D. (2016). Suite2p: Beyond 10,000 neurons with standard two-photon microscopy. *bioRxiv,* 061507. https://doi.org/10.1101/061507

Packard, M. G., Hirsh, R., & White, N. M. (1989). Differential effects of fornix and caudate nucleus lesions on two radial maze tasks: Evidence for multiple memory systems. *The Journal of Neuroscience*, *9*(5), 1465–1472. https://doi.org/10.1523/JNEUROSCI.09-05-01465.1989

Packard, M. G., & McGaugh, J. L. (1992). Double dissociation of fornix and caudate nucleus lesions on acquisition of two water maze tasks: Further evidence for multiple memory systems. *Behavioral Neuroscience*, *106*(3), 439–446. https://doi.org/10.1037//0735-7044.106.3.439

Penfield, W., & Milner, B. (1958). Memory deficit produced by bilateral lesions in the hippocampal zone. *A.M.A. Archives of Neurology and Psychiatry*, *79*(5), 475–497. https://doi.org/10.1001/archneurpsyc.1958.02340050003001

Phillips, R. G., & LeDoux, J. E. (1992). Differential contribution of amygdala and hippocampus to cued and contextual fear conditioning. *Behavioral Neuroscience*, *106*(2), 274–285. https://doi.org/10.1037//0735-7044.106.2.274

Quirk, G. J., Muller, R. U., & Kubie, J. L. (1990). The firing of hippocampal place cells in the dark depends on the rat's recent experience. *The Journal of Neuroscience*, *10*(6), 2008–2017. https://doi.org/10.1523/JNEUROSCI.10-06-02008.1990

Rich, P. D., Liaw, H.-P., & Lee, A. K. (2014). Large environments reveal the statistical structure governing hippocampal representations. *Science*, *345*(6198), 814–817. https://doi.org/10.1126/science.1255635

Roenneberg, T., & Merrow, M. (2016). The Circadian Clock and Human Health. *Current Biology: CB*, *26*(10), R432-443. https://doi.org/10.1016/j.cub.2016.04.011

Roenneberg, T., Wirz-Justice, A., Skene, D. J., Ancoli-Israel, S., Wright, K. P., Dijk, D.-J., Zee, P., Gorman, M. R., Winnebeck, E. C., & Klerman, E. B. (2019). Why Should We Abolish Daylight Saving Time? *Journal of Biological Rhythms*, *34*(3), 227–230. https://doi.org/10.1177/0748730419854197

Royer, S., Zemelman, B. V., Losonczy, A., Kim, J., Chance, F., Magee, J. C., & Buzsáki, G. (2012). Control of timing, rate and bursts of hippocampal place cells by dendritic and somatic inhibition. *Nature Neuroscience*, *15*(5), 769–775. https://doi.org/10.1038/nn.3077

Samsonovich, A., & McNaughton, B. L. (1997). Path Integration and Cognitive Mapping in a Continuous Attractor Neural Network Model. *The Journal of Neuroscience*, *17*(15), 5900–5920. https://doi.org/10.1523/JNEUROSCI.17-15-05900.1997

Savelli, F., Yoganarasimha, D., & Knierim, J. J. (2008). Influence of boundary removal on the spatial representations of the medial entorhinal cortex. *Hippocampus*, *18*(12), 1270–1282. https://doi.org/10.1002/hipo.20511

Schibler, U. (2005). The daily rhythms of genes, cells and organs. *EMBO Reports*, *6*(Suppl 1), S9–S13. https://doi.org/10.1038/sj.embor.7400424

Scoville, W. B., & Milner, B. (1957). Loss of recent memory after bilateral hippocampal lesions. *Journal of Neurology, Neurosurgery, and Psychiatry*, *20*(1), 11–21. https://doi.org/10.1136/jnnp.20.1.11

Selden, N. R., Everitt, B. J., Jarrard, L. E., & Robbins, T. W. (1991). Complementary roles for the amygdala and hippocampus in aversive conditioning to explicit and contextual cues. *Neuroscience*, *42*(2), 335–350. https://doi.org/10.1016/0306-4522(91)90379-3

Sharma, V. K., & Chandrashekaran, M. K. (2005). Zeitgebers (*time cues*) for biological clocks. *Current Science 89*(7), 1136–1146.

Sheintuch, L., Rubin, A., Brande-Eilat, N., Geva, N., Sadeh, N., Pinchasof, O., & Ziv, Y. (2017). Tracking the Same Neurons across Multiple Days in Ca2+ Imaging Data. *Cell Reports*, *21*(4), 1102–1115. https://doi.org/10.1016/j.celrep.2017.10.013

Skaggs, W., McNaughton, B., & Gothard, K. (1992). An Information-Theoretic Approach to Deciphering the Hippocampal Code. *Advances in Neural Information Processing Systems*, *5*. https://proceedings.neurips.cc/paper/1992/hash/5dd9db5e033da9c6fb5ba83c7a7ebea9-Abstract.html

Solstad, T., Boccara, C. N., Kropff, E., Moser, M.-B., & Moser, E. I. (2008). Representation of geometric borders in the entorhinal cortex. *Science (New York, N.Y.)*, *322*(5909), 1865–1868. https://doi.org/10.1126/science.1166466

Speakman, A., & O'Keefe, J. (1990). Hippocampal Complex Spike Cells do not Change Their Place Fields if the Goal is Moved Within a Cue Controlled Environment. *The European Journal of Neuroscience*, *2*(6), 544–555. https://doi.org/10.1111/j.1460-9568.1990.tb00445.x

Squire, L. R. (1992). Memory and the hippocampus: A synthesis from findings with rats, monkeys, and humans. *Psychological Review*, *99*(2), 195–231. https://doi.org/10.1037/0033-295X.99.2.195

Squire, L. R. (2009). The legacy of patient H.M. for neuroscience. *Neuron*, *61*(1), 6–9. https://doi.org/10.1016/j.neuron.2008.12.023

Squire, L. R., Knowlton, B., & Musen, G. (1993). The structure and organization of memory. *Annual Review of Psychology*, *44*, 453–495. https://doi.org/10.1146/annurev.ps.44.020193.002321

Squire, L. R., & Zola-Morgan, S. (1991). The medial temporal lobe memory system. *Science*, *253*(5026), 1380–1386. https://doi.org/10.1126/science.1896849

Steiger, A., Farfan, J., Fisher, N., Heller, H. C., Fernandez, F.-X., & Ruby, N. F. (2022). Reversible Suppression of Fear Memory Recall by Transient Circadian Arrhythmia. *Frontiers in Integrative Neuroscience*, *16*, 900620. https://doi.org/10.3389/fnint.2022.900620

Sutherland, R. J., Kolb, B., & Whishaw, I. Q. (1982). Spatial mapping: Definitive disruption by hippocampal or medial frontal cortical damage in the rat. *Neuroscience Letters*, *31*(3), 271–276. https://doi.org/10.1016/0304-3940(82)90032-5

Sutherland, R. J., & Rudy, J. W. (1989). Configural association theory: The role of the hippocampal formation in learning, memory, and amnesia. *Psychobiology*, *17*(2), 129–144. https://doi.org/10.3758/BF03337828

Taube, J., Muller, R., & Ranck, J. (1990a). Head-direction cells recorded from the postsubiculum in freely moving rats. I. Description and quantitative analysis. *The Journal of Neuroscience*, *10*(2), 420–435. https://doi.org/10.1523/JNEUROSCI.10-02-00420.1990

Taube, J., Muller, R., & Ranck, J. (1990b). Head-direction cells recorded from the postsubiculum in freely moving rats. II. Effects of environmental manipulations. *The Journal of Neuroscience*, *10*(2), 436–447. https://doi.org/10.1523/JNEUROSCI.10-02-00436.1990

Tavares, R. M., Mendelsohn, A., Grossman, Y., Williams, C. H., Shapiro, M., Trope, Y., & Schiller, D. (2015). A Map for Social Navigation in the Human Brain. *Neuron*, *87*(1), 231–243. https://doi.org/10.1016/j.neuron.2015.06.011

Teyler, T. J., & DiScenna, P. (1986). The hippocampal memory indexing theory. *Behavioral Neuroscience*, *100*(2), 147–154. https://doi.org/10.1037//0735-7044.100.2.147

Tolman, E. C. (1948). Cognitive maps in rats and men. *Psychological Review*, *55*(4), 189–208. https://doi.org/10.1037/h0061626

Vadnie, C. A., & McClung, C. A. (2017). Circadian Rhythm Disturbances in Mood Disorders: Insights into the Role of the Suprachiasmatic Nucleus. *Neural Plasticity*, *2017*, 1504507. https://doi.org/10.1155/2017/1504507

Van Esseveldt, L. (K.) E., Lehman, M. N., & Boer, G. J. (2000). The suprachiasmatic nucleus and the circadian time-keeping system revisited. *Brain Research Reviews*, *33*(1), 34–77. https://doi.org/10.1016/S0165-0173(00)00025-4

Wendeu-Foyet, M. G., Cénée, S., Koudou, Y., Trétarre, B., Rébillard, X., Cancel-Tassin, G., Cussenot, O., Boland, A., Olaso, R., Deleuze, J.-F., Blanché, H., Lamy, P.-J., Mulot, C., Laurent-Puig, P., Truong, T., & Menegaux, F. (2020). Circadian genes polymorphisms, night work and prostate cancer risk: Findings from the EPICAP study. *International Journal of Cancer*, *147*(11), 3119–3129. https://doi.org/10.1002/ijc.33139

White, N. M., & McDonald, R. J. (2002). Multiple parallel memory systems in the brain of the rat. *Neurobiology of Learning and Memory*, *77*(2), 125–184. https://doi.org/10.1006/nlme.2001.4008

Wilson, M. A., & McNaughton, B. L. (1993). Dynamics of the hippocampal ensemble code for space. *Science (New York, N.Y.)*, *261*(5124), 1055–1058. https://doi.org/10.1126/science.8351520

Xia, C. (2006). Understanding the human brain: A lifetime of dedicated pursuit. Interview with Dr. Brenda Milner. *McGill Journal of Medicine : MJM*, *9*(2), 165–172.

Yamada, K., & Toda, K. (2022). Pupillary dynamics of mice performing a Pavlovian delay conditioning task reflect reward-predictive signals. *Frontiers in Systems Neuroscience*, *16*, 1045764. https://doi.org/10.3389/fnsys.2022.1045764

Yin, H. H., Knowlton, B. J., & Balleine, B. W. (2004). Lesions of dorsolateral striatum preserve outcome expectancy but disrupt habit formation in instrumental learning. *The European Journal of Neuroscience*, *19*(1), 181–189. https://doi.org/10.1111/j.1460-9568.2004.03095.x

Yuan, R. K., Zitting, K.-M., Duffy, J. F., Vujovic, N., Wang, W., Quan, S. F., Klerman, E. B., Scheer, F. A. J. L., Buxton, O. M., Williams, J. S., & Czeisler, C. A. (2021). Chronic Sleep Restriction While Minimizing Circadian Disruption Does Not Adversely Affect Glucose Tolerance. *Frontiers in Physiology*, *12*, 764737. https://doi.org/10.3389/fphys.2021.764737

Zelinski, E. L., Hong, N. S., & McDonald, R. J. (2014). Persistent impairments in hippocampal function following a brief series of photoperiod shifts in rats. *Animal Cognition*, *17*(1), 127–141. https://doi.org/10.1007/s10071-013-0645-8

Zienolddiny, S., Haugen, A., Lie, J.-A. S., Kjuus, H., Anmarkrud, K. H., & Kjærheim, K. (2013). Analysis of polymorphisms in the circadian-related genes and breast cancer risk in Norwegian nurses working night shifts. *Breast Cancer Research*, *15*(4), R53. https://doi.org/10.1186/bcr3445

Zola-Morgan, S., Squire, L. R., Clower, R. P., & Alvarez-Royo, P. (1991). Independence of memory functions and emotional behavior: Separate contributions of the hippocampal formation and the amygdala. *Hippocampus*, *1*(2), 207–220. https://doi.org/10.1002/hipo.450010208

Zong, W., Obenhaus, H. A., Skytøen, E. R., Eneqvist, H., de Jong, N. L., Vale, R., Jorge, M. R., Moser, M.-B., & Moser, E. I. (2022). Large-scale two-photon calcium imaging in freely moving mice. *Cell*, *185*(7), 1240-1256.e30. https://doi.org/10.1016/j.cell.2022.02.017

Appendix A:

An accounting of all unusable data

Some of the data collected was found to be unusable for later analysis for various reasons. Mostly this is due to the necessity of obtaining multiple laps worth of data in each session. The minimum number of laps was set at ten. Mouse 7 in its entirety was excluded from analysis because it did not run the minimum number of laps on most sessions including the retention tests.

The sessions excluded due to the mouse failing to run the minimum ten laps were:
Mouse 4 days 4 and 13
Mouse 10 days 4 and 7
Mouse 13 days 5, 6, 7 and 12
Mouse 19 days 3 and 4

The sessions excluded due to MATLAB error that, without clear indication of any problem, halted recording of position and velocity data before the completion of ten laps were:
Mouse 2 day 11
Mouse 11 day 1
Mouse 13 days 3 and 4
Mouse 14 day 5

The session excluded due to an unexplained failure of AxoScope to record the timing of the microscope's frames was:
Mouse 1 day 3

The sessions excluded due to an unidentified error during recording that prevented processing by Suite-2p were:
Mouse 3 day 1
Mouse 4 days 1, 2, 3, 4 and 5

The session excluded due to a severe shift in field of view depth during imaging is:
Mouse 11 day 10

To sum up, the full list of recorded sessions excluded from analysis is:
Mouse 1 day 3
Mouse 2 day 11
Mouse 3 day 1

Mouse 4 days 1, 2, 3, 4, 5 and 13

Mouse 7 all sessions

Mouse 10 days 4 and 7

Mouse 11 days 3 and 10

Mouse 13 days 3, 4, 5, 6, 7 and 12

Mouse 14 day 5

Mouse 19 days 3 and 4

Appendix B:

Practical constraints on experimental design

There were a few practical constraints which limited this experiment in undesirable ways. Because multiple mice were imaged on each day, there was variation in the amount of time between when housing room lights turn on and when imaging begins. These variations exist between mice of the same group and cohort, as well as between days for any individual mouse. Some of this variation came about in an effort to reduce the amount of between group variation in the amount of time between imaging sessions. Since the experimental group is on a 21-hour light-dark cycle, the amount of time between imaging sessions had to be less than 24 hours as would have been the default for the control group. In an effort to minimize this difference, the spacing of the experimental group imaging sessions were advanced by only 2 and not three hours each day during phase shifting, meaning experimental group imaging sessions occurred approximately once every 22 hours. This was the case for the experimental groups of both cohorts. The control group imaging sessions occurred approximately once every 23 hours for cohort 1, and approximately once every 24 hours for cohort 2. This difference between cohorts was an unexpected change in plans made necessary due the scheduling challenges inherent to sharing use of the imaging equipment with other researchers. Because of all of this variation within and between groups and cohorts in regard to the time of day of imaging, it would be foolish to attempt any analysis of the effects of time of day.

Other undesirable practical constraints included the use of two different training treadmills which were in separate rooms, and small variations between days in the volume of each sugar water reward due to the pinch valve requiring frequent readjustment.

Appendix C:

Examples of firing activity of individual cells

The following figures are drawn from the data of mouse 6 day 10 using true offsets. Figure C.1 contains 80 place cells.

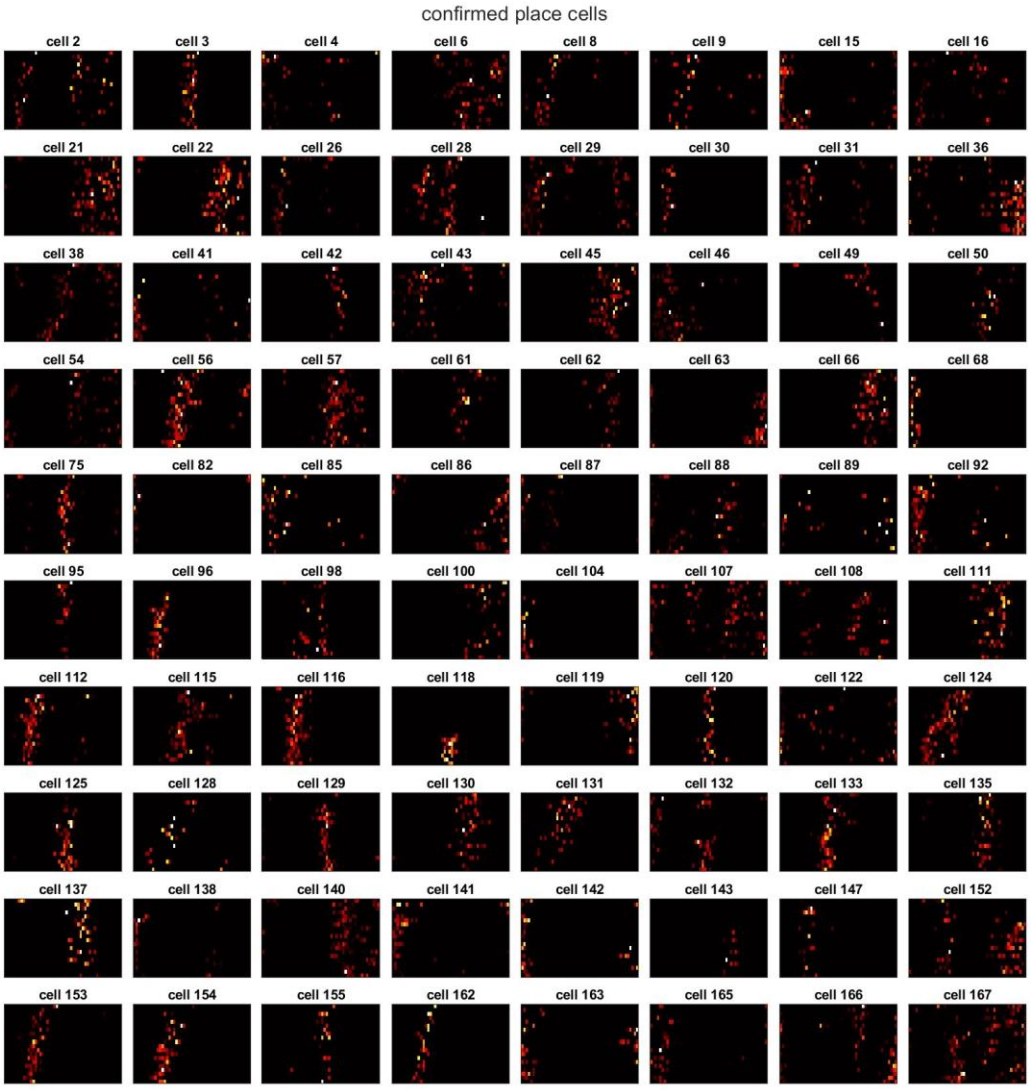

Figure C.1: 80 place cells from mouse 6 day 10 obtained with true offsets. Lap number is indicated by y-axis of each subfigure with the first lap being the top row. Bin number is indicated by x-axis.

Figure C.2 contains 80 cells which passed the first criteria of possessing sufficient spatial information, but failed the second criteria of possessing a sufficiently coherent place field.

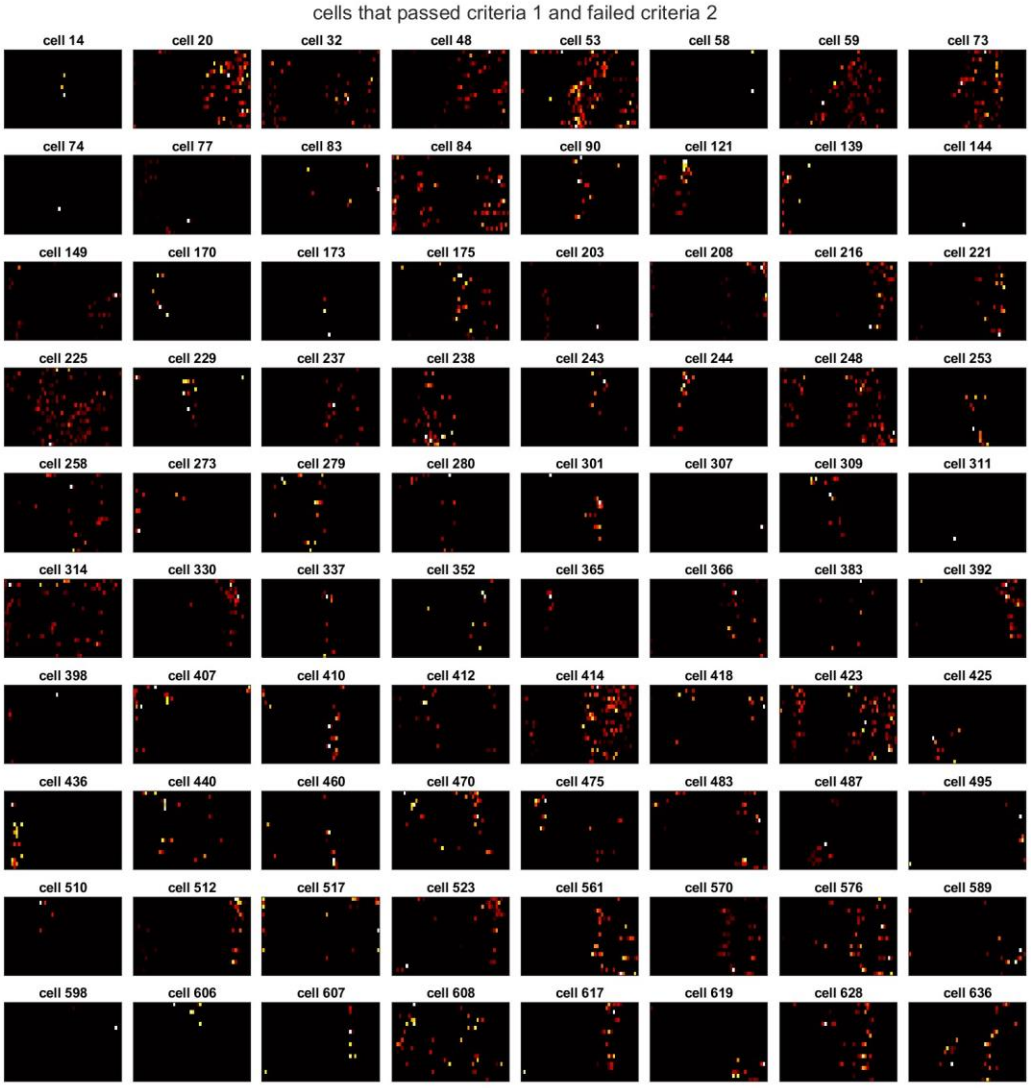

Figure C.2: 80 non-place cells that passed the first criteria and failed the second. All cells depicted are from mouse 6 day 10 obtained with true offsets. Lap number is indicated by y-axis of each subfigure with the first lap being the top row. Bin number is indicated by x-axis.

Figure C.2 contains all 11 cells which passed the second criteria of possessing a sufficiently coherent place field, but failed the first criteria of possessing sufficient spatial information.

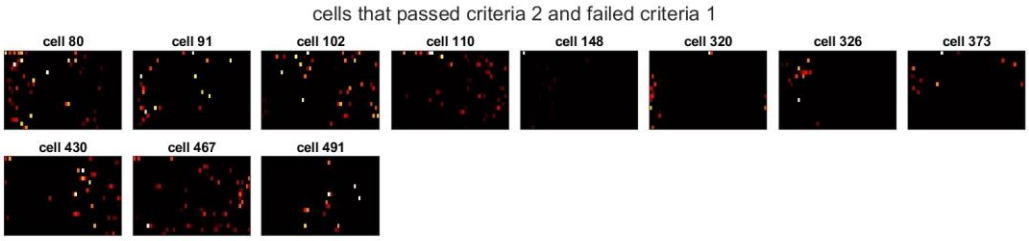

Figure C.3: All 11 non-place cells that passed the second criteria and failed the first. All cells depicted are from mouse 6 day 10 obtained with true offsets. Lap number is indicated by y-axis of each subfigure with the first lap being the top row. Bin number is indicated by x-axis.

Appendix D:

Behavioural data

As described in sections 2.2.1, 2.2.3 and 4.3.1, during imaging certain behavioral data was collected. The position and velocity of the mouse's movement along the treadmill was recorded, along with the timings of each lick of the reward spout. While running along the treadmill, mice would occasionally pause. Figure D.1 shows which sections of the treadmill each mouse spent time paused in on each day of imaging.

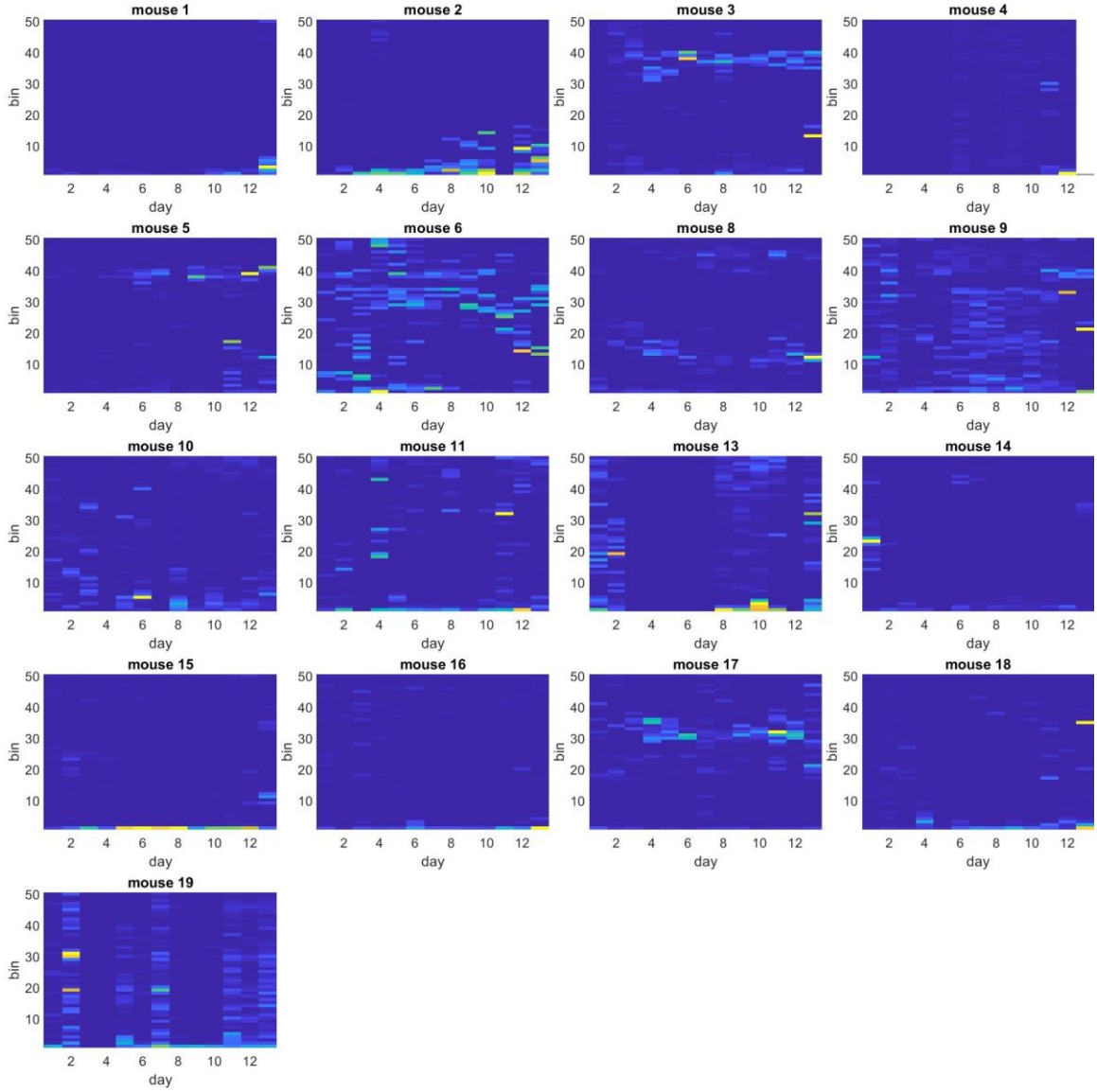

Figure D.1: Time spent paused in each bin on each day of imaging.

Since mice are generally inclined to pause most often in the first few bins immediately following the reward location, and since this data is primarily of use as a way to check for signs of anticipatory pausing in the last few bins, figure D.2 was made. Figure D.2 calculates the mean median and mode position of pausing for each day, using only the pausing data from bins 6 to 50. This allows for easy identification of consistent pausing behaviour across days. Some mice are more consistent than others in pausing in the same location each day.

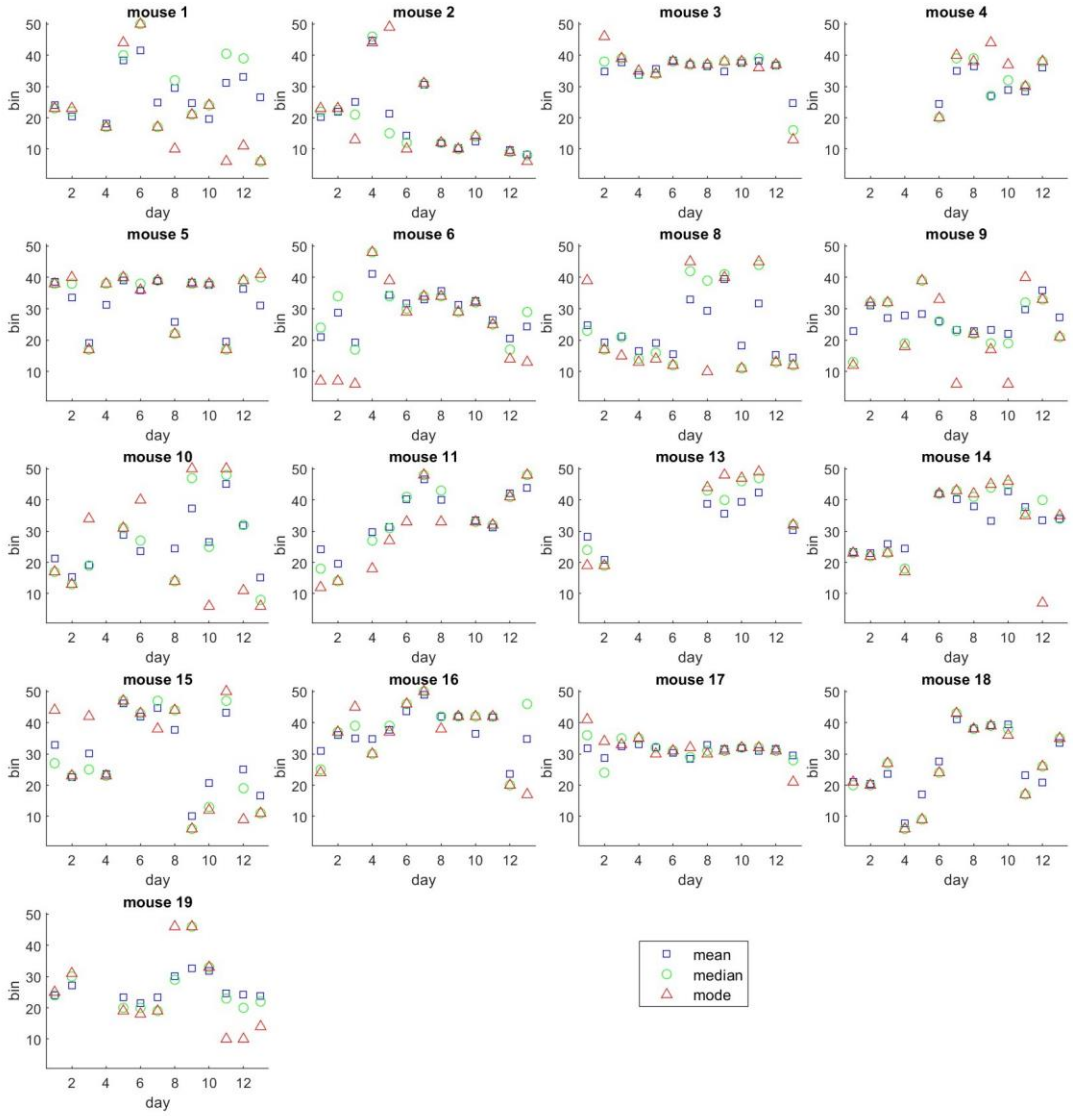

Figure D.2: Average position of pausing for each day of imaging. Each subfigure shows the mean, median and mode position of pausing for each imaging day. These were calculated after disregarding all time spent paused in the first 5 bins.

The lick sensor was non-functional throughout the imaging of cohort 1. This is in the process of being corrected, using the video from the infrared camera to calculate licking timings.

However, that data is not yet available. As such figures D.3 and D.4 contain only data from the mice of cohort 2. Figure D.3 displays the relative frequency of licking in each bin in each day of imaging. Unsurprisingly, in all mice there was an overwhelming preference for licking in the first bin due to it being immediately after the reward location.

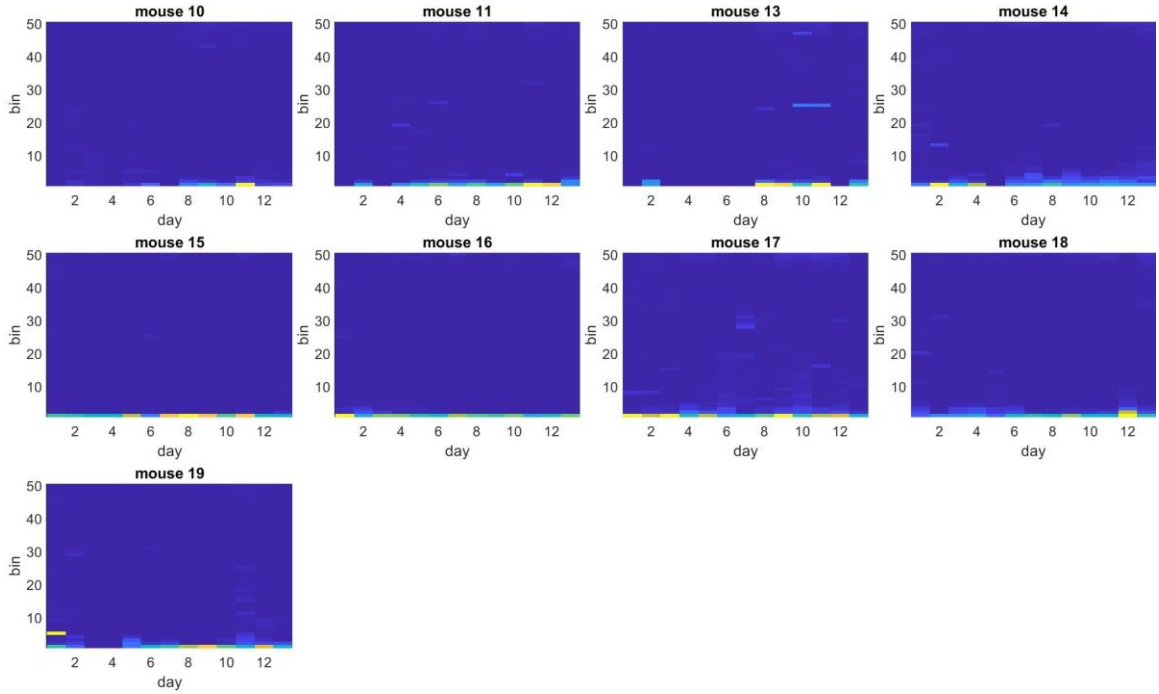

Figure D.3: Total number of licks in each bin for each day of imaging.

To translate this into a more useful format, figure D.4 was made by calculating the mean median and mode position of licking, using only data from bins 6 to 50. Figure D.5 shows that some mice engage in noticeable anticipatory licking behaviour in the last two bins. However, this is not a universal behaviour on all days, or for all mice.

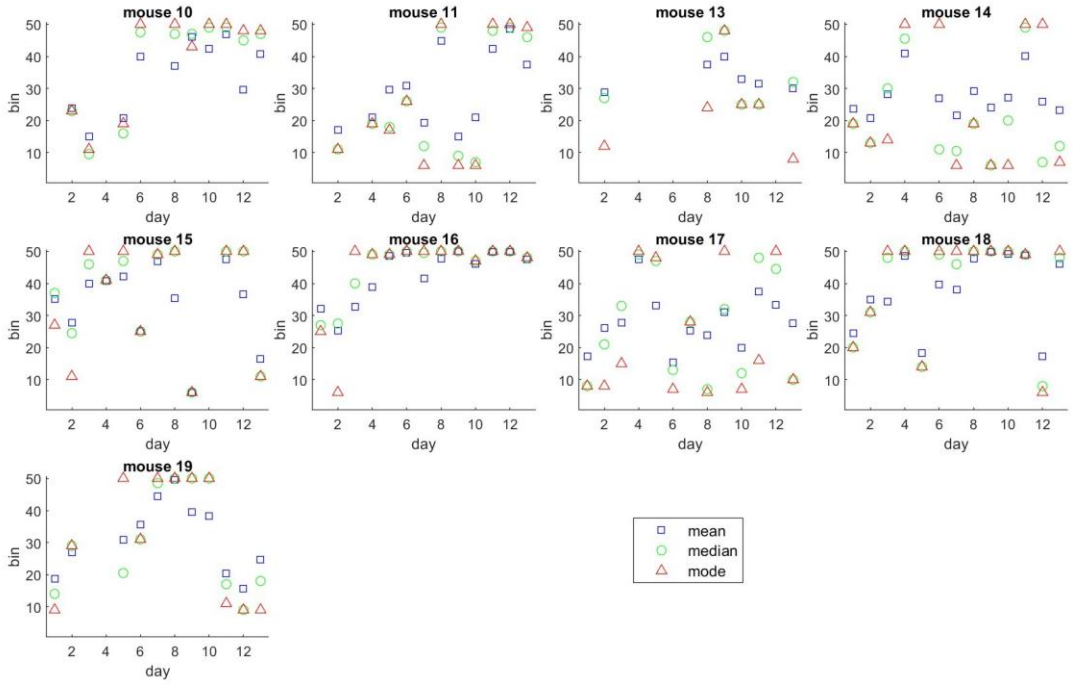

Figure D.4: Average position of licking for each day of imaging. Each subfigure shows the mean, median and mode position of pausing for each imaging day. These were calculated after disregarding all time spent paused in the first 5 bins.